ELEMENTA
Science of the Anthropocene

Neukermans, Harmel, Gali et al. 2018. Harnessing remote sensing to address critical science questions on ocean-atmosphere interactions. *Elem Sci Anth*, 6: 71. DOI: https://doi.org/10.1525/elementa.331

REVIEW

Harnessing remote sensing to address critical science questions on ocean-atmosphere interactions

Griet Neukermans[*], Tristan Harmel[*,†], Martí Galí[‡,§], Natalia Rudorff[‖], Jacek Chowdhary[¶], Oleg Dubovik[**], Chris Hostetler[††], Yongxiang Hu[††], Cédric Jamet[‡‡], Kirk Knobelspiesse[§§], Yoav Lehahn[‖‖], Pavel Litvinov[‖‖‖], Andrew M. Sayer[§§,¶¶], Brian Ward[***], Emmanuel Boss[†††], Ilan Koren[‡‡‡] and Lisa A. Miller[§§§]

Earth observing systems have proven to be a unique source of long-term synoptic information on numerous physical, chemical and biological parameters on a global scale. Merging this information for integrated studies that peruse key questions about the ocean-atmosphere interface is, however, very challenging. Such studies require interdisciplinary frameworks and novel insights into ways to address the problem. We present here a perspective review on how current and emerging remote sensing technologies could help address two scientific questions within the Surface Ocean-Lower Atmosphere Study (SOLAS) science plan: (1) to what extent does upper-ocean biology affect the composition and radiative properties of the marine boundary layer; and (2) to what extent does upper-ocean turbulence drive fluxes of mass and energy at the air-sea interface. We provide a thorough review of how these questions have been addressed and discuss novel potential avenues using multiplatform space-borne missions, from visible to microwave, active and passive sensors.

Keywords: Ocean; Atmosphere; Interface; Interactions; Remote sensing; Interdisciplinarity

1 The Problem: Upscaling air-sea interaction processes to the global system

Resolving the fluxes of material, heat, and momentum between the atmosphere and the ocean is essential to understand key climate processes (Stocker et al., 2013). However, our current level of understanding is limited by insufficient measurements of the governing processes, which are often highly nonlinear.

Air-sea exchanges occur between two relatively narrow boundary layers that vary on different time and space scales (Liss and Johnson, 2014). Problems of momentum exchange are dependent on processes occurring on the scales of waves, from capillary waves of millimetre scale to tsunamis tens of kilometres long. In contrast, heat exchange occurs on vertical scales of micrometres (near infra-red emission) to metres (light absorption). At larger scales, exchanges of

* Sorbonne Université, Centre National de la Recherche Scientifique (CNRS), Laboratoire d'Océanographie de Villefranche-sur-Mer, Villefranche sur Mer, FR
† Irstea, UR RECOVER, Pôle AFB-Irstea Hydroécologie des Plans d'eau, Aix-en-Provence, FR
‡ Takuvik Joint International Laboratory (Université Laval – CNRS) and Québec-Océan, Biology Department, Université Laval, Québec, CA
§ Barcelona Supercomputing Center (BSC), ES
‖ Divisão de Satélites e Sistemas Ambientais, Centro de Previsão do Tempo e Estudo Climáticos, Instituto Nacional de Pesquisas Espaciais, INPE, Cachoeira Paulista, São Paulo, BR
¶ Department of Applied Physics and Mathematics, Columbia University, New York, US
** Laboratoire d'Optique Atmosphérique, CNRS/Universite Lille, Villeneuve d'Ascq, FR
†† Langley Research Center, National Aeronautics and Space Administration, Hampton, Virginia, US
‡‡ Univ. Littoral Cote d'Opale, CNRS, Univ. Lille, UMR 8187, LOG, Laboratoire d'Océanologie et de Géosciences, Wimereux, FR
§§ Ocean Ecology Laboratory, NASA Goddard Space Flight Center, Greenbelt, Maryland, US
‖‖ Department of Marine Geosciences, Charney School of Marine Sciences, University of Haifa, Haifa, IL
¶¶ Goddard Earth Sciences Technology and Research (GESTAR), Universities Space Research Association (USRA), NASA Goddard Space Flight Center, Greenbelt, Maryland, US
*** AirSea Laboratory, School of Physics and Ryan Institute, National University of Ireland, Galway, IE
††† School of Marine Sciences, University of Maine, Orono, Maine, US
‡‡‡ Department of Earth and Planetary Sciences, Weizmann Institute of Science, Rehovot, IL
§§§ Centre for Ocean Climate Chemistry, Institute of Ocean Sciences, Fisheries and Oceans Canada, Sidney, British Columbia, CA
‖‖‖ GRASP-SAS, Remote sensing developments, Villeneuve d'Ascq, FR
Griet Neukermans, Tristan Harmel and Martí Galí contributed equally
Corresponding author: Martí Galí (marti.gali.tapias@gmail.com)

gases and aerosols are driven at the scale of mixed layers (hundreds of meters in the atmosphere and tens of meters in the ocean). Although remote sensing tools have the potential to help resolve these different spatial scales, the region encompassing the two boundary layers contains a sharp discontinuity in optical properties at the air-sea interface, which poses a challenge to remote sensing of these interface processes. This problem is a classic case of one scientist's noise being another's data: atmospheric remote sensing considers the ocean's contribution to measured spectral reflectance as a problem that requires a correction (Tanré et al., 1997; Remer et al., 2005) and vice versa, with ocean remote sensing viewing atmospheric signals as interferences (IOCCG, 2010; Müller et al., 2015). Both communities generally avoid or neglect interface processes.

Key challenges in the study of air-sea exchange include high interdisciplinarity and extreme nonlinearity between the processes to be described. A hypothetical, comprehensive air-sea exchange expert would need to understand ocean ecology, biogeochemistry and microbiology, fluid dynamics, micrometeorology, cloud dynamics and microphysics, thermodynamics, organic chemistry, heterogeneous chemistry, radiation transfer, and even glaciology (see for instance Le Quéré and Saltzman, 2013). Feedbacks between the processes described by each of these disciplines add to the inherent complexity in these systems (**Figure 1a**). SOLAS has had great success with in-situ measurements, laboratory experiments, and numerical models (Brévière et al., 2015), but scaling the knowledge generated by these approaches to the full Earth system

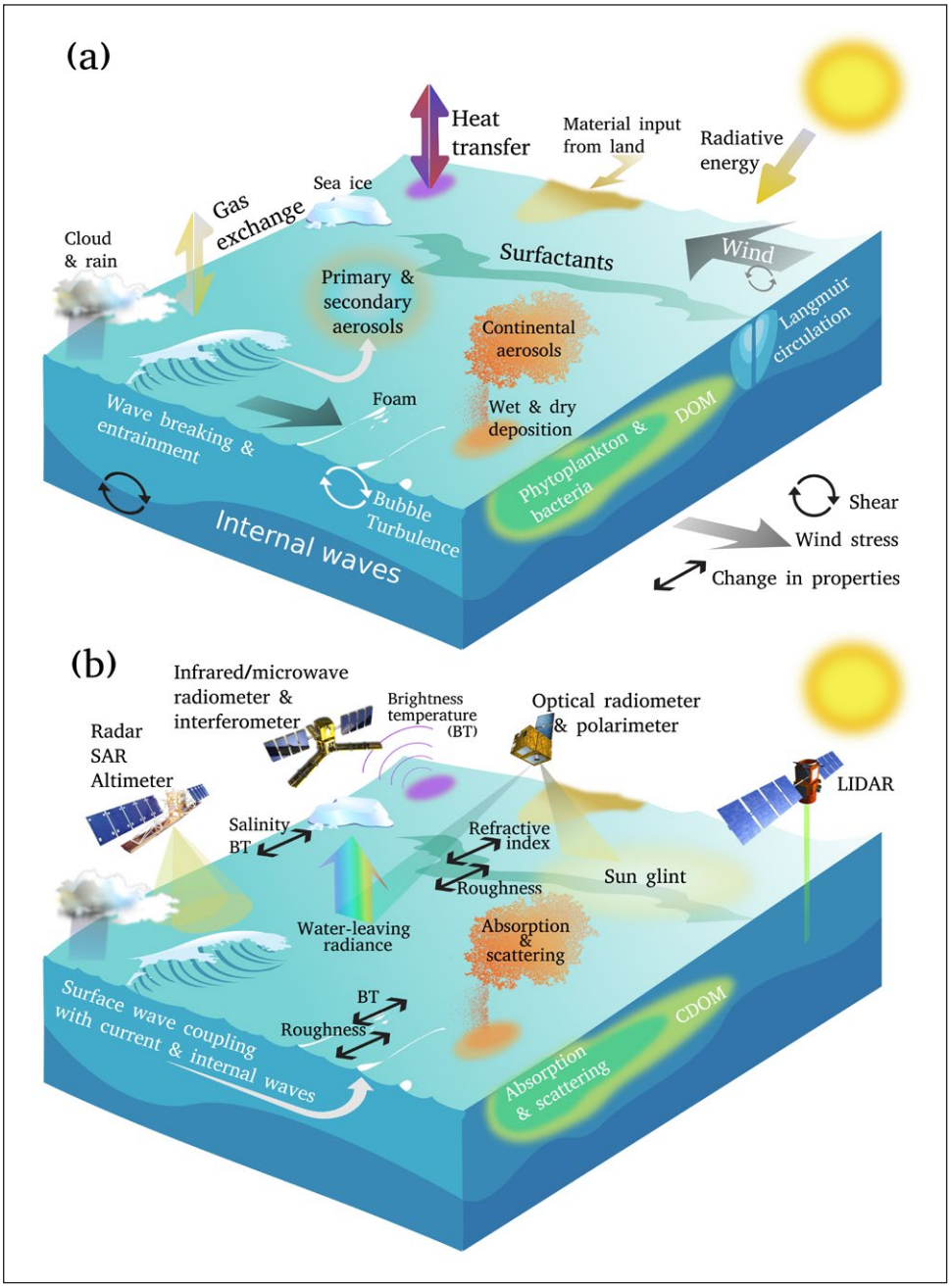

Figure 1: Remote sensing of ocean-atmosphere interactions. Conceptual view of **(a)** oceanic and atmospheric processes influencing air-sea interactions, and **(b)** corresponding properties observable by the remote sensing technologies discussed in this paper. DOI: https://doi.org/10.1525/elementa.331.f1

requires optimised utilisation of available and future remote sensing tools.

Remote sensing uses different parts of the electromagnetic spectrum to observe the Earth system, taking advantage of the fact that different parts of this spectrum are affected differently by properties and dynamic behaviour of matter within the ocean, the atmosphere, and at the interface between them (**Figure 1b**) (Shutler et al., 2016). Remote Earth observation sensors are deployed not only on satellites in Earth orbit, but also on aircraft and even ground or ship-based facilities. Passive sensors measure the electromagnetic radiation reflected or emitted by the Earth system (typically in the visible, near-infrared, thermal, or microwave spectral regions), the characteristics of which depend on the state of the atmosphere and surface. Active sensors provide an electromagnetic source on their own, and record the signal backscattered from interactions with material along the path. The temporal signal of the backscattered radiation provides information about the vertical profiles of scattering objects (Winker et al., 2009; Hostetler et al., 2018). See **Table 1** for a list of abbreviations and acronyms for satellite missions, instruments, geophysical terms, and models mentioned in this review.

For both passive and active signals, the radiation interacts with multiple components of the Earth system (clouds, aerosols, gases, the air-ocean interface, dissolved and particulate materials in the ocean). The complex mixture of competing interactions can mask certain components and limit their specific retrieval, owing to low signal-to-noise ratios. On the other hand, at any given moment, no more than one third of the ocean surface can be viewed in the visible range because of pronounced cloud cover (Harmel and Chami, 2013; Mace and Zhang, 2014). Satellite orbits and sensor fields of view also affect the spatial and temporal scales of the retrieved parameters, and, as in all scientific fields, the ability to answer a question of interest depends on the temporal and spatial scales of the available measurements. While polar-orbiting satellites provide global coverage every few days, geostationary satellites provide the possibility of observing the same location many times a day, enabling observations of processes and phenomena that operate at sub-diurnal time scales. Combining different remote sensing technologies with in-situ monitoring systems and/or with numerical models (Dubovik et al., 2014; Shutler et al., 2016) can generate a more accurate and useful understanding of the Earth system, while a single sensor can make contributions to the study of multiple disciplines (e.g., marine biogeochemistry, aerosols and cloud physics and chemistry, air-sea fluxes of mass and energy) (Gordon and Wang, 1994; Winker et al., 2009; Xu et al., 2016; Hostetler et al., 2018). Historically, these multiple disciplines have been studied largely by separate science communities leading to separate data products for aquatic and atmospheric applications.

This paper summarizes the outcomes of a workshop sponsored by SOLAS and the European Space Agency (ESA), held in Frascati, Italy, in June 2016 and dedicated to bridging gaps between scientists from various disciplines of remote sensing, ocean, and atmospheric sciences and to identifying innovative synergies between them. The invited participants were divided into groups with mixed scientific expertise and tasked with brainstorming new ways to answer their most persistent and thorny scientific questions. The participants focused on two questions that are central to the SOLAS program (Brévière, 2016) but that have received relatively little attention from the remote sensing community to date: (1) to what extent does upper-ocean biology affect the composition and radiative properties of the marine boundary layer, and (2) to what extent does upper-ocean turbulence drive fluxes of mass and energy at the air-sea interface. In this paper, we discuss how current and future remote sensing technologies may bring us closer to answering these questions and facing the challenges that lie ahead of us.

2 To what extent does upper-ocean biology affect the composition and radiative properties of the marine boundary layer?

2.1 Perspective on the problem

Biological activity in the upper ocean produces a range of particles and gases that influence the composition and radiative properties of marine boundary layer (MBL) aerosols, either by affecting the properties of wind-driven sea spray aerosols (primary aerosols) or by producing volatile compounds that nucleate into new particles and promote their growth (secondary aerosols). Away from continental and anthropogenic aerosol sources, marine biogenic aerosols can dominate MBL aerosol populations and provide a major source of cloud-seeding particles (cloud condensation nuclei, CCN). Hence, marine biogenic aerosols affect the amount of solar radiation reaching the Earth's surface by altering aerosol scattering (direct effects) and cloud radiative properties (indirect effects) (Twomey, 1974; Albrecht, 1989; Andreae and Rosenfeld, 2008; Brooks and Thornton, 2018).

Early research on the coupling between ocean biology, aerosols, and clouds focused mostly on the gas dimethylsulphide (DMS). DMS is produced by marine planktonic food webs through the decomposition of dimethylsulphoniopropionate (DMSP), a multifunctional compound produced by phytoplankton. The so-called CLAW hypothesis (**Table 1**; Charlson et al., 1987) proposed that DMS was the dominant source of CCN in the MBL. For a given liquid water content, an increase in CCN would result in clouds with more droplets of smaller size (smaller cloud droplet effective radius, CER) and higher cloud albedo (reflective power). The resulting decrease in photosynthetically available radiation (PAR) and sea surface temperature would decrease phytoplankton growth and DMS production. This effect would lead to a negative (regulatory) climate feedback between phytoplankton activity and cloud albedo. This hypothesis sparked a great amount of research across the fields of microbiology, oceanography, and atmospheric chemistry, advancing knowledge to a level unmatched for most biogenic volatile compounds (Simó, 2011; Carpenter et al., 2012). Although key aspects of the CLAW hypothesis have been challenged (Quinn and Bates, 2011), DMS still appears as a major source of CCN over most of the global ocean (Quinn et al., 2017), and can modulate the seasonal cycles of aerosols and CCN in remote atmospheres (Lana et al., 2012; Leaitch et al., 2013).

Table 1: List of abbreviations and acronyms mentioned in this review. DOI: https://doi.org/10.1525/elementa.331.t1

Abbreviation or acronym	Definition	Type
3MI	Multi-viewing Multi-channel Multi-polarisation Imaging	Instrument
(A)ATSR	(Advanced) along-track scanning radiometer	Instrument
AERONET	Aerosol Robotic Network	Observation network
AirMSPI	Airborne Multiangle Spectro Polarimetric Imager	Instrument
AMSR	Advanced Microwave Scanning Radiometer	Instrument
AOD	Aerosol optical depth (=aerosol optical thickness)	Geophysical term
ASCAT	Advanced Scatterometer	Satellite mission
ATLID	Atmospheric Lidar	Instrument
AVHRR	Advanced Very High Resolution Radiometer	Instrument
BRDF	Bidirectional reflectance distribution function	Geophysical term
BPDF	Bidirectional polarisation distribution function	Geophysical term
CALIOP	Cloud-Aerosol Lidar with Orthogonal Polarisation	Instrument
CALIPSO	Cloud-Aerosol Lidar and Infrared Pathfinder Satellite Observation	Satellite mission
CAPI	Cloud and Aerosol Polarimetry Imager	Instrument
CATS	Cloud/Aerosol Transport System	Instrument
CCN	Cloud condensation nuclei	Geophysical term
CDOM	Coloured (or chromophoric) dissolved organic matter	Geophysical term
CER	Cloud droplet effective radius	Geophysical term
CFOSAT	China-France Oceanography Satellite	Satellite mission
Chl-*a*	Chlorophyll-*a*	Chemical
CLAW	Charlson, Lovelock, Andreae, and Warren (hypothesis)	Geophysical term
CNES	Centre National d'Études Spatiales	Organisation
COD	Cloud optical depth	Geophysical term
COMS	Communication, Ocean and Meteorological Satellite (hosting GOCI)	Satellite mission
CPR	Cloud profiling radar	Instrument
DMS	Dimethylsulphide	Chemical
DMSP	Dimethylsulphoniopropionate	Chemical
EarthCARE	Earth Clouds, Aerosols and Radiation Explorer	Satellite mission
ESA	European Space Agency	Organisation
EUMETSAT	European Organisation for the Exploitation of Meteorological Satellites	Organisation
FAP	Functional assemblage of particles	Geophysical term
GMI	GPM Microwave Imager	Instrument
GOCI	Geostationary Ocean Colour Imager	Instrument
GOES	Geostationary Operational Environmental Satellite	Satellite mission
GPM	Global Precipitation Measurement	Satellite mission
GRASP	Generalised Retrieval of Aerosol and Surface Properties	Algorithm
HARP	Hyper-Angular Rainbow Polarimeter	Instrument
HSRL	High spectral resolution lidar	Instrument type
IASI	Infrared Atmospheric Sounding Interferometer	Instrument
ICARE	Cloud-Aerosol-Water-Radiation Interactions	Data server
IOCCG	International Ocean Colour Coordinating Group	Organisation
JAXA	Japan Aerospace Exploration Agency	Organisation
LIDAR	Light detection and ranging	Instrument type
MAN	Maritime Aerosol Network	Observation network
MBL	Marine boundary layer	Geophysical term
MERIS	Medium Resolution Imaging Spectrometer	Instrument
MetOP	Meteorological OPerational	Satellite mission

(Contd.)

Abbreviation or acronym	Definition	Type
MISR	Multiangle Imaging Spectroradiometer	Instrument
MODIS	Moderate Resolution Imaging Spectroradiometer	Instrument
MSI	MultiSpectral Instrument	Instrument
MSG	Meteosat Second Generation	Satellite mission
MUR	Multiscale Ultra-high Resolution	Data set
NASA	National Aeronautics and Space Administration	Organisation
NIR	Near-infrared	Geophysical term
NRCS	Normalised radar cross section	Geophysical term
OLCI	Ocean and Land Colour Instrument	Instrument
OLI	Operational Land Imager	Instrument
OLS	Operational Linescan System	Instrument
OPAC	Optical Properties of Aerosols and Clouds	Database
PACE	Plankton, Aerosols, Clouds, and ocean Ecosystems	Satellite mission
PAR	Photosynthetically available radiation	Geophysical term
PARASOL	Polarisation and Anisotropy of Reflectances for Atmospheric Sciences coupled with Observations from a Lidar	Satellite mission
PFT	Phytoplankton functional types	Geophysical term
POC	Particulate organic carbon	Geophysical term
POLAC	Polarised Atmospheric Correction	Algorithm
POLDER	Polarisation and Directionality of the Earth's Reflectance	Instrument
QuikSCAT	Quick Scatterometer	Satellite mission
RADARSAT	Radar satellite	Satellite mission
RGB	Red-green-blue	Image term
RSP	Research Scanning Polarimeter	Instrument
SAR	Synthetic Aperture Radar	Instrument type
SARAL-AltiKa	French-Indian Oceanography Mission	Satellite mission
SGLI	Second Generation Global Imager	Instrument
SeaWiFS	Sea-viewing Wide Field-of-view Sensor	Instrument
SEM	Small eddy model	Model
SEVIRI	Spinning Enhanced Visible and Infrared Imager	Instrument
SLSTR	Sea and Land Surface Temperature Radiometer	Instrument
SMAP	Soil Moisture Active/Passive	Satellite mission
SMOS	Soil Moisture Ocean Salinity	Satellite mission
SNAP	Sentinel Application Platform	Software
SOLAS	Surface Ocean-Lower Atmosphere Study	Project
SPEX	Spectropolarimeter for Planetary Exploration	Instrument
SSA	Single scattering albedo	Geophysical term
SSM/I	Special Sensor Microwave/Imager	Instrument
SSS	Sea surface salinity	Geophysical term
SST	Sea surface temperature	Geophysical term
SRAL	SAR radar altimeter	Instrument
SWIR	Shortwave infrared	Geophysical term
TMI	TRMM Microwave Imager	Instrument
TRMM	Tropical Rainfall Measuring Mission	Satellite mission
TIRS	Thermal Infrared Sensor	Instrument
UV	Ultraviolet (radiation)	Geophysical term
VIIRS	Visible Infrared Imaging Radiometer Suite	Instrument
VIS	Visible (radiation)	Geophysical term
Windsat	Windsat Polarimetric Radiometer	Instrument

More recently, attention has spread to a wider range of biogenic secondary aerosol precursor gases including amines and a variety of hydrocarbons (Simó, 2011; Carpenter et al., 2012; Mungall et al., 2017) as well as oxidant precursors such as the halocarbons (von Glasow and Crutzen, 2004; Saiz-Lopez et al., 2007). While sulphuric acid derived from the oxidation of atmospheric DMS is an important driver of nucleation, other substances such as ammonia, amines, hydrocarbons and ions also appear to play a critical role and are progressively being incorporated into atmospheric chemistry and nucleation models. Through different mechanisms, these compounds can stabilise sulphuric acid nanoclusters and thus enhance nucleation rates (Kulmala et al., 2013; Lehtipalo et al., 2016); they can also promote the growth of newly formed particles to sizes large enough to act as CCN (Willis et al., 2016; Collins et al., 2017; Dall'Osto et al., 2017). Despite rapid progress, several unknowns remain regarding sources and sinks of secondary aerosol precursors in the marine troposphere: for example, the biogeochemical production pathways of gaseous aerosol precursors, the magnitude and the sign of their net sea-air fluxes (Simó, 2011; Carpenter et al., 2012a), the prevalence of MBL nucleation compared to aerosol entrainment from the free troposphere (Burkart et al., 2017; Dall'Osto et al., 2017; Quinn et al., 2017), and the compounds driving aerosol growth (Willis et al., 2016; Dall'Osto et al., 2017; Mungall et al., 2017).

The effects of biological activity on primary marine aerosols have also received considerable attention, with several studies indicating that organic compounds emitted directly as particulates into the atmosphere might represent a sizable biogenic contribution to CCN (O'Dowd et al., 2004; Sellegri et al., 2006; Keene et al., 2007) and ice nuclei (Wilson et al., 2015). Primary aerosols are produced mainly through bubble bursting, which ejects into the atmosphere hydrophobic organic substances (surfactants) that are enriched in the sea surface microlayer, in bubble films, and in foams. Experimental bubbling studies have established that primary aerosol production rates, size distributions, and organic enrichments depend on bubble formation rates, size, and lifetime, which interact in complex ways with the physicochemical properties of seawater, such as surfactant concentration and temperature (Sellegri et al., 2006; Keene et al., 2007). Whereas a first-order relationship between wind-generated wave breaking and primary aerosol emission is expected, the relationship between phytoplankton bloom dynamics, the composition of sea-spray aerosols and their CCN-forming activity remains highly controversial.

For example, O'Dowd et al. (2015) showed that the composition of sea spray aerosols in the clean subpolar marine air over the Northeast Atlantic Ocean exhibits strong seasonal variability, with maximum organic enrichment during demise of the phytoplankton bloom. This enrichment was attributed to the massive release of fresh organic matter caused by viral lysis, bacterial activity and grazing processes in the surface ocean. On the other hand, Quinn et al. (2014) did not observe changes in CCN-forming activity of sea spray aerosol as a function of phytoplankton productivity, and attributed the organic matter enrichment of nascent aerosols to the large reservoir of aged organic carbon constantly found in surface seawater (see also Kieber et al., 2016). Collins et al. (2016), who analysed the CCN activity of sea spray derived from laboratory phytoplankton blooms, also failed to observe significant changes across a wide range of bloom stages with different abundances of phytoplankton, bacteria and viruses. Indeed, attempts to synthesize these opposing views using measurements (Ceburnis et al., 2016) or modelling (Burrows et al., 2014) need to invoke two or more organic matter pools with different composition and turnover times.

The contribution of sea spray aerosols to the CCN population was recently quantified by Quinn et al. (2017). By reanalysing a large historical dataset, they estimated that primary aerosols contribute less than 30% of the CCN over most of the global ocean, with higher values found only in the windy Southern Ocean. As their estimates combine primary organic and sea-salt aerosol, they set an upper bound for the biogenic (primary organic) contribution.

Biogenic effects on the properties of primary and secondary marine aerosols are expected to correlate with phytoplankton biomass because phytoplankton are the base of the oceanic food web and the production of organic matter. Consequently, remote sensing studies aimed at relating aerosol properties and biological activity commonly use satellite-retrieved chlorophyll-*a* concentration (Chl-*a*) at the sea surface as an indirect proxy for biogenic aerosol precursors. Here we distinguish between three groups of studies depending on the strategies used and the spatiotemporal scales addressed.

The first group includes regional-scale studies attempting to infer the source regions and atmospheric processing of aerosols measured in situ at coastal stations or on oceanographic cruises ("top-down" approach). These studies typically combine air mass back-trajectories derived from meteorological reanalysis with satellite-retrieved variables such as Chl-*a* concentration (Arnold et al., 2010; Park et al., 2013) and/or other derived quantities such as net primary production (O'Dowd et al., 2015; Becagli et al., 2016) or total DMSP concentration (Heintzenberg et al., 2017).

The second group of studies aims to predict sea surface concentrations of aerosol precursors from remote sensing data to subsequently estimate regional or global gas emission fluxes, which can be used as input to chemical transport and Earth system models ("bottom-up" approach). These approaches generally combine Chl-*a* concentration with geophysical variables (mixed layer depth, irradiance, sea surface temperature) and, less commonly, with estimates of phytoplankton functional types or size classes. Such empirical approaches have been proposed to estimate sea surface concentrations of DMS (see intercomparisons in Tesdal et al., 2016; Galí et al., 2018), its algal precursor DMSP (Galí et al., 2015), and hydrocarbons such as isoprene (Arnold et al., 2009; Ooki et al., 2015).

The third group includes studies that exploit simultaneous satellite observations of the surface ocean biota and the lower troposphere, including aerosols and cloud microphysics. With this approach, Vallina et al. (2006) and Meskhidze and Nenes (2006) revealed that CCN and CER correlated positively and negatively, respectively, with

Chl-*a* over the pristine Southern Ocean, postulating that this pattern is controlled by gaseous aerosol precursors. With the increasing awareness of the climatic role played by primary marine aerosols (Quinn and Bates, 2011), recent studies have tried to untangle the contribution of DMS, other secondary aerosol precursors, primary organic aerosols, and sea salt to cloud microphysical properties over the seasonal cycle (Lana et al., 2012; McCoy et al., 2015).

The outcomes of these different approaches can be summarized in two main points. First, that studying ocean-aerosol interactions with remote sensing data remains challenging. Large uncertainties arise from the use of empirical models and indirect proxy variables (e.g., Chl-*a*, coloured dissolved organic matter, CDOM) to estimate marine emissions, and are intertwined with atmospheric transport. Second, that despite large uncertainties, biogenic aerosol sources, CCN numbers and CER show robust relationships in pristine oceanic regions. For example, CCN (CER) over the Southern Ocean is maximal (minimal) during the productive summer season, when wind-driven sea-salt aerosol is at its minimum. Overall, these findings lend credit to hypothesized plankton-climate feedbacks (Charlson et al., 1987), though through complex and unforeseen mechanisms (Quinn and Bates, 2011).

How and to what extent upper-ocean biological activity affects the properties of MBL aerosols remains a subject of ongoing research and debate. There is currently no consensus on the effect of marine phytoplankton and organic matter on the number, size, and composition of aerosols in the MBL. By allowing long-term synoptic observations of ocean and atmosphere, satellite remote sensing provides a powerful tool for addressing this question, and for quantifying the linkage between biological activity in the ocean and properties of MBL aerosols. In what follows, we discuss how current and planned satellite missions of ocean colour, lidar, polarimetry, and other ocean and atmosphere sensing technologies may help advance studies on the coupling between the characteristics of surface ocean biology and the composition and radiative properties of the MBL.

2.2 Remote sensing of upper-ocean biology

2.2.1 Ocean colour radiometry

Studies linking ocean biology to clouds have used satellite observations of ocean colour primarily to derive proxies for phytoplankton biomass (concentration of the phytoplankton pigment Chl-*a* or phytoplankton carbon concentration). However, since the early 2000's the available ocean colour satellite products have boomed (**Table 2**) and now, for example, include indicators of phytoplankton functional groups (IOCCG, 2014; Bracher et al., 2017), phytoplankton size classes (Ciotti and Bricaud, 2006), and particle size distribution (Kostadinov et al., 2016), as well as phytoplankton carbon (Martinez-Vicente et al., 2013; Graff et al., 2015). Many of these new approaches, however, have not been appropriately validated on the scale

Table 2: Characteristics of upper-ocean biology that can be derived from current multispectral and planned hyperspectral ocean colour remote sensing missions. DOI: https://doi.org/10.1525/elementa.331.t2

Upper-ocean biology characteristic	Current multispectral ocean colour satellite radiometers	Future hyperspectral ocean colour satellite radiometers
Phytoplankton biomass	Concentration of Chl-*a* (non-calcifying phytoplankton) and calcite (coccolithophores); phytoplankton carbon concentration	Contributions of phytoplankton functional types (PFT) or size classes to total phytoplankton biomass; better separation of Chl-*a* from interference by CDOM
Phytoplankton composition and succession	Differentiation among limited number of broad phytoplankton groups (coccolithophores, diatoms, cyanobacteria)	Differentiation among larger number of PFT and phytoplankton size classes
Phytoplankton bloom phenology and bloom state	Bloom onset, peak date, decline, and duration from time series of phytoplankton abundance at daily resolution	PFT-specific bloom onset, peak date, decline, and duration from time series of phytoplankton abundance at daily resolution, concentration of Chl-a breakdown product (phaeophytin), properties of detrital material
Organic carbon pool	Concentrations of particulate organic carbon (POC), and absorption coefficients of CDOM and non-algal particles	Concentration and PFT-specific nature of POC, and CDOM concentration and composition
Particle size distribution	Slope of particle size distribution from light backscattering coefficient	Slope of particle size distribution from light backscattering coefficient with better accuracy
Bacterial biomass	Directly: Cyanobacteria; indirectly: using SST, CDOM, PAR, and Chl-*a*	Potential to differentiate microbes with specific spectral absorption signatures
Phytoplankton (photo) physiology	Ratio of Chl-*a* to phytoplankton carbon at given growth irradiance, nutrient limitation diagnosed from solar-stimulated fluorescence yields	Concentration of Chl-*a* breakdown products (phaeophytin, phaeophorbide), improved estimation of Chl-*a* to phytoplankton carbon
Ecological regime or structure	Limited differentiation among functional assemblages of suspended particles (FAP)	Differentiation among FAP

for which their products are being produced (e.g., daily and global); such validation of these new ocean colour satellite products is needed urgently. The capability to resolve phytoplankton functional groups, size classes or even particular species from space would significantly advance ocean-atmosphere interaction research because the production of aerosol precursors depends on the taxonomic composition of the phytoplankton assemblage (e.g., Le Quéré et al., 2005).

New and exciting possibilities are expected from planned ocean colour satellite missions with improved spectral resolution (**Table 2**) from multispectral to hyperspectral sensors, which are planned for launch in the next decade by various space agencies, including NASA's PACE. To date, optical differentiation among only a few phytoplankton functional types (PFT) in open ocean waters has been achieved using multispectral ocean colour data and with limited accuracy (Alvain et al., 2005; Bricaud et al., 2012). It is expected that hyperspectral ocean colour satellite sensors will substantially improve PFT identification (IOCCG, 2014; Bracher et al., 2017) and may even allow identification of individual species or genera such as *Phaeocystis spp.* (Lubac et al., 2008), an important DMS producer.

Inverse optical models allow us to extract the spectral light absorption and backscattering coefficients of seawater from ocean colour satellite radiance measurements (Lee et al., 2002; Maritorena et al., 2002; IOCCG, 2006). The shape of the phytoplankton absorption spectrum is controlled primarily by the concentration of various phytoplankton pigments, which may provide information on community structure (Morel and Bricaud, 1981; Bricaud et al., 2004; Ciotti and Bricaud, 2006). Physiological aspects of phytoplankton have been diagnosed with measurements of chlorophyll fluorescence from space (Behrenfeld et al., 2009). In addition, certain pigments like pheophorbide *a* and pheophytin *a* have been shown to be the main degradation products of Chl-*a* during phytoplankton senescence (Spooner et al., 1994) and grazing (see citations in Carpenter et al., 1986) and may provide, under certain conditions, a means to detect grazing optically. Thus, future hyperspectral space missions will be providing spectral information that may enable retrieval of information on taxonomic composition, PFT, and phytoplankton physiology and degradation.

Even though phytoplankton is an important determinant of optical variability in the open ocean and the primary source of organic material, other seawater constituents such as CDOM and non-algal particulate matter (detritus, bacteria, and viruses) also contribute to optical variability and represent essential components of the marine food web that may be of interest to studies of ocean biology-atmosphere interactions. The spectral shape of light absorption by non-algal particles is commonly modelled as an exponentially decreasing function of wavelength, and its slope is thought to depend on the composition of the non-algal matter (Babin and Stramski, 2002; Estapa et al., 2012). The same is true for CDOM (Carder et al., 1989). Simplifying assumptions on the spectral shape of CDOM and detrital matter absorption, on one hand, and phytoplankton absorption, on the other, enabled the development of inversion models that can partition absorption into its main algal and non-algal components. Semi- and quasi-analytical approaches pioneered by several groups (Roesler and Perry, 1995; Garver and Siegel, 1997; Lee et al., 2002; Maritorena et al., 2002) continue to be improved (Werdell et al., 2013; Zheng and Stramski, 2013; see review by Werdell et al., 2018). Separating absorption by CDOM from absorption by non-algal particles is, however, challenging (Siegel et al., 2005). Some recent works have presented potential approaches to separate these terms and even estimate the pool of bulk dissolved organic carbon (DOC) from CDOM in coastal regions (Matsuoka et al., 2013; Loisel et al., 2014), but such efforts remain challenging in the open ocean.

Future ocean colour missions, such as the hyperspectral PACE mission, will extend into UV wavelengths, which is expected to improve retrieval of CDOM (separately from non-algal particles) and its spectral slope from ocean colour reflectance. This improvement will facilitate the retrieval of DOC concentrations (Vantrepotte et al., 2015) and perhaps a rough estimation of bulk organic chemical properties. Because CDOM accumulates in surface waters throughout the growth season, it may be a good indicator of phytoplankton bloom state in waters outside the influence of rivers or upwelling. Being able to link temporal changes in CDOM with changes in DOC concentration would be useful, but important sources of uncertainty must be overcome: the absolute value of CDOM is generally not well correlated with DOC concentration in the open ocean (Nelson and Siegel, 2013), except in the Arctic Ocean (Matsuoka et al., 2017); and CDOM also reflects seasonal photo-bleaching (Vodacek et al., 1997) and vertical and horizontal mixing and deep water upwelling (Nelson and Siegel, 2013). Thus, further work is needed to link CDOM optical signatures to its sources and chemical properties.

The coefficient for light backscattering by particles, which is simultaneously derived with light absorption from ocean colour semi-analytical models, can be used to estimate particle concentration (Neukermans, Loisel, et al., 2012b) and phytoplankton carbon concentration (Martinez-Vicente et al., 2013; Graff et al., 2015). The wavelength dependency of light backscattering by particles, which can also be obtained from ocean colour remote sensing (Loisel et al., 2006), is commonly modelled as a power law function (Gordon and Morel 1983), which, according to Mie scattering theory, steepens with increasing slope of the particle size distribution (Gordon and Morel, 1983; Kostadinov et al., 2009). Some field and laboratory observations have provided general support for a relationship between the spectral shape of light backscattering by particles and their size distribution (Loisel et al., 2006; Stramski et al., 2008; Slade and Boss, 2015), whereas no observational support was obtained in other field studies (Reynolds et al., 2016). These discrepancies between optical theory and observations likely arise from the neglect of absorption effects on scattering and from the traditional use of Mie scattering theory which assumes sphericity and homogeneity of the in-water

particles. This problem is particularly relevant for light scattering in the back direction (e.g., Harmel et al., 2016). Scientific advances in optical modelling and experimental understanding of the backscattering properties of in-water particles are needed to establish such relationships. For example, recent studies (Zhai et al., 2013; Fournier and Neukermans, 2017; Neukermans and Fournier, 2018) provided an analytical model for light backscattering from populations of *Emiliania huxleyi*, the most ubiquitous species of coccolithophores (calcifying phytoplankton).

New connections between hyperspectral optical properties of marine particles and biogeochemistry are emerging. Neukermans et al. (2016) demonstrated the feasibility of identifying functional assemblages of particles (FAP), a concept which accounts for the coexistence of algal and non-algal particles, from hyperspectral optical properties. This concept goes beyond PFT by including non-algal material (e.g., detritus), which also contributes to optical variability and represents an essential component of marine ecosystem and biogeochemical models (Fasham et al., 1990; Dunne et al., 2005). For example, waters characterized by the same PFT but with increasing contributions of detrital material may reflect progressive stages of a phytoplankton bloom (Neukermans et al., 2014). FAP detection from hyperspectral sensors is thus expected to provide detailed information on the ecological condition of ocean waters, which may impact the oceanic source of primary and secondary aerosols (e.g., O'Dowd et al., 2015).

Some marine bacteria, such as the photosynthesizing cyanobacterium *Trichodesmium*, have unique optical properties that enable their detection from ocean colour satellite remote sensing, as reviewed by McKinna (2015). Other (non-photosynthesizing) bacteria, such as *Vibrio harveyi*, are bioluminescent and can cause nocturnal "milky seas", where the surface of the sea produces an intense, uniform, sustained glow at night. Miller et al. (2005) showed that this phenomenon was observable from space under lunar illumination conditions with the highly sensitive OLS of the US Defense Meteorological Satellite Program, suggesting a promising avenue to detect milky seas and other bioluminescent organisms from space. The OLS, however, stopped operating in 1996, and, to the best of our knowledge, no such highly sensitive sensors are currently operational nor planned by the various space agencies. The VIIRS on board the Joint Polar Satellite System has a day-night band with a dynamic sensitivity range that may enable such applications, but its suitability for detecting bacterial bioluminescence remains to be investigated. Indirect approaches to estimate bacterial activity using remote sensing data are reviewed by Grimes et al. (2014).

Other technological advances in radiometric ocean colour remote sensing, besides increased spectral resolution, include increased acquisition frequency and spatial resolution. Indeed, the first ocean colour satellite in geostationary orbit, the Korean GOCI (Kim et al., 2012), was launched in 2010 and provides hourly imagery for the Yellow Sea, a significant improvement from the daily imagery typically available from polar-orbiting ocean colour sensors. Such improved temporal resolution increases data availability in cloudy regions and, in cloud-free conditions, allows the study of processes with sub-diurnal variability, such as vertical migration or photo-acclimation (O'Malley et al., 2014), or tidal variability of suspended sediments, turbidity and light attenuation in coastal waters (Choi et al., 2012; Neukermans et al., 2012a; Ruddick et al., 2012). Ocean colour sensors with improved spatial resolution on the order of < 100 m could also enable studies of ocean-atmosphere interactions at finer scales, such as in mesoscale eddies and thin foams produced by phytoplanktonic DMS producers (see **Figure 2** for an example of a *Phaeocystis globosa* bloom observed by the sun-synchronous Sentinel 2A-MSI). Such improvements in spatial and temporal resolution may help to better match the exact location, timing, and strength of phytoplankton blooms, which can improve the correlation between the presence of oceanic phytoplankton and cloud properties, as previously suggested by McCoy et al. (2015).

2.2.2 Polarimetric remote sensing

Polarimeter instruments measure the polarization of light (i.e., the wave properties of electromagnetic radiation) in addition to the intensity of light (i.e., the energy of electromagnetic radiation) measured by photometer instruments. Compared to light intensity, light polarization is more sensitive to variations in the scattering angle caused

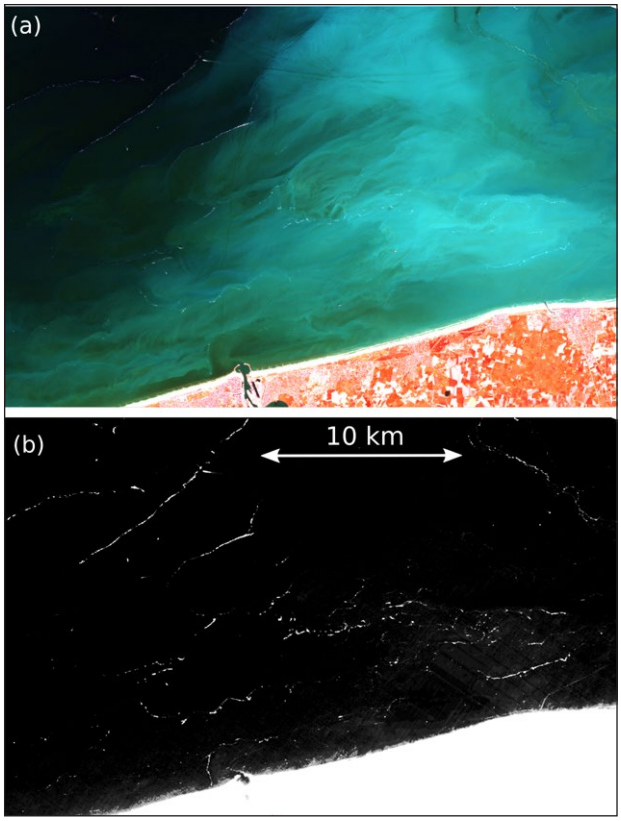

Figure 2: Fine-scale features of a coastal phytoplankton bloom. (a) Sentinel 2A/MSI RGB composite of the Belgian coastal zone on 1 May 2016 (10:53UTC) indicating fine-scale features in ocean colour satellite imagery, such as foam produced by *Phaeocystis globosa*, and **(b)** near infrared image of the same scene. Satellite image suggested by Q. Vanhellemont. DOI: https://doi.org/10.1525/elementa.331.f2

by particles, and less affected by multiple scattering events. Thus, polarization is more sensitive to, and easier to correlate with, particle microphysics (i.e., size, shape, and composition). Nevertheless, existing satellite polarimeters rarely have been used to retrieve information about particles suspended in oceans (with the exception of few studies: Loisel et al., 2008; Harmel, 2016), largely because the satellite instruments providing these observations, i.e., POLDER, were designed to characterize the radiative properties of clouds and aerosols but not the ones of the ocean (Deschamps et al., 1994). Consequently, pixel sizes are rather large (≥6 km), the number of polarised wavelength bands (443/490 nm, 670 nm and 865 nm) is limited, and the radiometric dynamic range is not optimally suited for ocean colour retrievals. Nevertheless, Loisel et al. (2008) provided a proof-of-concept study for the retrieval of suspended particle composition from POLDER data in highly scattering waters where the polarised light signal was sufficiently strong. Furthermore, theoretical computations (Chowdhary et al., 2006; Chami and McKee, 2007; Chami and Platel, 2007), laboratory measurements (Voss and Fry, 1984; Quinby-Hunt et al., 1989), and field measurements (Tonizzo et al., 2011; Ibrahim et al., 2016) show that the polarisation of the in-water light field is sensitive to the shape, size, and composition of suspended marine particles. On the other hand, the polarimetric and multidirectional characteristics of the third POLDER sensor on-board the PARASOL satellite were shown to significantly improve the accuracy of the atmospheric correction process (Harmel and Chami, 2008, 2011) and to be a practical means to correct for sun-glint contamination (Harmel and Chami, 2013). Other proposed ocean applications of POLDER data involve using one of the polarisation components measured by POLDER to limit the sun-glint contamination (He et al., 2015) and to increase the ocean signal contribution to space-borne observations (Liu et al., 2017).

2.2.3 Lidar remote sensing

While aircraft-based lidars have provided relevant ocean measurements for decades (see Churnside et al., 2013, Hostetler et al., 2018, and references therein), the power of satellite lidar for ocean biology measurements has been demonstrated only recently (Behrenfeld et al., 2013, 2017; Churnside et al., 2013; Lu et al., 2014). These studies involved analysis of data from the CALIOP instrument on the CALIPSO platform (**Table 1**; Winker et al., 2009). Although CALIOP was designed for atmospheric measurements of clouds and aerosols, its 532-nm channels are also sensitive to ocean backscatter. The relatively coarse vertical resolution of CALIOP (30 m in the atmosphere and 23 m in the ocean) and poor detector transient response make vertically resolved ocean retrievals challenging. However, significant scientific impacts have been realized using vertically integrated CALIOP subsurface ocean data. Behrenfeld et al. (2013) used CALIOP data to retrieve particulate backscattering coefficient (b_{bp}) for the global oceans and, employing published relationships based on b_{bp}, estimated particulate organic carbon (POC) and phytoplankton biomass (**Figure 3**).

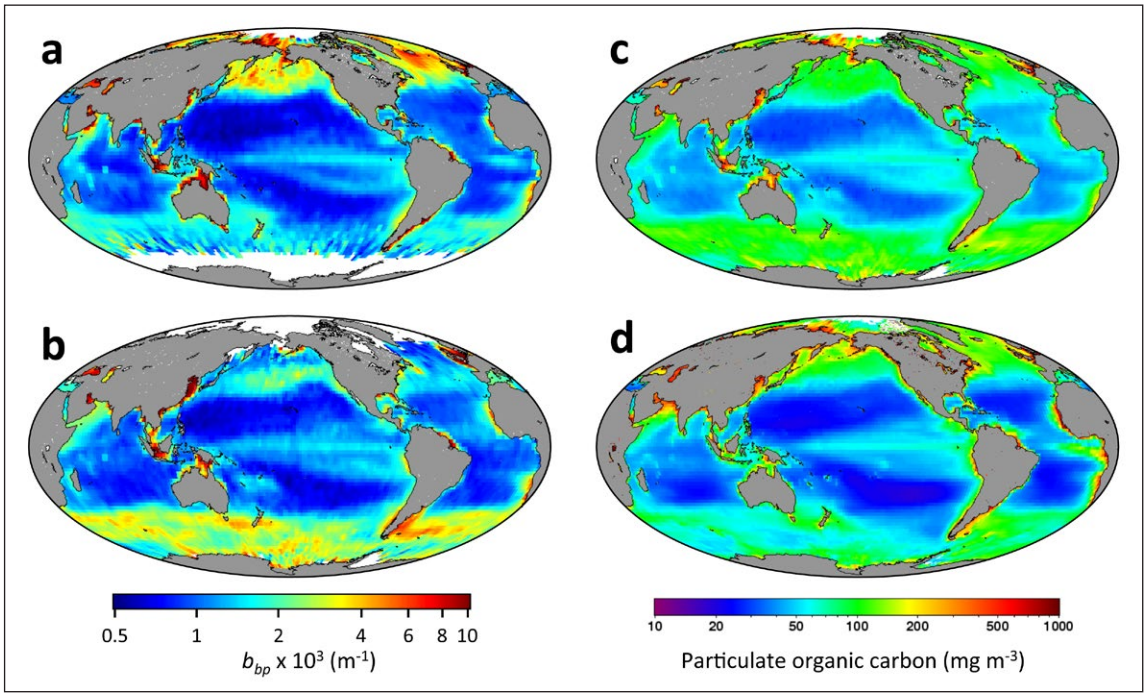

Figure 3: Retrieval of sea surface particulate backscatter coefficient and particulate organic carbon with satellite-borne lidar. Left: seasonal average b_{bp} retrieved from CALIOP space-borne lidar data for June–August **(a)** and December–February **(b)**. Note that the lidar provides measurements for wintertime high-latitude regions that are beyond the capability of satellite ocean colour due to low sun angles. Right: Annual average POC estimated from CALIOP b_{bp} **(c)**, which shows good agreement with MODIS POC retrieved using a wave band algorithm **(d)**. Data in each panel are from the 2006–2012 period and have been averaged to 2°latitude × 2°longitude pixels. Figures from Behrenfeld et al. (2013). DOI: https://doi.org/10.1525/elementa.331.f3

CALIOP data are particularly valuable in the polar oceans where the ocean colour record is incomplete from the late fall through the winter due to low sun angles. Supplying its own light source, CALIOP has provided an uninterrupted record of plankton stocks for the ice-free portions of the polar oceans. Behrenfeld et al. (2017) used a decade of monthly-resolved CALIOP data to demonstrate fundamental processes governing the balance between phytoplankton division and loss rates, thereby advancing a new and evolving understanding of plankton blooms (Behrenfeld, 2010; Behrenfeld and Boss, 2018). An additional finding was that interannual anomalies in northern and southern polar-zone plankton stocks were of similar magnitude but driven by different processes. Specifically, ecological factors dominated interannual changes in the northern polar zone, while variations in plankton stocks of the southern polar zone predominately reflected changes in ice-free area.

While the atmosphere-focused CALIOP instrument provides scientifically valuable ocean data products, it has exceeded its 3-year design lifetime by over 9 years. Significant advances in science capability are envisioned for a follow-on satellite lidar optimised for ocean as well as atmospheric measurements (Hostetler et al., 2018). One major advance would be to have higher vertical resolution. Lidar signals attenuate rapidly with depth, for instance, by a factor of 400 at three optical depths, beyond which the lidar signal is generally not useable due to low signal-to-noise. At CALIOP's 532-nm wavelength, this three-optical-depth limit corresponds to about 50 m in geometric depth in the clearest waters and much less in more turbid waters, which leaves only one or two useable points in the 23-m resolution CALIOP profile. In future space-borne lidars, vertical resolutions of less than 3 m are easily achievable, and would enable true profiling of vertical structure in backscatter to three optical depths. Such profiling would represent a significant advantage over passive radiometric measurements, for which the measured signals are weighted exponentially toward the ocean surface (with 92% of the signal coming from the first optical depth). Vertically resolved lidar data of phytoplankton biomass, for instance, will reduce errors in estimates of net primary productivity that result from using surface-weighted retrievals to represent ocean properties at greater depths (Platt and Sathyendranath, 1988; Zhai et al., 2012; Hill et al., 2013; Schulien et al., 2017).

Further major advances are expected from a high-spectral-resolution-lidar (HSRL) instrument, summarized in **Table 3**. The standard elastic backscatter lidar technique used for CALIOP data requires assumptions on the change of attenuation with depth and to single out the backscatter from particles from the backscatter of seawater molecules. These assumptions can introduce large errors. By adding one or more channels in the receiver to resolve the optical signal spectrally, the HSRL technique enables independent and accurate retrieval of particulate backscatter and attenuation coefficients. The HSRL technique has been used for decades for aerosol measurements (Shipley et al., 1983; Piironen and Eloranta, 1994; Esselborn et al., 2008; Hair et al., 2008), and more recently to retrieve ocean particulate backscatter and the diffuse attenuation coefficient (Hair et al., 2016; Schulien et al., 2017). **Figure 4** shows coincident atmosphere and ocean measurements made at 532 nm with an airborne HSRL. A future space-borne 532-nm HSRL with high-vertical-resolution capability would enable vertically resolved estimates of phytoplankton biomass, POC, and net primary productivity. Adding HSRL capability at 355 nm in addition to that at 532 would allow independent estimates of algal and CDOM absorption and information on the slope of the particle size distribution.

A further promising direction for application of space-borne lidar is the retrieval of the fluorescence signature of Chl-*a* and CDOM, which would allow studies of

Table 3: Characteristics of upper-ocean biology that can be derived from current and potential future satellite lidar missions. DOI: https://doi.org/10.1525/elementa.331.t3

Upper-ocean biology characteristic	Current satellite lidar: CALIOP on CALIPSO	Future satellite lidar: ocean-optimised
Phytoplankton biomass	Surface-weighted values consistent with weighting of passive ocean colour estimates	Vertically resolved profiles to ~ three optical depths; separate estimates of pigment absorption and CDOM (with addition of 355-nm measurements)
Phytoplankton composition and succession	Not available	Potential for crude PFT discrimination from depolarisation and wavelength dependence of backscatter
Phytoplankton bloom phenology and bloom state	Biomass retrieval under conditions impossible for ocean colour: high-latitude winter, night, through aerosol and optically thin clouds, between clouds in broken cloud systems, and in the proximity of ice; ~ monthly resolution	Same plus vertically resolved profile of phytoplankton abundance to ~ three optical depths
Organic carbon pool	Surface-weighted estimates of POC	Vertically resolved estimates of POC and CDOM.
Particle size distribution	Not available	Slope of particle size distribution from particle backscatter at two wavelengths
Phytoplankton physiology	Not available	Nutrient and radiative stress from day-night comparisons of Chl-*a* fluorescence

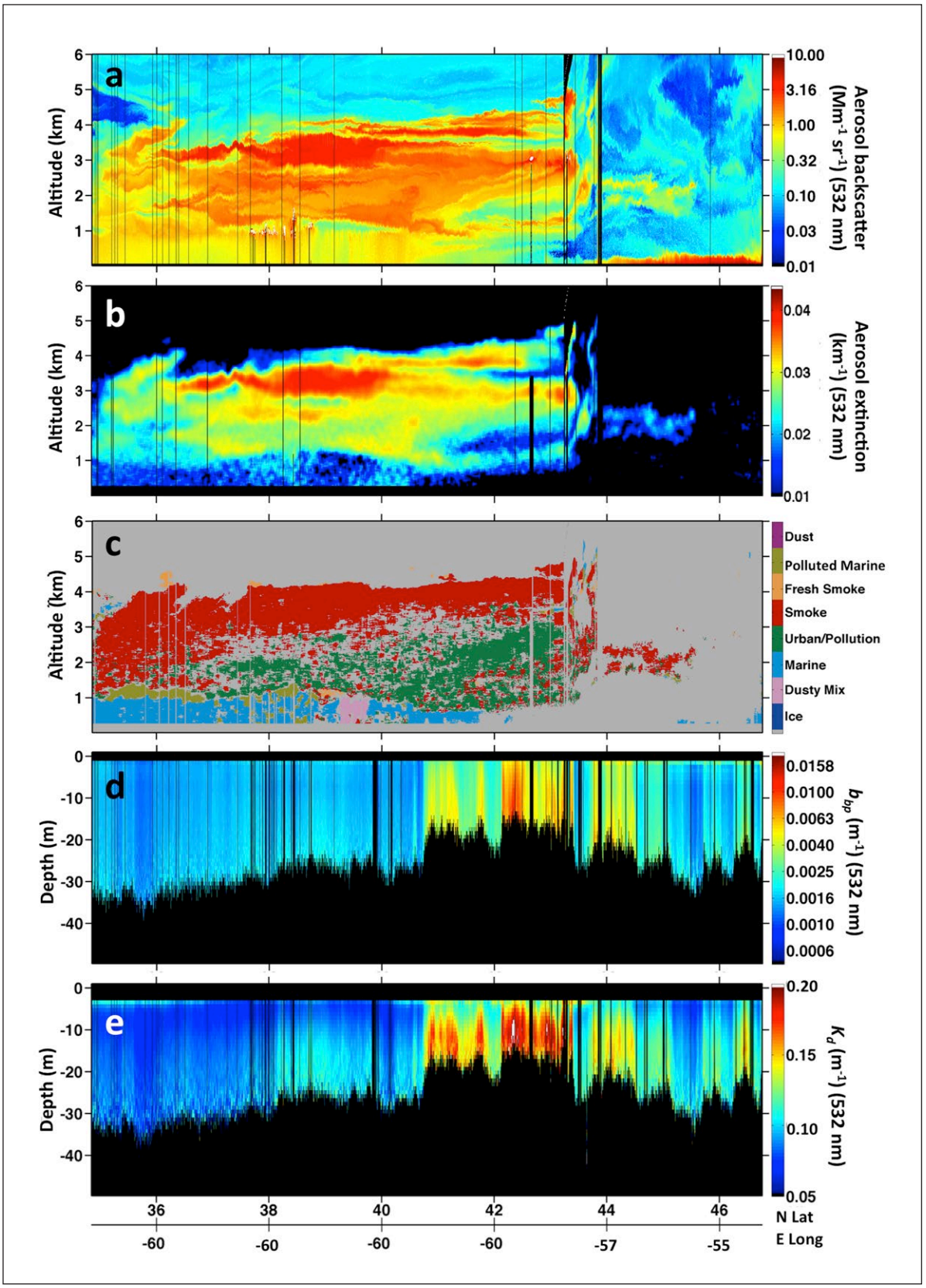

Figure 4: Aerosol and ocean parameters retrieved from NASA airborne high-spectral-resolution-lidar (HSRL-1), highlighting vertical and horizontal variability. Data acquired on the North Atlantic Aerosol and Marine Ecosystems Study off the East Coast of North America in May 2016. In the atmosphere, the HSRL technique enables independent retrieval of aerosol backscatter **(a)** and extinction **(b)**, and the ability to infer aerosol type **(c)**. In the ocean, the technique enables independent retrieval of particulate backscatter **(d)** and diffuse attenuation coefficients **(e)** regardless of aerosol conditions, including, in this case, an optically thick layer of smoke from forest fires in Canada, as indicated in the aerosol backscatter and extinction coefficients (a and b) and aerosol type mask (c). DOI: https://doi.org/10.1525/elementa.331.f4

phytoplankton physiology and a better separation of the different pools of organic carbon in the upper ocean. Laser-excited fluorescence of both Chl-*a* and dissolved organic matter have already been shown to be measurable by airborne lidar instruments in both coastal and open-sea waters (Hoge et al., 1993).

Overall, lidar is a natural complement to passive radiometric remote sensing. While lidar lacks the swath, it has many sampling advantages over passive remote sensing techniques. Lidar can provide measurements at any solar angle (even at night), enabling sensing during all seasons at high latitudes, which are very challenging with passive radiometric remote sensing due to cloudiness and low sun elevation. An ocean-optimised HSRL can provide measurements through aerosol layers of any type (absorbing, as well as non-absorbing) and through optically thin clouds. Lidar's small footprint (e.g., 90 m for CALIOP) enables measurements in gaps between clouds, regardless of cloud shadowing or adjacency effects that can contaminate passive retrievals. As shown with CALIOP (Behrenfeld et al., 2017), these sampling advantages provide annual coverage comparable to MODIS at high latitudes, despite its small footprint. Furthermore, with the addition of high vertical resolution capability, a future lidar would enable the first global three-dimensional view of the ocean surface layer. For more detail on lidar ocean remote sensing, past, present, and future, see Hostetler et al. (2018).

2.3 Remote sensing of the lower atmosphere

2.3.1 Passive radiometric remote sensing

As noted in the Introduction, one discipline's signal is another's noise. Passive satellite instruments used for ocean colour radiance retrieval perform an 'atmospheric correction' for cloud-free pixels, to remove the atmospheric radiance from the total signal measured by the satellite sensor and obtain the spectrum of the visible (VIS) water-leaving radiance. Over clear waters, this atmospheric contribution is typically about 90% of the total signal in the VIS, due to interaction with aerosols and air molecules (Gordon, 1997). A common assumption (e.g., Gordon and Wang, 1994) is that seawater completely absorbs in the near-infrared (NIR) part of the spectrum, such that a pair of spectral bands can be used to infer information on aerosol type, aerosol optical depth (AOD), and Angström exponent (α) (Ahmad et al., 2010). This information is then used to remove the aerosol contribution from the signal in the VIS. In waters with highly scattering particles (e.g., inorganic sediments and floating algae), such as in some coastal areas, this assumption becomes invalid, and more sophisticated schemes have been developed to estimate aerosol optical properties in the VIS (Ruddick et al., 2000; Wang and Shi, 2007; Bailey et al., 2010). While AOD estimated from these approaches has been validated (e.g., Mélin et al., 2010), resulting in high-quality retrievals of ocean colour parameters on the global average, the necessity of extrapolating NIR aerosol properties to the VIS induces aerosol loading-dependent and type-dependent biases in the retrieved AOD (Kahn et al., 2016). Additionally, these algorithms are typically applied only for low- and non-absorbing AOD scenes, so that correction for thick dust or smoke plumes, for example, is more difficult and typically not performed in standard data products.

On the other hand, dedicated AOD retrieval algorithms have been developed to accurately retrieve aerosol loading (amount and type), but they make simplifying assumptions about the signal coming from the ocean. Such algorithms typically pair VIS and NIR measurements in the retrieval process, omitting shorter blue-wavelength bands where the ocean colour signal is more variable. Turbid or shallow water pixels are also often identified and removed for similar reasons. One exception is described in Limbacher and Kahn (2017), although this work was performed for the comparatively narrow MISR swath and still requires significant assumptions about ocean optics. While ocean colour retrieval algorithms are often run at full instrumental resolution to resolve small-scale ocean features, dedicated AOD algorithms are typically produced at scales of several to tens of kilometres for reasons of computational efficiency and noise reduction, and because aerosol features typically vary on longer spatial scales (Anderson et al., 2003).

Single-view sensors (i.e., sensors that view each pixel from a single angle) on polar-orbiting platforms, such as AVHRR, MERIS, MODIS, SeaWiFS, and VIIRS, have broad swaths and can provide AOD retrievals typically once per day in cloud-free conditions and away from sun glint. Regardless of sensor, most of these algorithms perform a multispectral inversion from multiple bands in the VIS and NIR spectral regions, to obtain mid-visible AOD and some weighting between different aerosol modes (Tanré et al., 1997; Ignatov et al., 2004; Sayer et al., 2012). Similar sensor types on geostationary platforms, such as SEVIRI and GOCI, have also been used for AOD retrieval from this type of algorithm as their more frequent repeat cycle increases data set coverage (De Paepe et al., 2008). Although older geostationary imagers were typically less capable than polar-orbiting imagers for aerosol retrieval, the Flexible Combined Imager (FCI) on the Meteosat Third Generation Platform (planned for launch in 2020) and the recently launched Himawari-8, COMS/GOCI, and GOES-16 have enhanced the capabilities (spectral, spatial, and radiometric) of geostationary sensors to be more comparable with multispectral ocean colour satellite instruments.

Multi-view (or multidirectional) sensors are able to acquire several optical measurements with different viewing geometries for a given ground target. Deployment of these sensors on polar-orbiting platforms, such as the (A)ATSRs (see Popp et al., 2016, for a comparison of various approaches) and MISR (Martonchik et al., 1998), can provide more information on aerosol type and are not so strongly limited by sun glint, because when one view sees glint, generally others do not (Sayer et al., 2010). However, multi-view sensors generally have narrower swaths and so view a given location on the Earth's surface only once every several days. Synergistic use of radiance measurements from several satellite platforms also results in improved characterisation of aerosol properties, for example, by combining the spectral and angular information provided by the MERIS and the AATSR sensors (Benas et al., 2013), which could also be achieved from their follow-on sensors

OLCI and SLSTR on the recently-launched Sentinel 3 platform. Coarse, elevated aerosols, such as mineral dust and volcanic ash, are optically active in the thermal infrared, and in recent years several efforts to retrieve mineral dust AOD from the IASI sensor have made progress on this front (Klüser et al., 2011; Vandenbussche et al., 2013). However, these aerosols are easier to quantify at altitude than near the surface.

For all these passive radiometric sensor types, aerosols are often modelled as mixtures of aerosol populations with lognormal distribution; aerosol 'types' are also reported in the product (giving rise to derived quantities such as spectral AOD, α, and single scattering albedo, SSA), although they are somewhat constrained by the required assumptions underlying aerosol optical models. Aerosol components are often derived from either AERONET inversions (Dubovik and King, 2000) or databases such as OPAC (Hess et al., 1998). Validation results vary depending on algorithm and sensor (e.g., Kokhanovsky et al., 2010; Petrenko and Ichoku, 2013). In recent years, the Maritime Aerosol Network (MAN) of ship-based observations (Smirnov et al., 2011) has enabled data validation not only at coastal/island AERONET sites but also in open-ocean conditions more representative of the bulk of the data. Generally, AOD can be retrieved with one-standard-deviation relative uncertainties on the order of 5–20% (with a lower limit of 0.03–0.05) and typical biases of 0.025 or smaller. Other quantities tend to be unreliable in low-AOD conditions but more quantitative for thicker aerosol plumes (e.g., α or fine-mode weighting), or harder to validate objectively (e.g., SSA or aerosol type).

The same polar-orbiting and geostationary sensors have also been used widely to retrieve cloud properties, chiefly COD, CER, and phase, as well as (for sensors with thermal bands, multi-angle views, and/or observations in the O_2 A-band) cloud height (Baum et al., 2012). Sensors observing in the microwave spectral region (TRMM, SSM/I, AMSR, GPM) also provide information on cloud liquid water path (related to COD and CER), as well as precipitation and surface quantities (Wentz, 2015). Thermal and microwave-based techniques also have the advantage in that they are able to perform retrievals at night. However, microwave approaches cannot generally be employed over or near land surfaces, a limitation for coastal studies.

A limiting characteristic of these sensor types for studies of the near-surface region is that they are typically most sensitive to cloud-top properties, rather than the lower parts of the clouds that are in closer contact with the surface and marine boundary layer. However, innovative techniques to infer information about cloud vertical structure using the available data have been developed (Rosenfeld et al., 2016). Satellite instruments designed specifically to probe CCN concentrations and cloud profiles more directly have also been proposed (Martins et al., 2011; Rosenfeld et al., 2012). **Table 4** summarizes the MBL characteristics that can be inferred remotely using passive radiometric sensors with current satellite missions and expected improvements in future missions.

2.3.2 Polarimetric remote sensing

A number of satellite polarimeters have been launched (e.g., POLDER) in order to support long-term climate change research and ecological monitoring. Others are currently being prepared (e.g., 3MI/MetOP, HARP (Martins et al., 2014), and MAIA (Liu and Diner, 2017), or planned for launch (e.g., on the NASA/PACE platform). The requirement for multi-angle, multispectral photopolarimetric measurements to achieve extended and accurate aerosol and ocean surface characterisation from space-borne instruments has long been recognized in numerical sensitivity studies (Mishchenko and Travis, 1997; Hasekamp and Landgraf, 2007; Mishchenko et al., 2007; Knobelspiesse et al., 2012). The conclusions from these numerical studies were subsequently confirmed in analyses of data obtained by airborne polarimeters, such as the RSP, the AirMSPI and the SPEX, for aerosols (Chowdhary et al., 2001; Xu et al., 2016; Stamnes et al., 2018) and cloud properties (van Diedenhoven et al., 2013; Alexandrov et al., 2016; Xu et al., 2018). Despite confirmation, the only polarimeters successfully launched in orbit were those from the POLDER series (Deuzé et al., 2001; Herman et al., 2005). The longest lasting was POLDER-3 on-board the PARASOL platform, which provided nine years of continuous global polarimetric measurements (Tanré et al., 2011).

Table 4: Radiative properties of the marine boundary layer that can be derived from current and planned satellite radiometric missions. DOI: https://doi.org/10.1525/elementa.331.t4

MBL atmospheric characteristic	Current passive satellite radiometers	Future passive satellite radiometers
Aerosol optical properties	Midvisible (primary) and spectral (secondary) aerosol optical thickness (AOD), and related quantities (e.g., Angström exponent α)	Increased retrieval accuracy of AOD and its spectral variations, better spatial coverage and resolution, single-scattering albedo (for absorbing aerosols)
Aerosol microphysical properties ('type')	Best-fitting aerosol models (based on AERONET statistics and/or databases), weighting between fine and coarse modes (i.e., fine mode fraction), single-layer column-effective parameters	More robust identification of likely microphysical properties, better spatial coverage and resolution, more aerosol models possibility to identify and separate properties of distinct aerosol layers
Cloud macrophysical properties	Cloud cover, water content, top height	Increased accuracy and resolution
Cloud microphysical/optical properties	Cloud optical depth (COD), cloud droplet effective radius (CER), particle phase	Increased accuracy and resolution
Precipitation	Rain rate, rain phase	Increased accuracy with multichannel approaches

The design of a potential future space-borne polarimetric sensor, 3MI, is largely inherited from POLDER/PARASOL missions (Marbach et al., 2013). However, important improvements include higher radiometric accuracy, extended spectral coverage, and finer spatial resolution. These improvements in 3MI data are expected to provide more advanced aerosol/cloud and surface characterisation than the POLDER instruments. Other space-borne polarimeters that are currently being designed (e.g., SPEX) or prepared (e.g., MAIA) for future launch will inherit higher polarimetric accuracies from the above-mentioned airborne polarimeters (RSP and AirMSPI, respectively). These polarimetric accuracy improvements will lead, in turn, to higher retrieval accuracies of aerosol, cloud, and surface properties. Some of these future polarimeters will provide global coverage (e.g., HARP), whereas others (e.g., MAIA) will only target specific locations. In addition, several other polarimeters have been launched or are planned for launch by the Japanese and Chinese space agencies. The SGLI instrument was recently launched on the JAXA GCOM-C spacecraft and combines single view angle, multispectral VIS/NIR/SWIR/TIR channels with slant-view polarisation sensitivity at two VIS wavelengths (Hashiguchi et al., 2016). The CAPI instrument launched on-board the Chinese Tansat satellite obtains images of radiance in five channels in the VIS/NIR/SWIR spectrum, two of which also measure the polarisation at 0.67 and 1.64 μm (Chen et al., 2017).

The POLDER-3 observations were initially analysed using traditional look-up-table algorithms, which enable fast and robust retrievals, providing long records of aerosols over land and ocean (Tanré et al., 2011). As an example, **Figure 5** shows the yearly mean value of the contributions of fine and coarse aerosol modes to the atmosphere optical thickness as retrieved with the POLAC algorithm, which retrieves both aerosol and surface properties implementing a statistically optimised fitting based on elaborated look-up-table approach (Harmel and Chami, 2011, 2013).

Another class of retrieval algorithms considers a continuous parameter space of aerosol and surface properties and retrieves them simultaneously by taking into account differences in angular, spectral, and polarisation (if available) features of atmosphere and surface signals (Dubovik et al., 2011; Hasekamp et al., 2011; Xu et al., 2016). The first results of this approach were encouraging and demonstrated that the quality of space-borne retrieval is comparable to ground-based AERONET retrievals. These algorithms do not use look-up tables and implement all radiative transfer calculations on-line during retrieval. As a result, they require significantly longer time for the

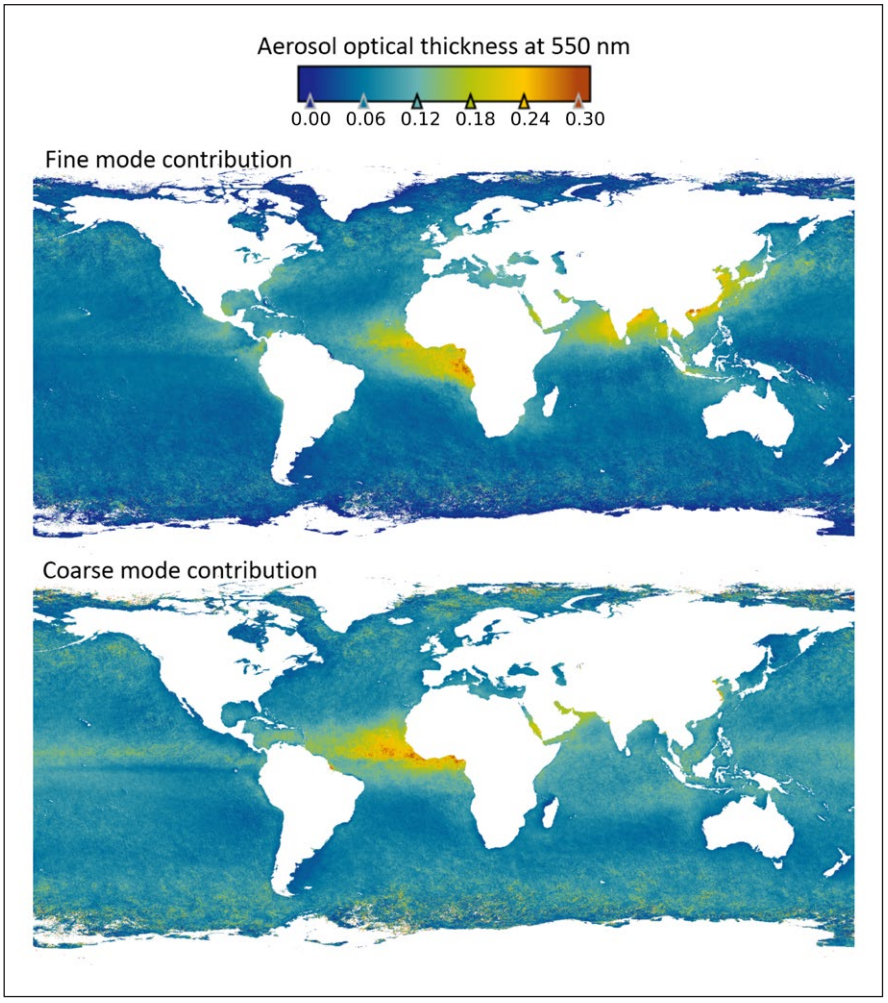

Figure 5: Aerosol retrieval with polarimetric instruments. Yearly mean value for 2007 of the fine and coarse aerosol optical depths as retrieved by the POLAC algorithm (Harmel and Chami, 2011) applied to the PARASOL imagery.
DOI: https://doi.org/10.1525/elementa.331.f5

retrievals compared to traditional algorithms and are rarely used for processing large volumes of the data.

Recently, a set of atmosphere and surface products was generated for the entire PARASOL archive using GRASP, an open source software (Dubovik et al., 2014; https://www.grasp-open.com) that implements statistically optimised fitting using a new multi-pixel concept. This new approach allows for additional a priori constraints on aerosol and surface variability, improving the retrieval accuracy (Dubovik et al., 2011). PARASOL/GRASP provides an extended set of aerosol parameters including spectral AOD and SSA, Angström exponent, fraction of spherical particles, and information about aerosol height (**Figure 6**). Together with aerosol properties, the bidirectional reflectance distribution function (BRDF) and the bidirectional polarisation distribution function (BPDF) of the land or ocean surface are also retrieved. A comprehensive set of the atmosphere parameters potentially provided by advanced polarimetric algorithms is listed in **Table 5**, although these may vary for different instruments and algorithms.

2.3.3 Lidar remote sensing

The chief advantage of lidar is the ability to resolve backscatter in the vertical dimension. Unlike passive techniques, there is unambiguous separation of lidar signals arising from the ocean and the atmosphere. Within the atmosphere, lidar provides vertically resolved aerosol optical properties as opposed to only a column AOD. While passive IR measurements provide information on cloud top height for well-posed cases, lidar achieves higher precision and provides vertical distributions of multi-layer cloud systems (e.g., top height of marine stratus beneath optically thin cirrus) and vertical structure within optically thin clouds.

Efficient lidar measurements of aerosols and clouds were first demonstrated from space with the Lidar In-space Technology Experiment from the NASA Space Shuttle in 1994 (Winker et al., 1996), and the most recent lidar deployed in space was the CATS, in operation from 2015 to 2017 (Yorks et al., 2016). Here we focus our discussion on CALIOP (launched in 2006; Winker et al., 2009), because of the length of its data record and extensive use

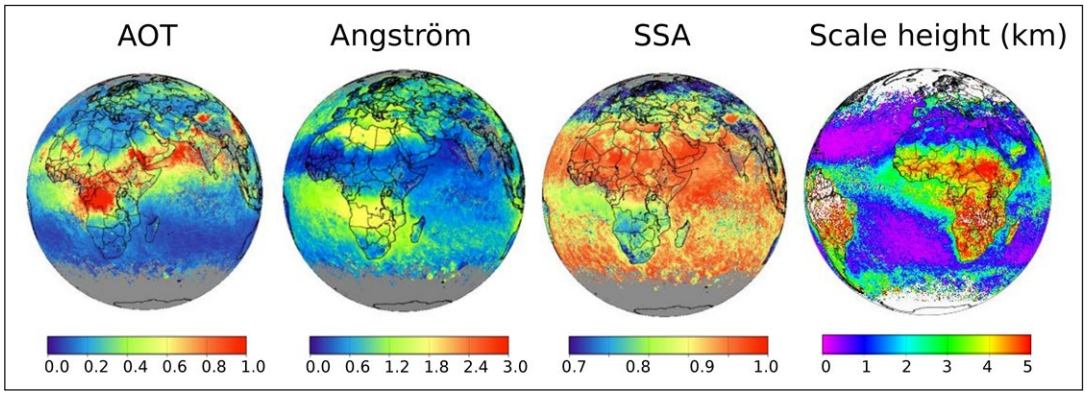

Figure 6: PARASOL/GRASP retrieval of seasonal mean aerosol parameters for summer 2011. From left to right: Aerosol optical depth (or thickness, AOT) at 565 nm, Angström exponent (α), single scattering albedo (SSA) at 670 nm, and aerosol scale height. PARASOL/GRASP retrievals were implemented at the original 6-km resolution using all available PARASOL angular and polarimetric measurements (at 440, 490, 560, 670, 870 and 1020 nm), and using a single set of a priori constraints at the global scale (with no location-specific assumptions). DOI: https://doi.org/10.1525/elementa.331.f6

Table 5: Radiative properties of the marine boundary layer that can be derived from current and planned satellite polarimeters. DOI: https://doi.org/10.1525/elementa.331.t5

MBL atmospheric characteristic	Current satellite polarimeters: PARASOL/POLDER	Potential future polarimeters: 3MI, multi-angular polarimeter on PACE mission
Microphysical aerosol properties	Complex refractive index, size distribution, aerosol nonsphericity, aerosol concentration	Increased retrieval accuracy (for polarimetric uncertainty <0.5%), increased spatial coverage and resolution
Optical aerosol properties	Aerosol optical depth (AOD), single scattering albedo (SSA), Angström exponent, aerosol extinction profile, aerosol type, aerosol backscatter	Increased retrieval accuracy (for polarimetric uncertainty <0.5%), increased spatial coverage and resolution
Aerosol vertical profile	Estimated accuracy of 1–2 km limited by sensitivity to aerosol height distribution	Better accuracy due to addition of polarisation channels in the blue and UV wavelength regime (and reduction in polarimetric uncertainty)
Cloud microphysics	Cloud droplet size distribution, cloud phase, ice crystal shape, cloud top height and thickness	Increased accuracy (for polarimetric uncertainty <0.5%), increased spatial coverage and resolution

that has been made from those data (to date, nearly 2000 publications are based on CALIOP observations). The CALIOP sensor employs the standard elastic backscatter lidar technique, which, fundamentally, measures attenuated backscatter from air molecules and cloud/aerosol particles at 532 and 1064 nm. In addition, measurement of backscatter polarised parallel and perpendicular to the transmitted laser pulse provides the ability to determine the presence of non-spherical particles. The calibration procedure used in CALIOP retrievals eliminates concerns about calibration drift over the lifetime of the instrument (Powell et al., 2009), an important consideration in long-term cloud/aerosol trend studies.

The discrimination between clouds and aerosols is based on backscatter signal level, the ratio of 532- and 1064-nm backscatter signals, and depolarisation (Liu et al., 2009). For detected aerosol layers, computation of aerosol extinction and backscatter relies on the assumption of the aerosol extinction-to-backscatter ratio (Young et al., 2009, 2013), which is highly dependent on aerosol type (i.e., desert dust, biomass burning, clean continental, polluted continental, marine, and polluted dust). Aerosol type is assigned based on geographic location, underlying surface type (e.g., ocean vs. land), altitude, and an approximate estimate of depolarisation from the lidar measurement (Omar et al., 2009). An average extinction-to-backscatter ratio is assigned to each type based on AERONET climatology and other relevant data. Consequently, retrieval errors can arise from misclassification of aerosol type and the natural uncertainty of extinction-to-backscatter ratios within a type (Burton et al., 2013). These errors can accumulate as the retrieval proceeds downward through the atmosphere toward the surface.

The CALIOP sensor provided the first global view of the three-dimensional distribution of aerosols (Winker et al., 2013) which, along with data from other sensors and models, has enabled several important breakthroughs, including quantification of the direct radiative effects of aerosols above low clouds (e.g., Chand et al., 2009; Oikawa et al., 2013; Zhang et al., 2016), the first global estimates of all-sky aerosol radiative forcing (e.g., Oikawa et al., 2013; Matus et al., 2015), and assessments of the vertical distribution of aerosol in transport models (e.g., Yu et al., 2010; Koffi et al., 2016). CALIOP data have also been used to help quantify transport of desert dust and associated iron fertilization of regions remote from dust sources (e.g., Johnson et al., 2011; Tan and Shi, 2012; Yu et al., 2015). **Figure 7** displays a 532-nm browse image from CALIOP showing examples of many relevant aerosol and cloud features.

In addition to information on aerosols, CALIOP provides cloud top height and, for non-opaque clouds, base height and optical depth. It is much more sensitive to optically thin clouds than passive remote sensors and does not suffer ambiguities arising from, for instance, viewing warm marine boundary layer clouds through a veil of thin cirrus. CALIOP also provides information on the vertical profile of backscatter and depolarisation within clouds (i.e., down to the point that the signal is not so attenuated as to become useless). Together with the CPR on Cloudsat (Stephens et al., 2008, 2017), which is more sensitive to strongly scattering clouds, CALIOP has provided the first global data set on the vertical distribution of cloud occurrence (Mace et al., 2009) and heating rates (Haynes et al., 2013). The CALIOP and CPR data have been combined with MODIS observations to provide accurate estimates of surface downward radiative fluxes (Kato et al., 2011).

Moreover, CALIOP depolarisation measurements have been key in identifying cloud thermodynamic phase (ice vs. water droplets) including, for instance, the identification of super-cooled liquid droplets at the tops of boundary layer clouds over the Southern Ocean (Hu et al., 2010). These clouds had been misclassified in passive imagery and hence improperly parameterized in models, creating errors in estimated shortwave and longwave

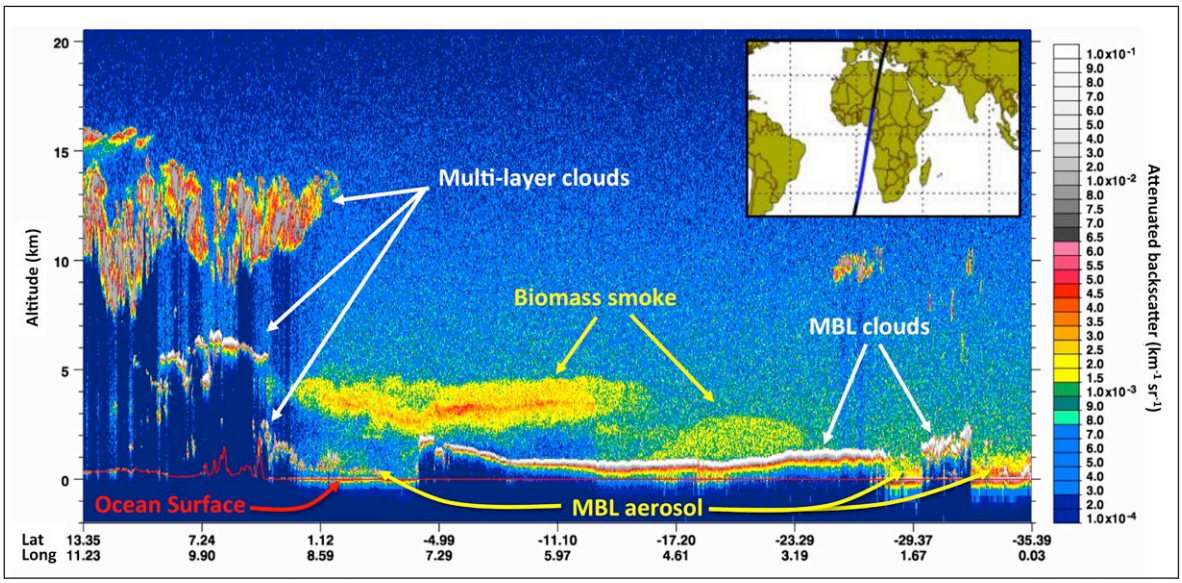

Figure 7: Lidar image showing many features relevant to radiation budgets and aerosol-cloud-ocean interactions. As shown in this browse image of CALIOP attenuated backscatter, lidar provides the vertical dimension, enabling accurate measurement of cloud top height (even for multi-layered clouds) and determination of whether aerosol layers are located at cloud altitude or lofted above clouds. DOI: https://doi.org/10.1525/elementa.331.f7

radiative fluxes (e.g., Bodas-Salcedo et al., 2016; Forbes et al., 2016). Depolarisation measurements have also been used to characterize multiple scattering and cloud microphysics in strongly scattering water clouds, enabling lidar retrievals of cloud-top extinction and combined CALIOP-MODIS retrievals of cloud droplet number density that do not rely on the adiabatic assumption of MODIS retrievals (Zeng et al., 2014).

As indicated previously, CALIOP is well past its design lifetime. The next cloud-aerosol lidar to come online will be the ATLID, a 355-nm HSRL instrument with polarisation sensitivity on the EarthCARE satellite (Illingworth et al., 2015). The HSRL capability overcomes the need to assume an extinction-to-backscatter ratio in the retrieval of aerosol extinction and backscatter, thereby providing more accurate retrievals through the column and into the MBL. Independent HSRL measurements of aerosol extinction and backscatter (Esselborn et al., 2008) from ATLID will enable calculation of the aerosol extinction-to-backscatter ratio, which along with aerosol depolarisation ratio will be used to infer aerosol type (Groß et al., 2015). However, the ability to unambiguously resolve aerosol types may be limited using data at only one wavelength (Burton et al., 2015). Cloud products from ATLID will include cloud top height and, for optically thin clouds, vertical structure and optical depth. In combination with measurements from other sensors on EarthCARE, ATLID data will also be used to retrieve CER and ice water content. We note that ATLID's coarse vertical resolution of 100 m precludes ocean subsurface profiling.

In the future, we can envision a more capable space-borne HSRL operating at multiple wavelengths. Airborne lidars with HSRL capability at 532 nm, backscatter capability at 1064 nm, and polarisation sensitivity have been conducting routine measurements for over a decade (Esselborn et al., 2008; Hair et al., 2008). These two-wavelength polarisation-sensitive lidars provide highly accurate aerosol extinction, backscatter, depolarisation, and optical depth measurements, and significantly greater aerosol typing skill than that achievable with CALIOP (Burton et al., 2012, 2013, 2014; Groß et al., 2013) and anticipated to be possible with ATLID. **Figure 4** shows examples of the independent aerosol extinction and backscatter products as well as the aerosol type mask retrievable from one of these airborne HSRLs. The vertical resolution of that same lidar was increased to ~1 m to enable coincident ocean profiling (**Figure 4**), which is serendipitously enabling advances in MBL cloud property retrievals. The addition of HSRL capability at 355 nm would enable vertically resolved retrievals of aerosol effective radius and concentration, as demonstrated by recent airborne lidar measurements (Müller et al., 2014; Sawamura et al., 2017), and polarisation sensitivity at all three wavelengths provides increased skill in classifying smoke (Burton et al., 2015).

As with ocean remote sensing, lidar is a natural complement to passive radiometry and polarimetry. While lidar lacks swath, the vertical profiling capability provides information critical to studies of marine aerosols and clouds. Lidar provides aerosol measurements over bright clouds, including layer optical depth and the distribution of aerosols above clouds. The ability to determine whether an aerosol layer is lofted high above MBL clouds or interacting with those clouds is critical to accurately correlate the effect of marine aerosols on cloud microphysical and macrophysical properties (Costantino and Bréon, 2013) (**Figure 7**). In broken cloud systems, lidar provides vertical profiles of aerosols within the MBL, thereby providing information on aerosol loading at cloud base altitude. In addition to locating aerosols with respect to cloud altitude, lidar aerosol retrievals do not suffer from artefacts due to adjacency effects or cloud shadowing. In combination with passive data, lidar can provide advanced retrievals of cloud microphysics relevant to the study of aerosol-cloud interaction. **Table 6** summarizes properties of the MBL that can be retrieved with current and potential future space-borne lidars.

Table 6: Properties of the marine boundary layer that can be derived from current, planned, and potential future satellite lidars. DOI: https://doi.org/10.1525/elementa.331.t6

MBL atmospheric characteristic	Current satellite lidar capability: CALIOP on CALIPSO	Potential future HSRL capability
Aerosol backscatter and extinction	Derived from attenuated backscatter via assumption of extinction-to-backscatter ratio or optical depth constraint	Accurate independent retrieval of backscatter and extinction without assumptions
Aerosol type	Crude typing capability	Improved skill with ATLID 355-nm extinction, backscatter, and polarisation sensitivity. High skill with two-wavelength lidar: 532-nm HSRL, 1064-nm backscatter, and polarisation sensitivity at both wavelengths
Aerosol effective radius and concentration	Not available	Vertically resolved estimates via three-wavelength lidar: 355- and 532-nm HSRL, 1064-nm backscatter
CCN	Proxy based on extinction as retrieved from attenuated backscatter	Proxy based on aerosol extinction or aerosol concentration estimate
Cloud top height	Precise and unambiguous	Precise and unambiguous
Cloud base height	For non-opaque clouds	For non-opaque clouds
Cloud microphysics	Thermodynamic phase, cloud droplet concentration (with data from passive sensors)	Thermodynamic phase, cloud droplet concentration (with data from passive sensors)

3 To what extent does upper-ocean turbulence drive fluxes of mass and energy at the air-sea interface?

3.1 Perspective on the problem

The air-sea interface is the critical zone where the coupled ocean-atmosphere system constantly exchanges heat, momentum, gases, and particulate matter. Understanding these exchanges has been one of the underpinning foci of SOLAS (Law et al., 2013; Brévière, 2016). Ocean-atmosphere fluxes usually scale with turbulence at the air-sea interface. Surface turbulence is generated primarily by wind stress, which produces short capillary-gravity waves and wave micro-breaking or bubble entrainment caused by breaking of large gravity waves. Other sources of turbulence include buoyancy convection, rainfall, or interactions with sea ice. As a ubiquitous phenomenon, turbulence should be accounted for when estimating sea-air fluxes at both local and global scales.

Gas exchange across the air-sea interface plays a critical role in the climate system by regulating the global carbon cycle. In particular, molecular exchanges are thought to contribute to partitioning approximately 30% of the emitted anthropogenic CO_2 into the ocean (Wanninkhof et al., 2009). Other crucial processes controlled by the air-sea interface include the exchange of heat, the exchange of powerful greenhouse gases like methane and nitrous oxide, ocean oxygenation (with growing concern about ocean deoxygenation and hypoxia; Schmidtko et al., 2017), the emission of gaseous aerosol precursors (Carpenter et al., 2012), and the transport of pollutants (González-Gaya et al., 2016). Therefore, scientific progresses in modelling and remote sensing activities related to air-sea exchange are critical to better understand a wide range of contemporary environmental issues and key processes in the Earth system, as well as to project future climate and support the development of science-informed climate policies.

Gas fluxes (F) across the air-sea interface are generally parameterized for each specific gas with a simple product of the concentration gradient across the sea-air interface, ΔC, and the gas transfer coefficient, k. The gradient ΔC is defined as $C_w - s_g \cdot C_a$, the difference between the waterside gas concentration, C_w, and the airside gas concentration, C_a, scaled by the gas solubility coefficient, s_g. Given that the concentrations of many gases of interest can be measured with sufficient accuracy, and that gas solubility is generally a well-constrained function of temperature and salinity (Johnson, 2010), the gradient term ΔC is a secondary source of uncertainty in gas flux calculations. However, much larger uncertainties are associated with the transfer coefficient, k (Wanninkhof et al., 2009), which is primarily determined by the physics at the air-sea interface, and particularly the waterside turbulence, at least for insoluble gases (**Figure 8**).

The gas transfer velocity is usually characterized by accessible measurements, wind speed being the most widely used parameter. An advantage of this practice is that wind speed can be derived routinely from satellite data with relatively good accuracy (~1 m s^{-1} at spatial resolution of 12.5–50 km) (Vogelzang et al., 2011). However, parameterisations using wind speed alone often fail to match directly measured gas-exchange rates, and estimates from different parameterisations often disagree by more than a factor of two (Goddijn-Murphy et al., 2016).

At high wind speeds (>20 m s^{-1}), this uncertainty has been attributed to the effect of bubble-mediated gas transfer (Woolf, 2005), which can greatly enhance the flux of low-solubility gases like CO_2. At low wind speeds

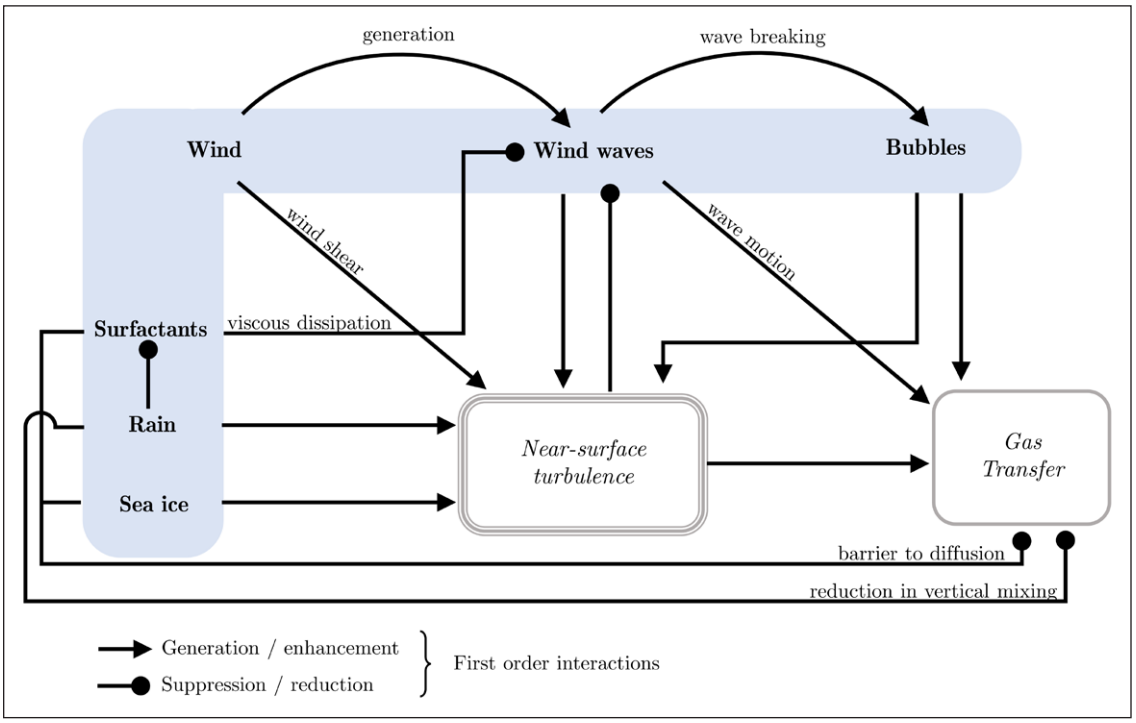

Figure 8: Turbulence at the air-sea interface. First order interactions between parameters observable from remote sensing devices (bold) and near-surface phenomena (italic) related to air-sea gas exchange. DOI: https://doi.org/10.1525/elementa.331.f8

(<5 m s^{-1}), buoyancy-driven convection has been proposed as a dominant transfer mechanism (McGillis et al., 2004). The picture is even more complicated in polar oceans due to the presence of sea ice, which itself directly exchanges gases with the atmosphere (e.g., Loose et al., 2011) and alters the propagation of kinetic energy within the water through processes that are poorly understood (Loose et al., 2017; Prytherch et al., 2017).

The relatively poor predictive skill of wind-speed based *k*-parameterisations has triggered the development of alternative approaches. For example, a number of empirical formulations have been proposed to estimate *k* from the wave slope variance, a proxy for interfacial turbulence that can be retrieved by satellite radar altimeters (Glover et al., 2002, 2007; Goddijn-Murphy et al., 2012, 2013). Other studies suggest that empirical fits to observations of *k* are insufficient because they do not rely on the underlying physics of the exchange process. Thus, improvements in air-sea flux quantification could rely on parameterisations of *k* along with the dissipation rate of turbulent kinetic energy (Kitaigorodskii and Donelan, 1984; Asher, 1997). Lamont and Scott (1970) derived a direct relation between *k* and turbulence using the surface renewal theory (Higbie, 1935; Danckwerts, 1951). This theory describes periodic events of small eddies disturbing the sea surface with water from below (small eddy model: SEM). More recently, Esters et al. (2017) showed from field observations in the North Atlantic that kinetic energy dissipation and gas (DMS and CO_2) air-sea fluxes are generally consistent with the theoretical SEM approach. This experimental demonstration paves the way towards developing mechanistic approaches to estimate gas exchange from sea roughness parameters observable by space-borne sensors.

Exchange across the air-sea interface is also strongly affected by surfactants accumulating and spreading at the sea surface. For instance, experiments have shown that addition of artificial surfactants to the sea surface can significantly decrease *k* by up to 55% at low to moderate wind speeds (Salter et al., 2011). In the oceans, surfactants accumulate in the sea surface microlayer, the water-side interfacial layer, as thin as 50 μm (e.g., Zhang et al., 2003), where viruses, bacteria, and phytoplankton, as well as dissolved and particulate organic matter, including exopolymeric gels, also accumulate (Engel et al., 2017). Despite its very small vertical extent, the microlayer forms a physicochemical barrier that subsequently alters the hydrodynamics of the air-sea-interface and ultimately suppresses a substantial amount of turbulent energy (**Figure 8**). For instance, a surfactant-enriched microlayer increases the surface tension of the air-sea interface, thereby damping surface capillary waves and modifying the entrainment or bursting of air bubbles and surface renewal (e.g., Engel et al., 2017). Hence, full consideration of wind and microlayer properties could help further our capacity to determine air-sea exchanges for all types of coastal and oceanic waters. The first attempts to determine surfactant effects on air-sea exchange from remotely sensed data were based on estimates of surfactant proxies such as Chl-*a* (Lin et al., 2002), but a universal relationship linking Chl-*a*, surfactant properties, and *k* has thus far proved elusive (Engel et al., 2017; Sabbaghzadeh et al., 2017).

The inherent complexities of turbulent exchanges across the air-sea interface cannot be fully accessed via remote sensing techniques. However, several observables (here, defined as turbulence-related parameters interacting with the electro-magnetic field) might be readily or potentially measurable using space-borne sensors (see **Figure 1** for a general picture). Based on historical, current, and near-future space missions, this section provides a short overview of remote sensing technologies and methods that could be used to address the problem of scaling turbulence in the surface ocean boundary layer. Previous reviews on remote sensing of turbulent fluxes pointed out general capabilities and challenges (Bourassa et al., 2010b; Shutler et al., 2016). Here, we focus on some different approaches using non-conventional techniques (e.g., exploitation of surface-reflected sunlight from passive imagery) and emerging technologies for more broad and operational applications (e.g., polarimetric, SAR, and lidar sensors). We also discuss different sources of turbulence, not yet considered in general formulations, and how remote sensing could aid in understanding and better scaling bulk turbulent transfers at the air-sea interface. Going beyond wind-produced or wind-derived turbulence, we address the potential of remote sensing techniques to comprehensively characterize the sea state and the air-sea interface in the hope of strengthening interactions between the biogeochemistry and remote sensing communities.

3.2 Active remote sensing of the ocean-atmosphere interface

This section gives a brief overview of the current and potential capabilities of the space-borne active sensors in relation to air-sea flux parameterisation. The various instrumental configurations allow different characteristics of the air-sea interface to be identified with different spatial-temporal resolutions. These remote sensing capabilities are also summarized in **Table 7**.

3.2.1 Active microwave sensors

Active microwave sensors, i.e., scatterometers, altimeters and SAR, emit a pulse at a certain frequency and measure the energy backscattered from the roughened surface. Practically, a dimensionless quantity is used: the normalised radar cross section (NRCS), also called backscatter coefficient, which is defined as the radar cross section per unit surface area. The NRCS is sensitive to the trait of the material under the radar's observation, and is a function of the frequency, incidence angle and polarisation of the emitted pulse, and the scattering characteristics of the target. For a given frequency and polarisation, the NRCS depends on the quantity of capillary waves that satisfy a resonance condition with the pulse (Bragg scattering), and the geometry between the incident pulse and wave facets. As wind blows on the ocean surface, the capillary waves respond virtually immediately, propagating in the same direction and growing as wind intensity grows. Hence, for a given viewing angle, sea surface wind speed (conventionally defined as 10 m above the surface) can be estimated from NRCS. Nevertheless, the solution is not trivial with multiple combinations of wind speed and direction providing the same

Table 7: Characteristics of upper-ocean turbulence relevant to sea-air fluxes that can be derived from active satellite sensors, current and planned. DOI: https://doi.org/10.1525/elementa.331.t7

Interface geophysical parameters/properties	Current capabilities	Future capabilities
Sea surface wind	Wind speed, direction, and stress (good accuracy from 0 to 20 m s^{-1}); multiplatform daily global coverage only for scatterometry; higher spatial resolution (lower coverage) for SAR and lidar	Improved estimates at very high wind speed (e.g., typhoons), improved geophysical models to solve ambiguities, better coverage with higher spatial resolution, and better accuracy in coastal regions
Waves	Significant height and direction of gravity waves (altimetry and polarised SAR) and internal waves (SAR)	Improved accuracy over coastal regions, improved coverage of higher spatial resolution products (e.g., SWOT, SAR, and lidar missions)
Currents	Speed and direction of geostrophic currents (global coverage with multiplatform altimetry missions)	Higher spatial-temporal resolution, submesoscale currents in open ocean and coastal regions
Surface slicks	Feature detection (size, shape) (SAR)	Type of surfactant, concentration, thickness (SAR and optical sensors)
Ship wakes	Feature detection (SAR)	Vertical profile (lidar)
Sea surface roughness	Wave slope variance (capillary waves) (all active sensors)	Improved wave slope estimates to account for bulk interface properties and sea-state condition
Whitecaps (foam and bubbles)	Feature detection (SAR and lidar) or estimate of whitecap fraction from wind speed	Increased accuracy (detection, duration and type-source), spatial coverage and resolution, vertical profile (lidar)

NRCS. Such ambiguities are solved using multiple viewing angles and constraints from geophysical models.

An advantage of active microwave sensors is that the pulse can travel through clouds, providing a large coverage of the ocean surface. Only heavy rain cells can attenuate shorter pulses (e.g., Ku-band) adding noise to the signal and causing distortions in wind retrievals. Raindrops on the ocean surface also smooth the capillary waves. This effect can be a problem for wind retrieval from scatterometry or altimetry techniques, but it is actually another source of turbulence in the upper layer that could be resolved.

Traditional, global, wind-driven k parameterisations have relied on multi-mission satellite wind fields (Bourassa et al., 2010a; Wanninkhof, 2014). However, with the growing awareness that many other sea surface phenomena affect the gas transfer velocity, other ways to derive sources of bulk turbulence are being proposed and investigated. In particular, wind stress or mean square slope of the surface wave spectrum could be used instead of wind speed to parameterize k (Glover et al., 2007; Goddijn-Murphy et al., 2012, 2013) and thus could be better suited to resolve air-sea exchange processes from space observations (e.g., Shutler et al., 2016).

3.2.2 Scatterometry

Scatterometers routinely have been used to derive multi-mission global daily wind vectors, starting with the first space-borne scatterometer on-board SeaSat, launched in 1978, and continued with many other missions up to date (e.g., SeaWinds-QuikSCAT, ASCAT-MetOPA/B, OceanSat, ScatSat, CFOSAT). An advantage of scatterometers is that multi-angle NRCS measurements (with different antennas or a rotating one) allow derivation of not only the wind speed, but also the directional components of the wind vector, inverted with geophysical models. Scatterometers can derive wind speed with high accuracy (~1 m s^{-1}) at resampled resolutions of 12.5, 25, and 50 km for a wide range of wind speeds (~0–30 m s^{-1}) (Vogelzang et al., 2011). Although certainly not the only factor controlling air-sea gas transfer velocity, wind speed may provide a reasonable first-order estimate of k for moderate wind conditions (~4–15 m s^{-1}) over the global ocean (e.g., Wanninkhof, 2014). Scatterometry retrievals of wind stress, accounting for wind vector, buoyancy, surface currents, gravity waves, and air density, should be even more robustly related to gas transfer for all sea state conditions (Bourassa et al., 2010a, 2010b).

3.2.3 Altimetry

Satellite altimetry measures the NRCS with a nadir viewing single antenna. The timing of the returned microwave pulse is used to estimate the sea surface height, after careful corrections for atmospheric interference, geoid deformations, and tides. The first space-borne altimeter was also on-board SeaSat (launched in 1978). With the growing awareness of sea level rises with storm surges and climate change, altimetry missions have gained importance and support for scientific and operational missions (e.g., Geosat, TOPEX, ERS, Jason, Cryosat, Envisat, SARAL-AltiKa, Sentinel-3 SRAL).

In addition to sea surface height and derived properties, such as significant wave height and geostrophic currents (Isern-Fontanet et al., 2017), altimetry can be used to derive sea surface wind speed, because the intensity of the returned pulse is altered by the surface roughness. Glover et al. (2007) and Goddijn-Murphy et al. (2013) have shown that in-situ gas flux measurements are more strongly correlated with the wave mean square slope retrieved by dual

frequency altimetric radar (e.g., TOPEX, AltiKa) than with the wind speed derived from wave slope. This stronger correlation suggests that the altimetric radar wave slope can be used as a proxy for interfacial turbulence, including the effects of wind stress, small scale roughness, and surface films, and thus contribute to better *k* parameterisations.

Future missions with finer spatial resolution (~2 km), in particular the Surface Water and Ocean Topography (SWOT) mission (Fu et al., 2009; Durand et al., 2010), are expected to improve the estimation of the upper-ocean circulation at the submesoscale. The forthcoming data from these altimeters could permit significant advances in our understanding of the impacts of upper-ocean eddies, fronts, and filaments on surface waves (Ardhuin et al., 2017; Isern-Fontanet et al., 2017) and, in turn, in the evaluation of the role upper-ocean circulation plays in modulating the interfacial turbulence.

3.2.4 Synthetic Aperture Radar (SAR)

SAR is sensitive to small variations in surface roughness, which makes detection of slicks through their wave damping effect a straightforward application of SAR data. Specifically, natural and anthropogenic surfactants can modify physical properties of the ocean surface by altering surface tension, damping short capillary waves, and hence changing roughness and turbulence production. Under low-to-moderate wind conditions, these changes in physical properties may lead to the formation of slicks that are detectable by SAR remote sensing (Gade et al., 1998). Slick detection may improve our understanding of what organisms and meteorological conditions are responsible for surfactant production. For example, Kurata et al. (2016) were able to link surface roughness, surface slicks, and the presence of surfactant-associated bacteria in the near-surface layer of the ocean by combining satellite SAR data with genetic analysis of in situ collected water samples.

Another avenue for application of SAR data is information on organic matter concentration derived from its effect on the longevity of bubbles, which is expected to increase in the presence of organic matter. An example of this approach is the quantification of the persistence of boat wakes under low wind conditions, as observed in high resolution SAR imagery (Lyden et al., 1988). Thus, wind speed and foam fraction inferred from SAR measurements could potentially be used to predict organic matter concentration in the microlayer or subsurface layer.

Many challenges still remain in exploiting SAR imagery to identify more accurately sea surface features, particularly the extent and types of surfactants that may have different effects on the microlayer and upper layer turbulence. Combining different techniques and data sources, such as optical imagery (ocean colour, sun glint) and in-situ data collections, might be required to solve such problems.

We are now just starting an exciting new era of SAR imagery with openly distributed data (through the Copernicus Program (ESA/EUMETSAT), for example). Sentinel-1A was launched in April 2014, and Sentinel 1B in April 2016, extending the temporal/spatial coverage, which is mostly concentrated around Europe and in continental and coastal areas elsewhere. Software developed within the Copernicus Program (SNAP) is also helping to broaden the user community of both scientists and operational services. The open distribution policy of optical imagery in the 1980s and 1990s (introduced with the Landsat legacy) revolutionized various applications, and free SAR imagery will surely spur progress in other areas.

Phenomena in the MBL that have important effects on turbulent fluxes can also be observed in SAR imagery, including rain cells, boundary layer roll vortices (Zhang et al., 2008), atmospheric gravity waves, vortex streets (Li et al., 2013), hurricanes, typhoons (Li, 2015), and meso- and submesoscale vortices (see examples in **Figure 9**).

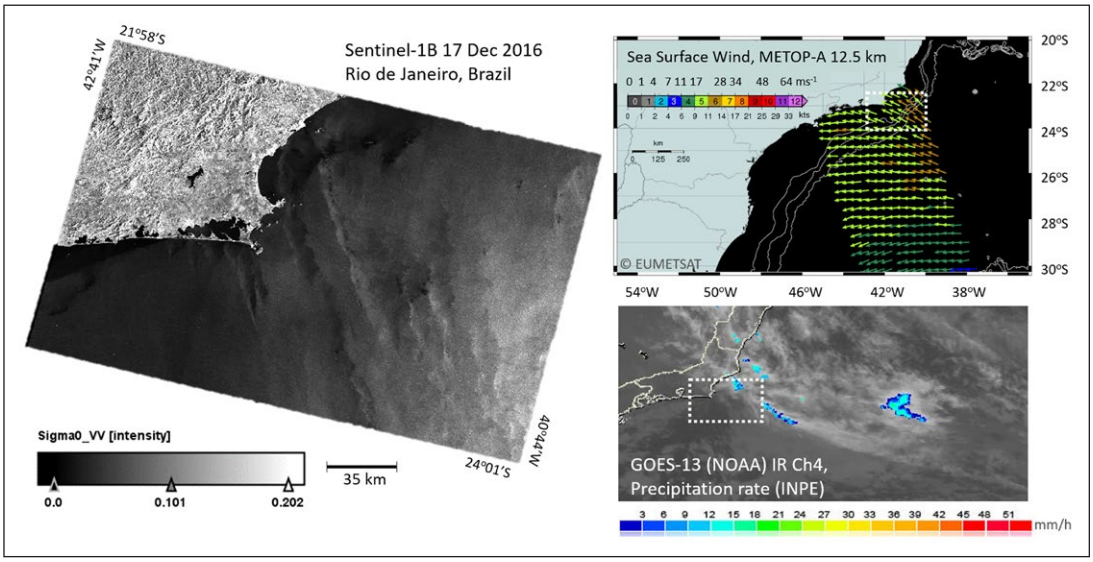

Figure 9: Quasi-simultaneous retrieval of turbulence-relevant parameters with microwave and infrared sensors. Example of Sentinel-1B SAR backscatter (sigma_0) VV polarization showing the imprints of rain cells on ocean surface roughness (left); ASCAT-MetOP-A (EUMETSAT) scatterometer-derived sea surface wind field (top right); and GOES-13 (NOAA) channel 4 (11 μm, passive infrared) image showing precipitation rate estimates (bottom right) (Vila et al., 2001). All scenes were obtained over southeast Brazil on 17 December 2016. DOI: https://doi.org/10.1525/elementa.331.f9

Estimation of air-sea fluxes at very high wind speeds associated with tropical storms, cyclones, and typhoons is particularly challenging; under such conditions, SAR data can play an important role in revealing fine scale structures (Li, 2015). High-resolution polarised SAR imagery (e.g., TerraSAR-X) provides further information that can be used to derive several sea surface characteristics, such as oceanic gravity waves (significant height and direction), whitecaps from breaking waves, surfactants, ship wakes, and internal waves (Pleskachevsky et al., 2016). All of these features have different effects on the interface and upper-ocean turbulence. Future exploitations of SAR data can be safely foreseen to provide new and complementary information to better constrain in-water turbulence estimates at the global scale, provided coincident advances in turbulence parameterisation.

Sea-ice properties (e.g., extent, concentration, thickness), which are important for sea-air fluxes and interface turbulence, have traditionally been mapped and globally monitored with passive microwave sensors. Such measurements enable high temporal resolution retrievals, but with coarse spatial resolution. Active microwave sensors, particularly SAR, complement passive microwave datasets by providing higher-resolution imagery and additional properties that are relevant for sea-air flux estimates, such as sea-ice thickness, type, age, drift and melting rate (Dierking, 2013). However, more detailed small-scale studies are still needed to fully exploit advanced SAR technology. The series of RADARSAT satellites, operated by the Canadian Space Agency, has provided SAR imagery for ice monitoring since 1995.

3.2.5 Lidar

Like scatterometers and radar altimeters, lidar also provides a measurement of the backscatter coefficient of the ocean surface. The lidar measurement of the ocean surface backscatter coefficient is directly related to the wave mean square slope variance. Hu et al. (2008) demonstrated the value of the lidar technique by computing wave slope variance from CALIOP data and using that to estimate wind speed. Favourable comparisons with AMSR-E wind speeds have demonstrated the validity of this approach (**Figure 10**).

An advantage of lidar is that the signal is more sensitive to smaller scale capillary waves, because of the much shorter wavelength of the electromagnetic pulse than those used by radio-frequency and microwave sensors. Another advantage derives from the small lidar footprint at the ocean surface. For the CALIOP lidar on-board CALIPSO, surface backscatter from 90-m diameter areas are collected for each laser pulse, a significantly finer resolution than kilometric scale of scatterometers. The smaller footprint provides more information on small-scale variability of the wave slope spectrum that can be averaged out in the larger footprints of microwave instruments. The greatest uncertainty in the lidar technique for estimating wave-slope variance is due to the difficulty in estimating the transmittance of the overlying atmosphere. The atmospheric transmittance can be estimated from the lidar signal itself, from co-located passive radiometric estimates of optical depth, or with two-wavelength techniques for high-spectral-resolution-lidar (HSRL) instrument (see Hu et al., 2008). Due to the accuracy of its atmospheric transmittance measurements, a space-borne HSRL would provide the highest accuracy wave-slope variance estimates. While lidar cannot probe the ocean surface through optically thick clouds and has limited spatial coverage due to the lack of cross-track sampling, the advantages provided by its smaller wavelength and footprint make it a natural complement to other active techniques for estimating wave spectrum.

3.3 Passive remote sensing of the ocean-atmosphere interface

This section gives a brief overview of the current and potential capabilities of the space-borne passive sensors in relation to the parameterisation of air-sea fluxes. Sensors dedicated to observation of the brightness temperature of the sea surface are now routinely used to infer air-sea interface parameters. Optical sensors working in the visible/near-infrared part of the spectrum, though less exploited, can also be used for this purpose, based on measurements of the sunlight reflected from the air-sea interface (i.e., sun glint). These remote sensing capabilities are also summarized in **Table 8**.

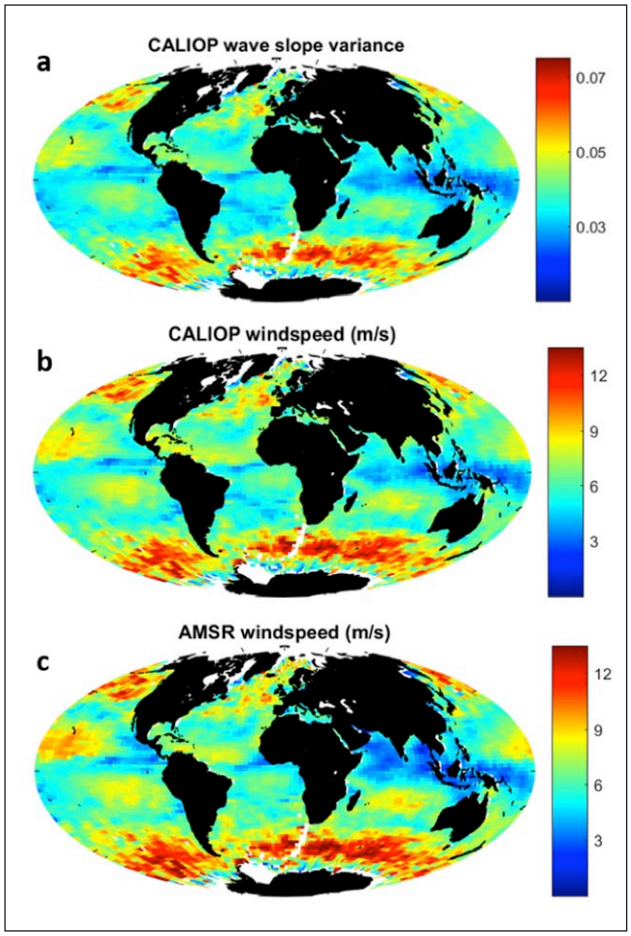

Figure 10: Lidar retrieval of sea surface wave slope variance and derived wind speed. Monthly average for April 2010 of **(a)** wave slope variance and **(b)** sea surface wind speed retrieved from CALIOP lidar data. Retrieved wind speeds satisfactorily compare with **(c)** the AMSR-E (microwave-based) wind speed products. DOI: https://doi.org/10.1525/elementa.331.f10

Table 8: Characteristics of upper-ocean turbulence relevant to sea-air fluxes that can be derived from passive satellite sensors, current and planned. DOI: https://doi.org/10.1525/elementa.331.t8

Interface geophysical parameters	Current capabilities	Future capabilities
Sea surface temperature (SST)	Skin and surface (~1 m) SST with daily global coverage at 750 m to 1 km	Improved spatial-temporal coverage and resolution with multi-mission approaches ("filtering clouds")
Sea surface salinity (SSS)	Global SSS at 35 km resolution (can be numerically enhanced to 0.05°) with 3–5 day revisit time	Improved accuracy, coverage and spatial resolution
Sea surface wind	Wind speed and direction with global daily coverage only at coarse spatial resolution (few to tens of kilometres); higher spatial resolution using sun-glint approaches, but with lower temporal coverage	Improved accuracy and coverage with higher spatial resolution
Whitecaps	Whitecap fraction	Increased accuracy of detection and estimation of duration and type-source
Rainfall	Rainfall rate	Improved accuracy and spatial-temporal resolution with multiplatform missions (infrared and microwave sensors)
Sea surface roughness	Wave slope variance	Improved coverage (optical sensors: using sun glint)
Slicks	Slick detection (SAR, sun glint)	Type-source, thickness, concentration

3.3.1 Infrared and microwave sensors

Buoyancy-driven turbulence, in the form of water-side convection during cooling in deep surface mixed layers (>20 m), can have a significant effect on k at wind speeds typically lower than 5 m s^{-1} (MacIntyre et al., 2010; Rutgersson et al., 2011; Tedford et al., 2014). With loss of surface heat (during night-time, on cloudy days, or with evaporation in tropical regions) denser surface water sinks, producing turbulent eddy flows within the seasonal mixed layer, increasing k and gas fluxes.

This kind of turbulence might be evaluated through monitoring of the sea surface temperature (SST), which has been measured systematically from space since 1980, with day and night revisits over the entire globe (with AVHRR). The AVHRRs lacked on-board calibration for solar and thermal bands, and the orbits of the earlier platforms were not well-controlled, leading to drift. Launch of the (A)ATSRs, beginning in 1991 and continuing through the recently launched SLSTR, overcame both of these limitations. The (A)ATSR generation sensors also provided near-simultaneous dual-views of the atmosphere enabling refinement of the atmospheric correction procedure and thus improving the overall accuracy of SST retrieval. The (A)ATSRs have been used to create stable long-term SST climate data records with small biases (<0.1 K) and high stability (e.g., Merchant et al., 2012).

A constellation of polar-orbiting and geostationary satellites with thermal infrared and passive microwave sensors provide global coverage several times a day, allowing resolution of not only the seasonal, but also the diurnal cycle of SST. The amplitude of seasonal and diurnal SST cycles could be used to understand heat fluxes in specific regions, which could be used further to parameterize buoyancy-driven fluxes. A major challenge for SST coverage of the first space missions was under-sampling due to cloud blocking. Passive microwave satellites (e.g., ISSM, AMSR, TRMM, GPM) helped overcome this issue, but with a much degraded spatial resolution (~25 km, compared to 1 km for AVHRR and MODIS). As an alternative, the MUR data set (Chin et al., 2013) gathers information from both infrared and microwave sensors, and provides ~1-km daily global product. Next-generation geostationary satellites (MSG, Himawari-8, GOES-16) are also equipped with multispectral sensors that allow the retrieval of high temporal resolution (~15 min) SST products. Besides providing more continuous daily surface fields (with temporally binned products), hourly resolved SST can be used to retrieve information regarding diurnal processes. For small scale variability and fine structure in coastal regions, the TIRS on-board Landsat-8 can also be used to derive SST at 100-m spatial resolution (with a 16-day revisit cycle).

In addition to temperature, evaporation can also stimulate convective mixing on the water side, whereas freshwater inputs from rain, large river outflows, and ice melt stratify surface waters and reduce turbulence. Hence, for large-scale processes, salinity from space is also a valuable measurement. In addition to its importance to the stratification problem, surface salinity influences gas solubility, and thereby air-sea exchange. Sea surface salinity (SSS) is estimated from passive microwave sensor data using inversion models that rely on differences in the relationship between the brightness temperature and the actual temperature due to the emissivity coefficient, which is dependent on salinity (and surface roughness). Global maps of SSS have been available since 2009 from the SMOS mission with 35-km resolution and a 3-day revisit time (Reul et al., 2014) complemented by the measurements of AQUARIUS (Lagerloef et al., 2008) over the

2011–2015 period. The broad spatial resolution limits the current SSS products (with 0.2–0.5 accuracy on the practical salinity scale) to large-scale variations, but exploitation of those data is very promising for various applications (Boutin et al., 2014; Matsuoka et al., 2016). Moreover, the spatial resolution of SMOS-retrieved SSS can be increased to 0.05° × 0.05° (<6 km) by relating, through data fusion techniques, the SSS and a second variable (usually SST) retrieved with higher resolution (Olmedo et al., 2016).

Besides sea surface temperature and salinity, which are more relevant for upper-ocean turbulent fluxes under low wind conditions, passive microwave radiometers have been used extensively to retrieve sea surface wind speed globally. Given that ocean emissivity in the microwave range (>0.15 cm) is dependent on sea surface roughness, surface wind speed can also be retrieved from passive microwave radiometers (e.g., Windsat, SSM, TMI, AMSR, GMI). Note that polarimetric radiometers can help retrieve wind direction (e.g., Windsat).

An important challenge for regional and global air-sea flux estimates is to account for bubble entrainment, sea spray, and foam formation by breaking waves. Estimation of the whitecap fraction improves regional and global sea spray production estimates and consequent impacts on CO_2 fluxes (Anguelova, 2016). Two main approaches are used to estimate the whitecap/foam fraction from space: (i) parameterisation based on the available wind speed measurements, and (ii) direct retrieval from the brightness temperature measured by microwave radiometers (Anguelova and Webster, 2006; Albert et al., 2016; Anguelova, 2016; Yin et al., 2016). The first approach is limited by the fact that numerous factors, in addition to wind, influence foam formation. The second one is more promising but also arduous, due to the large variability in dielectric properties of foam itself. Novel and future space missions with improved capabilities, such as the SMAP satellite (launched in the beginning of 2015), may improve sea surface wind speed retrievals at very high intensities under tropical storms (>30 m s^{-1}) based on the low frequency L-band (Meissner et al., 2017). This potential should also encourage further studies for whitecap fraction estimates under severe weather conditions which, although more spatially restricted, may have significant impacts on global fluxes due to the intensity of the exchange processes.

Another potential source of surface turbulence that may significantly impact air-sea fluxes at regional and global scales is the effect of rain drops on the ocean surface (Ashton et al., 2016). Rain rate can be inferred using infrared and microwave radiometric sensors and used to scale rain-induced surface turbulence. The challenge is to obtain accurate rainfall estimates due to the complexity of the measurement (see discussions in Section 3.2.1). Further efforts combining passive infrared, microwave, and active radar measurements should provide more insights into cloud microphysics and improve global rainfall, and hence air-sea flux estimates. Another benefit of passive microwave sensors is their utility to monitor sea-ice extent, which plays a critical role in sea-atmosphere exchange processes. The retrievals are based on changes of the brightness temperature due to emissivity differences of sea ice (including type, age) and the ocean surface. Despite the coarse spatial resolution (~25 km), the historical satellite dataset of sea-ice properties reaches down to 1973 with the Nimbus-5 mission (NASA), providing a long-term record for detecting changes and understanding feedback responses in the exchange processes.

3.3.2 Visible and near-infrared sensors

Active satellite sensors such as scatterometers, altimeters, or synthetic aperture radars (SAR) have been extensively used to detect wind speed and direction, as well as wave heights (Shutler et al., 2016). Passive spectroradiometers have been underutilized for such observations but could be further exploited to retrieve sea surface characteristics (e.g., wave spectrum) and related wind speed out of sun-glint observations (Harmel, 2016; Kudryavtsev et al., 2017a). That passive radiometric measurements are limited by the need for cloud-free conditions, daylight, and proper observation geometry is worth remembering. This limitation is the major disadvantage in comparison to SAR sensors, for example, which are capable of observing the sea surface under all-weather conditions throughout the diel cycle. However, radiometers do not suffer from the speckle noise characteristics of coherent SAR observations, thus allowing better observation of weaker features. Furthermore, radiometers provide an extensive dataset with worldwide coverage at a spatial resolution on the order of a kilometre (e.g., SeaWiFS, MODIS) down to a few meters (e.g., Pleiades, Spot, Landsat series, Sentinel-2). Therefore, low-to-high resolution optical images can be used independently or as a useful complement to active techniques for retrieving surface winds and sea roughness to better constrain near-surface oceanic turbulence.

Physically, sun glint is defined as the peak of intensity due to the sunlight reflection on the rough sea surface occurring in the vicinity of the theoretical location of the specular reflection spot that would be obtained for a flat sea (i.e., a mirror-like surface). The full sun-glint area is spread by a myriad of glints generated by reflection of sunlight on the facets of the water surface that are tilted toward the observer (Torrance et al., 1966) (**Figure 11**). Thus, the sun-glint region contains valuable information on the sea surface roughness, which can be expressed through quasi-specular scattering theory (Cox and Munk, 1954; Munk, 2009). The variations of the surface roughness induce specific patterns of the sun glint highlighting small-scale geophysical phenomena (**Figure 11a**) and the presence of biogenic slicks (**Figure 11b**). **Figure 11c–d** displays different geophysical patterns (slicks, eddies, wave packets, etc.) accessible via passive optical remote sensing thanks to the presence of sun glint over the image.

Based on the sun-glint characteristics, some studies have focused on turning the ocean glint signal into useful information for estimating some geophysical parameters of interest, including microphysical and optical properties of aerosols (Kaufman et al., 2002; Ottaviani et al., 2013), submarine topography (Shao et al., 2011), internal

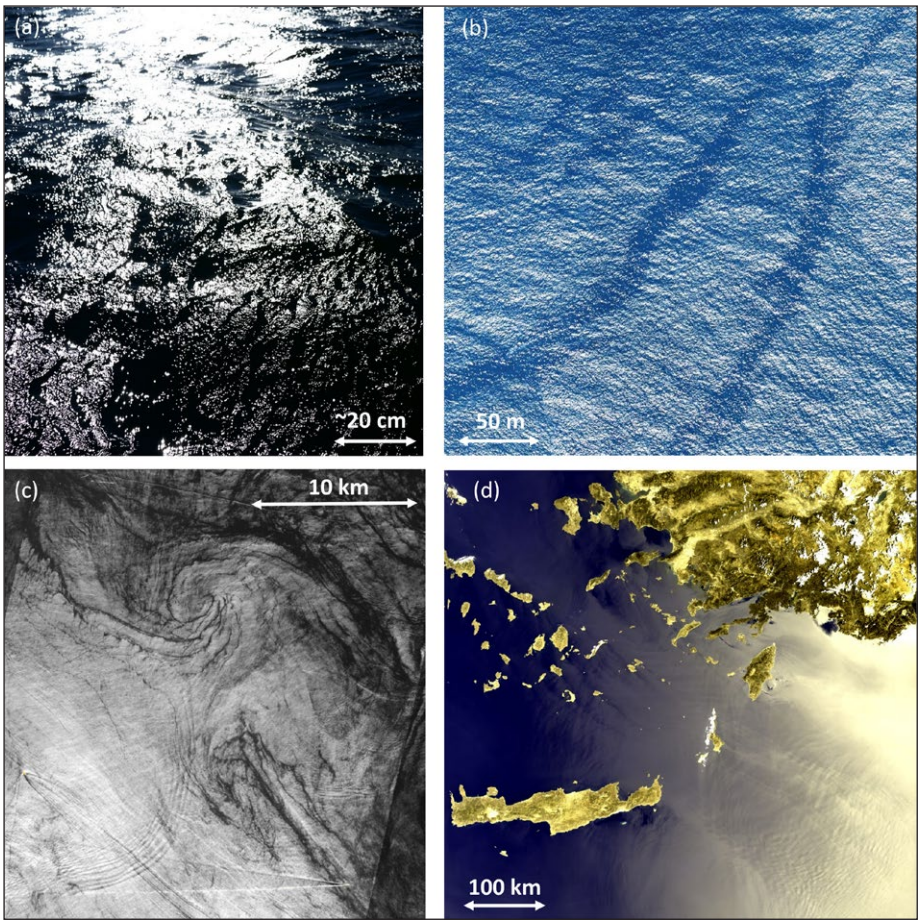

Figure 11: Examples of sun-glint patterns at different spatial scales. (a) Image of the sea surface under gust wind conditions taken from a reflex digital camera. **(b)** Aerial photography of sea surface with visible surfactant filaments. **(c)** Sentinel-2A image (4 July 2015) in the 2190-nm channel where sun glint is the most intense signal over water; the sun-glint patterns highlight some geophysical phenomena such as eddies, ship wakes, and wave packets; **(d)** Sentinel-3 RGB image (10 May 2016) over the eastern Mediterranean Sea; high sun glint is readily visible on the right side of the image. DOI: https://doi.org/10.1525/elementa.331.f11

waves (Jackson, 2007), extent of oil spills (Hu, 2011; Lu et al., 2016), and wind speed (Wald and Monget, 1983; O'Brien and Mitchell, 1988; Harmel and Chami, 2012). With regards to momentum transfer across the air-sea boundary, short gravity and capillary waves are the most interesting. Fortunately, intensity and spread of the sun glitter are mostly generated by those short waves. The links between sun glint and the dynamic mechanisms at the sea surface therefore offer practical means for optically sensing some of the turbulence-related parameters. Toward this goal, recent studies showed that decametre spatial resolution sensors, such as MSI/Sentinel-2 or OLI/Landsat-8, can be exploited to derive surface roughness and correlated sub-surface currents from pixels impacted by sun glint (Kudryavtsev et al., 2017a, 2017b). In this case, the wave mean square slope is estimated and could be used as a suitable alternative to wind speed for estimating air-sea transfer velocity (e.g., Goddijn-Murphy et al., 2013).

Hyperspectral radiance data obtained in the VIS/NIR from future missions, such as the Ocean Colour Imager (OCI) on-board the planned NASA/PACE mission, will offer other information of interest to characterizing ocean surface properties. More precisely, substances that float on ocean surfaces change the spectrum of light reflected by clean ocean surfaces. In general, they will increase the ocean surface brightness, which can be mistaken for aerosol scattering contributions in space-borne observations, as is a recognized problem for whitecaps (Gordon, 1997). However, these floating substances may also have absorption bands at specific wavelengths that manifest themselves as 'dips' in hyperspectral remote sensing observations. For example, Garaba and Dierssen (2018) found that marine-harvested macro- and microplastics show distinct absorption bands. Two of these bands (1215 and 1732 nm) occur in atmospheric windows and can therefore be noticed in space-borne observations. Floating material can also have reflectance dips in bands coinciding with enhanced liquid water absorption. Dierssen et al. (2015) used the band depth at 990 nm to estimate the age of floating seagrass from airborne hyperspectral imagery. Recent studies have also identified near infrared liquid water absorption bands in reflectance spectra of foam and whitecaps resulting from multiple scattering in and around the bubbles of whitecaps (HM Dierssen, personal communication). The whitecap absorption band at 980 nm lies at the edge of an atmospheric window, which implies that it can be noticed in

space-borne observations. Hence, hyperspectral remote sensing with appropriate spectral and spatial resolution allows for developing novel methods to identify and retrieve whitecaps and various types of floating vegetation and debris.

3.3.3 Polarimetric and multidirectional sensors

Direct sunlight, originally unpolarised, becomes partially polarised after reflection off the sea surface (Kattawar, 2013). Polarimetric measurements therefore can provide additional information to better discriminate the sun-glint signal from space (Harmel, 2016). As for intensity, the polarisation signal of sun glint is highly directional. The use of multi-angular (or multidirectional) data is most suitable for exploitation of remotely sensed sun glint in the marine environment (Harmel and Chami, 2013).

The sun-glint radiance as measured by a satellite sensor depends on the reflectivity of the air-sea interface and the atmospheric transmission. The former is highly directional and controlled by both the wave facet orientations and the refractive index of the sea surface. For example, oil slicks change the wave facet orientations and the surface refractive index. The resulting change in surface reflectivity has been exploited in multi-angular data obtained by MISR to detect oil slicks (Chust and Sagarminaga, 2007). The water refractive index is slightly variable over the VIS/NIR spectral range (e.g., by a few percent), but this small spectral variation can induce much more significant variation in the surface reflectivity (over 30%) and thus on the sun-glint signal (Harmel et al., 2018). The atmospheric transmission is modulated by the aerosol load and type. Therefore, for remote sensing applications, multispectral and multidirectional capabilities offer important information on aerosol optical properties and on the surface properties (Ottaviani et al., 2013).

The first advantage of polarimetric multidirectional sensors comes from the capability of acquiring the polarised optical signal within and outside the sun-glint influence for the same sea surface target. In this manner, atmospheric optical properties can be assessed from the viewing directions outside of the glitter. Here, the ability to measure the Stokes vector of light (i.e., polarisation state) is a significant asset to retrieve the aerosol optical properties more accurately (Mishchenko et al., 2007). Then, these retrieved optical properties might be used to correct the signal measured for the viewing directions impacted by the sun-glint contribution. After such a correction, the sun-glint signal can be quantified for a given geometry of observation. The second advantage of multidirectional measurements is the possibility to repeat this sun-glint radiance estimation for a series of distinct viewing geometries. Such multidirectional sun-glint data could allow reconstruction of the BRDF of the air-sea interface, which provides information on the sea surface roughness and could further help estimate the transfer coefficient k (Lin et al., 2016).

Bréon and Henriot (2006) showed, based on the multidirectional POLDER-1 mission (1996–1997), that the sun-glint radiance might be exploited to characterize the sea surface wind accurately. Harmel and Chami (2012, 2013) expanded those results by exploiting the polarisation, in addition to the radiance signal, to estimate sea surface wind speed from the PARASOL satellite (2005–2013). This method provides wind speed at the native spatial resolution of PARASOL (i.e., ~6 km) for more than 75% of the PARASOL swath and can be used to obtain a global assessment of the "clear sky" wind speed distribution (**Figure 12**). However, wind direction is not resolved by this method partly due to the limited number of directional observations per pixel (~14). A way to increase the

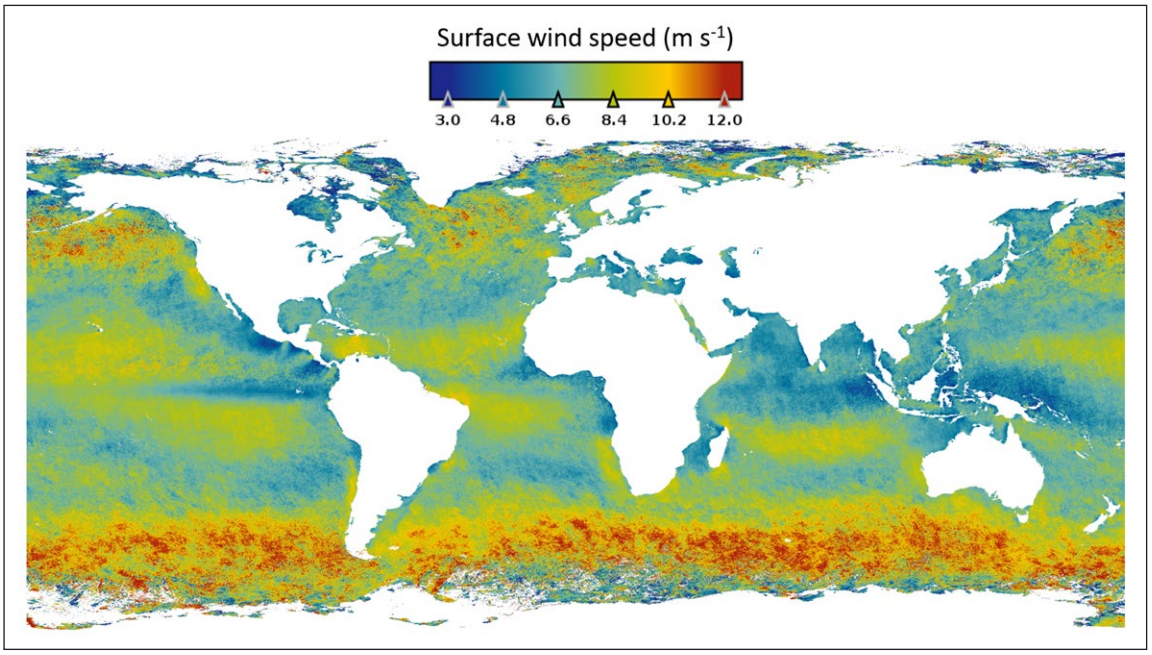

Figure 12: Global wind speed fields derived from the sun-glint signal. Annual average of the sea surface wind speed for 2007 obtained from inversion of the sun-glint signal measured by PARASOL for clear sky conditions (data available from ICARE/CNES). DOI: https://doi.org/10.1525/elementa.331.f12

number of available directions to scan the directional patterns of sun-glint reflectance would be to consider several contiguous pixels within the image. In such a way, appropriate inversion algorithms could be able to fully retrieve the wind vector components in preparation for the next 3MI mission.

As already mentioned, the surfactant-enriched microlayer increases the surface tension of the air-sea interface, modifying sea surface roughness and, in turn, the sun-glint signal. On the other hand, surfactant compounds have a refractive index significantly higher than bulk sea water (Decho et al., 2003). The presence of natural or anthropogenic surfactants in the microlayer therefore affects both the intensity and the polarisation state of the sun-glint signal. Recent studies showed that space-borne polarimetric measurements of sun glint can be used to estimate the presence of oil slicks from the change in refractive index between oiled and oil-free waters (Ottaviani et al., 2012; Lu et al., 2017). However, further studies are required to demonstrate whether this method could be applied to the detection of natural surfactants in order to provide estimations of the surfactant distributions and their impacts on the air-sea exchange processes at the global scale.

4 Challenges and opportunities in addressing science questions on ocean-atmosphere interactions using remote sensing

In this paper we have provided a review and future perspectives for the use of remote sensing technologies to study two key aspects of ocean-atmosphere interaction science: (1) the extent to which upper-ocean biology affects the composition and radiative properties of the marine boundary layer; and (2) the extent to which upper-ocean turbulence drives fluxes of mass and energy at the air-sea interface. Remote sensing is an outstanding tool for addressing these questions because it provides synoptic, multiscale, and long-term information on key physical-chemical-biological properties of the ocean-atmosphere system. Thanks to continued technological advances, we can probe the ocean-atmosphere system with ever-growing capacity in terms of available techniques, spatial-temporal-spectral resolution, measurement accuracy and stability, and data processing and storage capabilities. To transform this wealth of historical and upcoming observations into predictive understanding, oceanic and atmospheric scientists, as well as engineers, observational scientists and modellers, should routinely work in closer collaboration. Only interdisciplinary observational and data exploitation frameworks can significantly improve approaches to solve the two SOLAS research questions that motivated this review.

First, there is a need to overcome the traditional separation in the retrieval of atmosphere and ocean signals, and to integrate observations from various types of sensors and platforms. A model of the latter is the GRASP algorithm (Dubovik et al., 2014), which currently enables a simultaneous highly accurate retrieval of aerosol and land surface properties using spectral, multi-angular polarimetric remote sensing observations. We envision an extended GRASP-type framework that could solve for aerosol and hydrosol characteristics given near-simultaneous independent measurements of radiometry, polarimetry and lidar. In this way, a coherent retrieval of sea surface organic materials, atmospheric particles and cloud properties would be achieved. This approach would benefit from the high complementarity between passive radiometers, lidar, and polarimeters, in terms of both the optical characterisation capacity and the different spatial scales and dimensions resolved. Such a framework would largely contribute toward answering question (1).

A similar approach would be useful to address question (2). For example, space-borne retrievals of the sea surface wave spectrum, from capillary waves through gravity waves and swell, could be constrained by combining passive radiometry in the visible and near-infrared (i.e., sun-glint) and passive and active microwave sensors. Combined with retrievals of sea surface slicks, whitecaps, rain rate, sea ice, and buoyancy fluxes (driven by temperature and salinity), this approach would enable a much more accurate estimation of turbulent kinetic energy and bubble-mediated fluxes of gases and particles.

Beyond the retrieval process, we need innovative frameworks for data management, access and analysis. Space-borne sensors produce huge (and rapidly growing) amounts of data, such that handling and analysis with traditional systems and techniques will become increasingly challenging, being a clear example of a big data problem. Widespread implementation of big data approaches, like NOAA's Big Data Project (http://www.noaa.gov/big-data-project), will improve our ability to utilise remote sensing data to study the ocean-atmosphere interface while leveraging the observational efforts. For example, such approaches can greatly facilitate the task of sorting/controlling observations by meteorological state, aerosol type (pristine marine vs. continental influence), cloud type, and ocean ecosystem state, in order to separate ecosystem influences from other effects (e.g., McCoy et al., 2015). The on-going revolution in artificial intelligence and machine learning techniques is poised to play a key role in the development of remote sensing applications for the Earth Sciences (Lary et al., 2016). Efficient exploitation of multisensor datasets and extensive data mining can lead to new discoveries based on statistical relationships, which should ultimately result in better mechanistic understanding and predictive power.

Going a step further, we also envision data exploration platforms that simplify the task of tracking air and water mass trajectories as they are advected, an approach called Lagrangian tracking. Such tracking is currently done using models such as HYSPLIT (Stein et al., 2015) and by analysing sequences of satellite images (Lehahn et al., 2018). Analysing temporal changes in oceanic and atmospheric parameters in a Lagrangian manner greatly improves the ability to link statistically the history of particles at one side of the air-sea interface with those on the other side, revealing processes and suggesting productive avenues for future research. Satellite-based Lagrangian diagnostic tools were shown to be very useful in quantifying the dynamics of phytoplankton blooms (Lehahn et al., 2017), cloud fields (Koren and Feingold, 2013) and marine

aerosols (Lehahn et al., 2014) over time scales ranging from days to months. Such a modelling framework would be most informative if utilized simultaneously with in-situ measurements of aerosol properties and marine aerosol precursors over the relevant spatial-temporal scales.

Breakthroughs in ocean-atmosphere studies may also result from new in-situ observation platforms. Paralleling the revolution brought about by the ARGO autonomous floats to observe ocean circulation and heat content (Riser et al., 2016) and biogeochemistry (Claustre et al., 2010; Sauzède et al., 2017), autonomous platforms operating at the air-sea interface are being proposed. Examples include the Wave Glider (Krug et al., 2018), Saildrones (Cross et al., 2015) and a so-called "flying sailboat", a wind-powered drone, inspired by the albatross, which operates between 1 and 10 m above the air-sea interface (Gabriel Bousquet, personal communication). Such autonomous platforms would allow in-situ observation of fine-scale ocean-atmosphere interactions, and a swarm of them could bridge the gap between local (e.g., ship-based) and space-borne observations.

5 Summary

We hereby summarize this paper in eight key points.

I. Remote sensing from space offers practical means to upscale our understanding of ocean-atmosphere interactions from local to global scales. Essential to this upscaling is to (1) improve retrievals of the abundance, size spectrum and composition of particle assemblages in both the ocean and the atmosphere, and of dissolved organic matter, foams and bubbles at the ocean surface; (2) improve retrievals of sea-air interfacial turbulence and sea state at all relevant scales, and identify relevant sources of turbulence beyond wind stress; and (3) improve mechanistic models that link remotely observed properties and locally measured processes.

II. A wide range of observation platforms and techniques can be used to better understand ocean-atmosphere interactions, including passive and active sensors (e.g., radiometer, lidar, radar) sounding both intensity and polarisation characteristics of the electromagnetic field; we advocate for synergies between these remote sensing observations to better tackle multidisciplinary ocean-atmosphere science questions. Such synergies require (1) theoretical advances in the radiative transfer models in use for simultaneous retrieval of atmosphere-ocean properties, (2) merging multi-sensor and multiplatform datasets using advanced data assimilation schemes, (3) further developing user- and problem-oriented geophysical datasets, and (4) jointly exploiting space-borne sensors with in-situ data sets (acquired from ships or autonomous platforms) using newly developed artificial intelligence methods and facilities. This last point could help disentangle potential complex relationships between these two kinds of data sets, thereby furthering satellite retrieval algorithms.

III. Upcoming developments in passive radiometry include the launch of hyperspectral sensors and the extension into UV wavelengths. In the ocean, these developments will enhance (1) the simultaneous retrieval of algal pigments, non-algal particles, and coloured dissolved organic matter; (2) the differentiation between several particle functional types and size classes; and (3) the estimation of phytoplankton physiological state; and will perhaps enable (4) detection of zooplankton grazing, discrimination among different types of coloured dissolved organic matter, and assessment of the bulk dissolved carbon pool. In the atmosphere, hyperspectral and UV sensors will enhance (1) the discrimination of aerosol types, size classes and associated optical properties; and (2) the retrieval accuracy for cloud micro- and macro-physical properties.

IV. Multi-angle multispectral polarimetry largely enhances the accuracy in retrievals of atmospheric and oceanic particle concentration, size and shape distribution, and scattering and absorption characteristics, as well as sea surface roughness and wind speed. Planned instruments will provide better spatial coverage and resolution and more polarisation channels. This will enhance the retrieval of ocean signals, which were not explicitly targeted in previous missions.

V. Lidar offers an unmatched skill to resolve the vertical profiles of distinct particle populations. In the atmosphere, this skill allows the observation of multi-layered cloud and aerosol properties, which has powered breakthroughs in our understanding of aerosol transport and aerosol-cloud interactions. Current space-borne lidar provides year-round estimates of vertically averaged concentration of the subsurface particles independently of solar illumination and the presence of thin/scattered clouds. Future generations of ocean-optimised lidar satellites will also enable vertical profiling of the upper water column.

VI. Active microwave techniques provide all-weather observations of sea surface roughness and derived variables. Space-borne scatterometers and altimeters have provided a decades-long record of wind speed, widely used to determine sea-air gas exchange under simplifying assumptions. Microwave techniques are now increasingly used to obtain an integral view of interfacial turbulence, directly related to the wave spectrum, bubbles, foams, whitecaps, surfactants and rain. Recently launched synthetic aperture radars (SAR) offer an unmatched capacity to resolve these processes with extremely high resolution across multiple scales.

VII. Passive observations of the infrared and microwave signal from the sea skin have provided decades-long, accurate records of sea surface temperature and wind speed. They are now complemented by passive microwave retrieval of sea surface salinity, better resolving buoyancy fluxes and therefore convection-driven turbulence. Though less exploited, the sun-glint signal in the visible and

near-infrared (both radiometric and polarimetric) provides a powerful means to retrieve sea surface roughness (and thus turbulence-related parameters) at multiple scales.

VIII. The aforementioned advances are accompanied by growing constellations of polar-orbiting satellites with wide swaths, geostationary sensors with capacity to resolve diurnal cycles, and generalized increases in spatial resolution. Synergistic use of these datasets will soon enable the routine retrieval of a large variety of 3D geophysical fields with high resolution. Combined with powerful computational frameworks, such synergies should produce a leap forward in the understanding, modelling, and prediction of ocean-atmosphere interactions.

Acknowledgements

We would like to thank all other participants to the ESA/SOLAS workshop held at ESA-ESRIN in Frascati, Italy, 13–15 June 2016: Paulo Artaxo, Vittorio Brando, Cristina Facchini, Véronique Garçon, Roberto Sabia, Eric Saltzman, Yeala Shaked and Knut Stamnes. We thank Macarena Ortiz and one anonymous reviewer for their insightful comments, which helped improve an earlier version on the manuscript.

Funding information

Support for the workshop was provided by the European Space Agency (ESA), the Scientific Committee for Ocean Research (SCOR), the Surface Ocean-Lower Atmosphere Study (SOLAS), and the International Geosphere-Biosphere Programme (IGBP). The participation of NASA scientists was supported by NASA.

Competing interests

The authors have no competing interests to declare.

Author contributions

G.N. led section 2, T.H. led section 3, M.G. led sections 4 and 5. I.K., E.B., and L.M. led section 1. C.H. and Y.H. contributed on lidar remote sensing, O.D., P.L. and J.C. contributed on polarimetry, C.J. contributed on atmospheric correction of ocean colour satellite data, N.R. contributed on active microwave and passive infrared and microwave remote sensing, and A.S. on passive aerosol, cloud, and SST remote sensing and acronym lists. All authors contributed to the writing. All authors approved the submitted version of the publication.

References

Ahmad, Z, Franz, BA, McClain, CR, Kwiatkowska, EJ, Werdell, J, Shettle, EP and **Holben, BN.** 2010. New aerosol models for the retrieval of aerosol optical thickness and normalized water-leaving radiances from the SeaWiFS and MODIS sensors over coastal regions and open oceans. *Appl Opt* **49**(29): 5545. DOI: https://doi.org/10.1364/AO.49.005545

Albert, MFMA, Anguelova, MD, Manders, AMM, Schaap, M and **de Leeuw, G.** 2016. Parameterization of oceanic whitecap fraction based on satellite observations. *Atmos Chem Phys* **16**(21): 13725–13751. DOI: https://doi.org/10.5194/acp-16-13725-2016

Albrecht, BA. 1989. Aerosols, Cloud Microphysics, and Fractional Cloudiness. *Science (80-)* **245**(4923).

Alexandrov, MD, Cairns, B, van Diedenhoven, B, Ackerman, AS, Wasilewski, AP, McGill, MJ, Yorks, JE, Hlavka, DL, Platnick, SE and **Arnold, GT.** 2016. Polarized view of supercooled liquid water clouds. *Remote Sens Environ* **181**: 96–110. DOI: https://doi.org/10.1016/j.rse.2016.04.002

Alvain, S, Moulin, C, Dandonneau, Y and **Bréon, FM.** 2005. Remote sensing of phytoplankton groups in case 1 waters from global SeaWiFS imagery. *Deep Sea Res Part I Oceanogr Res Pap* **52**(11): 1989–2004. DOI: https://doi.org/10.1016/j.dsr.2005.06.015

Anderson, TL, Charlson, RJ, Winker, DM, Ogren, JA and **Holmén, K.** 2003. Mesoscale Variations of Tropospheric Aerosols. *J Atmos Sci* **60**(1): 119–136. DOI:https://doi.org/10.1175/1520-0469(2003)060<0119:MVOTA>2.0.CO;2

Andreae, MO and **Rosenfeld, D.** 2008. Aerosol – cloud – precipitation interactions. Part 1. The nature and sources of cloud-active aerosols. *Earth-Science Rev* **89**(1–2): 13–41. DOI: https://doi.org/10.1016/j.earscirev.2008.03.001

Anguelova, MD. 2016. Assessing the utility of satellite-based whitecap fraction to estimate sea spray production and CO_2 transfer velocity. *IOP Conf Ser Earth Environ Sci* **35**: 012002. DOI: https://doi.org/10.1088/1755-1315/35/1/012002

Anguelova, MD and **Webster, F.** 2006. Whitecap coverage from satellite measurements: A first step toward modeling the variability of oceanic whitecaps. *J Geophys Res* **111**(C03): C03–017. DOI: https://doi.org/10.1029/2005JC003158

Ardhuin, F, Gille, ST, Menemenlis, D, Rocha, CB, Rascle, N, Chapron, B, Gula, J and **Molemaker, J.** 2017. Small-scale open ocean currents have large effects on wind wave heights. *J Geophys Res Ocean* **122**(6): 4500–4517. DOI: https://doi.org/10.1002/2016JC012413

Arnold, SR, Spracklen, DV, Gebhardt, S, Custer, T, Williams, J, Peeken, I and **Alvain, S.** 2010. Relationships between atmospheric organic compounds and air-mass exposure to marine biology. *Environ Chem* **7**(3): 232. DOI: https://doi.org/10.1071/EN09144

Arnold, SR, Spracklen, DV, Williams, J, Yassaa, N, Sciare, J, Bonsang, B, Gros, V, Peeken, I, Lewis, AC, Alvain, S and **Moulin, C.** 2009. Evaluation of the global oceanic isoprene source and its impacts on marine organic carbon aerosol. *Atmos Chem Phys* **9**: 1253–1262. DOI: https://doi.org/10.5194/acp-9-1253-2009

Asher, WE. 1997. The sea-surface microlayer and its effect on global air-sea gas transfer. In: Liss, PS and Duce, R (eds.), *The Sea Surface and Global Change*, 251–286. DOI: https://doi.org/10.1017/CBO9780511525025.009

Ashton, IG, Shutler, JD, Land, PE, Woolf, DK and **Quartly, GD.** 2016. A sensitivity analysis of the impact of rain on regional and global sea-air fluxes of CO_2. *PLoS One* **11**(9): e0161105. DOI: https://doi.org/10.1371/journal.pone.0161105

Babin, M and **Stramski, D.** 2002. Light absorption by aquatic particles in the near-infrared spectral region. *Limnol Oceanogr* **47**(3): 911–915. DOI: https://doi.org/10.4319/lo.2002.47.3.0911

Bailey, SW, Franz, BA and **Werdell, PJ.** 2010. Estimation of near-infrared water-leaving reflectance for satellite ocean color data processing. *Opt Express* **18**(7): 7521. DOI: https://doi.org/10.1364/OE.18.007521

Baum, BA, Menzel, WP, Frey, RA, Tobin, DC, Holz, RE, Ackerman, SA, Heidinger, AK, Yang, P, Baum, BA, Menzel, WP, Frey, RA, Tobin, DC, Holz, RE, Ackerman, SA, Heidinger, AK and **Yang, P.** 2012. MODIS Cloud-Top Property Refinements for Collection 6. *J Appl Meteorol Climatol* **51**(6): 1145–1163. DOI: https://doi.org/10.1175/JAMC-D-11-0203.1

Becagli, S, Lazzara, L, Marchese, C, Dayan, U, Ascanius, SE, Cacciani, M, Caiazzo, L, Di Biagio, C, Di Iorio, T, di Sarra, A, Eriksen, P, Fani, F, Giardi, F, Meloni, D, Muscari, G, Pace, G, Severi, M, Traversi, R and **Udisti, R.** 2016. Relationships linking primary production, sea ice melting, and biogenic aerosol in the Arctic. *Atmos Environ* **136**: 1–15. DOI: https://doi.org/10.1016/j.atmosenv.2016.04.002

Behrenfeld, MJ. 2010. Abandoning Sverdrup's Critical Depth Hypothesis on phytoplankton blooms. *Ecology* **91**(4): 977–989. DOI: https://doi.org/10.1890/09-1207.1

Behrenfeld, MJ and **Boss, ES.** 2018. Student's tutorial on bloom hypotheses in the context of phytoplankton annual cycles. *Glob Chang Biol* **24**(1): 55–77. DOI: https://doi.org/10.1111/gcb.13858

Behrenfeld, MJ, Hu, Y, Hostetler, CA, Dall'Olmo, G, Rodier, SD, Hair, JW and **Trepte, CR.** 2013. Space-based lidar measurements of global ocean carbon stocks. *Geophys Res Lett* **40**(16): 4355–4360. DOI: https://doi.org/10.1002/grl.50816

Behrenfeld, MJ, Hu, Y, O'Malley, RT, Boss, ES, Hostetler, CA, Siegel, DA, Sarmiento, JL, Schulien, J, Hair, JW, Lu, X, Rodier, S and **Scarino, AJ.** 2017. Annual boom–bust cycles of polar phytoplankton biomass revealed by space-based lidar. *Nat Geosci* **10**(2): 118–122. DOI: https://doi.org/10.1038/ngeo2861

Behrenfeld, MJ, Westberry, TK, Boss, ES, O'Malley, RT, Siegel, DA, Wiggert, JD, Franz, BA, McClain, CR, Feldman, GC, Doney, SC, Moore, JK, Dall'Olmo, G, Milligan, AJ, Lima, I and **Mahowald, N.** 2009. Satellite-detected fluorescence reveals global physiology of ocean phytoplankton. *Biogeosciences* **6**(5): 779–794. DOI: https://doi.org/10.5194/bg-6-779-2009

Benas, N, Chrysoulakis, N and **Giannakopoulou, G.** 2013. Validation of MERIS/AATSR synergy algorithm for aerosol retrieval against globally distributed AERONET observations and comparison with MODIS aerosol product. *Atmos Res* **132–133**: 102–113. DOI: https://doi.org/10.1016/j.atmosres.2013.05.011

Bodas-Salcedo, A, Hill, PG, Furtado, K, Williams, KD, Field, PR, Manners, JC, Hyder, P and **Kato, S.** 2016. Large Contribution of Supercooled Liquid Clouds to the Solar Radiation Budget of the Southern Ocean. *J Clim* **29**(11): 4213–4228. DOI: https://doi.org/10.1175/JCLI-D-15-0564.1

Bourassa, M, Bonekamp, H, Chang, P, Chelton, D, Courtney, J, Edson, R, Figa, J, He, Y, Hersbach, H and **Hilburn, K.** 2010a. Remotely sensed winds and wind stresses for marine forecasting and ocean modeling. Hall, J, Harrison, DE and Stammer, D (eds.), *Proceedings of OceanObs* **9**(1). DOI: https://doi.org/10.5270/OceanObs09.cwp.08

Bourassa, M, Gille, S, Jackson, D, Roberts, JB and **Wick, G.** 2010b. Ocean Winds and Turbulent Air-Sea Fluxes Inferred From Remote Sensing. *Oceanography* **23**(4): 36–51. DOI: https://doi.org/10.5670/oceanog.2010.04

Boutin, J, Martin, N, Reverdin, G, Morisset, S, Yin, X, Centurioni, L and **Reul, N.** 2014. Sea surface salinity under rain cells: SMOS satellite and in situ drifters observations. *J Geophys Res Ocean*: 5533–5545. DOI: https://doi.org/10.1002/2014JC010070. Received.

Bracher, A, Bouman, HA, Brewin, RJW, Bricaud, A, Brotas, V, Ciotti, AM, Clementson, L, Devred, E, Di Cicco, A, Dutkiewicz, S, Hardman-Mountford, NJ, Hickman, AE, Hieronymi, M, Hirata, T, Losa, SN, Mouw, CB, Organelli, E, Raitsos, DE, Uitz, J, Vogt, M and **Wolanin, A.** 2017. Obtaining Phytoplankton Diversity from Ocean Color: A Scientific Roadmap for Future Development. *Front Mar Sci* **4**: 55. DOI: https://doi.org/10.3389/fmars.2017.00055

Breon, FM and **Henriot, N.** 2006. Spaceborne observations of ocean glint reflectance and modeling of wave slope distributions. *J Geophys Res* **111**: C06005. DOI: https://doi.org/10.1029/2005JC003343

Brévière, E and **the SOLAS Scientific Steering Committee.** 2016. SOLAS 2015-2025: Science Plan and Organisation. Kiel, Germany.

Brévière, EHG, Bakker, DCE, Bange, HW, Bates, TS, Bell, TG, Boyd, PW, Duce, RA, Garçon, V, Johnson, MT, Law, CS, Marandino, CA, Olsen, A, Quack, B, Quinn, PK, Sabine, CL and **Saltzman, ES.** 2015. Surface ocean-lower atmosphere study: Scientific synthesis and contribution to Earth system science. *Anthropocene* **12**: 54–68. DOI: https://doi.org/10.1016/j.ancene.2015.11.001

Bricaud, A, Ciotti, AM and **Gentili, B.** 2012. Spatial-temporal variations in phytoplankton size and colored detrital matter absorption at global and regional scales, as derived from twelve years of SeaWiFS data (1998–2009). *Global Biogeochem Cycles* **26**: GB1010. DOI: https://doi.org/10.1029/2010GB003952

Bricaud, A, Claustre, H, Ras, J and **Oubelkheir, K.** 2004. Natural variability of phytoplanktonic absorption in oceanic waters: Influence of the size structure of

algal populations. *J Geophys Res* **109**(C11): C11010. DOI: https://doi.org/10.1029/2004JC002419

Brooks, SD and **Thornton, DCO.** 2018. Marine Aerosols and Clouds. *Ann Rev Mar Sci* **10**: 289–313. DOI: https://doi.org/10.1146/annurev-marine-121916-063148

Burkart, J, Willis, MD, Bozem, H, Thomas, JL, Law, K, Hoor, P, Aliabadi, AA, Köllner, F, Schneider, J, Herber, A, Abbatt, JPD and **Leaitch, WR.** 2017. Summertime observations of elevated levels of ultrafine particles in the high Arctic marine boundary layer. *Atmos Chem Phys* **17**(8): 5515–5535. DOI: https://doi.org/10.5194/acp-17-5515-2017

Burrows, SM, Ogunro, O, Frossard, AA, Russell, LM, Rasch, PJ and **Elliott, SM.** 2014. A physically based framework for modeling the organic fractionation of sea spray aerosol from bubble film Langmuir equilibria. *Atmos Chem Phys* **14**(24): 13601–13629. DOI: https://doi.org/10.5194/acp-14-13601-2014

Burton, SP, Ferrare, RA, Hostetler, CA, Hair, JW, Rogers, RR, Obland, MD, Butler, CF, Cook, AL, Harper, DB and **Froyd, KD.** 2012. Aerosol classification using airborne High Spectral Resolution Lidar measurements – methodology and examples. *Atmos Meas Tech* **5**(1): 73–98. DOI: https://doi.org/10.5194/amt-5-73-2012

Burton, SP, Ferrare, RA, Vaughan, MA, Omar, AH, Rogers, RR, Hostetler, CA and **Hair, JW.** 2013. Aerosol classification from airborne HSRL and comparisons with the CALIPSO vertical feature mask. *Atmos Meas Tech* **6**(5): 1397–1412. DOI: https://doi.org/10.5194/amt-6-1397-2013

Burton, SP, Hair, JW, Kahnert, M, Ferrare, RA, Hostetler, CA, Cook, AL, Harper, DB, Berkoff, TA, Seaman, ST, Collins, JE, Fenn, MA and **Rogers, RR.** 2015. Observations of the spectral dependence of linear particle depolarization ratio of aerosols using NASA Langley airborne High Spectral Resolution Lidar. *Atmos Chem Phys* **15**(23): 13453–13473. DOI: https://doi.org/10.5194/acp-15-13453-2015

Burton, SP, Vaughan, MA, Ferrare, RA and **Hostetler, CA.** 2014. Separating mixtures of aerosol types in airborne High Spectral Resolution Lidar data. *Atmos Meas Tech* **7**(2): 419–436. DOI: https://doi.org/10.5194/amt-7-419-2014

Carder, KL, Steward, RG, Harvey, GR and **Ortner, PB.** 1989. Marine humic and fulvic acids: Their effects on remote sensing of ocean chlorophyll. *Limnol Oceanogr* **34**(1): 68–81. DOI: https://doi.org/10.4319/lo.1989.34.1.0068

Carpenter, LJ, Archer, SD and **Beale, R.** 2012. Ocean-atmosphere trace gas exchange. *Chem Soc Rev* **41**: 6473–6505. DOI: https://doi.org/10.1039/c2cs35121h

Carpenter, SR, Elser, MM and **Elser, JJ.** 1986. Chlorophyll production, degradation, and sedimentation: Implications for paleolimnology. *Limnol Oceanogr* **31**(1): 112–124. DOI: https://doi.org/10.4319/lo.1986.31.1.0112

Ceburnis, D, Masalaite, A, Ovadnevaite, J, Garbaras, A, Remeikis, V, Maenhaut, W, Claeys, M, Sciare, J, Baisnée, D and **O'Dowd, CD.** 2016. Stable isotopes measurements reveal dual carbon pools contributing to organic matter enrichment in marine aerosol. *Sci Rep* **6**: 36675. DOI: https://doi.org/10.1038/srep36675

Chami, M and **McKee, D.** 2007. Determination of biogeochemical properties of marine particles using above water measurements of the degree of polarization at the Brewster angle. *Opt Express* **15**(15): 9494. DOI: https://doi.org/10.1364/OE.15.009494

Chami, M and **Platel, MD.** 2007. Sensitivity of the retrieval of the inherent optical properties of marine particles in coastal waters to the directional variations and the polarization of the reflectance. *J Geophys Res* **112**(C5): 037. DOI: https://doi.org/10.1029/2006JC003758

Chand, D, Wood, R, Anderson, TL, Satheesh, SK and **Charlson, RJ.** 2009. Satellite-derived direct radiative effect of aerosols dependent on cloud cover. *Nat Geosci* **2**(3): 181–184. DOI: https://doi.org/10.1038/ngeo437

Charlson, RJ, Lovelock, JE, Andreae, MO and **Warren, SG.** 1987. Oceanic phytoplankton, atmospheric sulphur, cloud albedo and climate. *Nature* **326**(6114): 655–661. DOI: https://doi.org/10.1038/326655a0

Chen, X, Wang, J, Liu, Y, Xu, X, Cai, Z, Yang, D, Yan, C-X and **Feng, L.** 2017. Angular dependence of aerosol information content in CAPI/TanSat observation over land: Effect of polarization and synergy with A-train satellites. *Remote Sens Environ* **196**: 163–177. DOI: https://doi.org/10.1016/j.rse.2017.05.007

Chin, TM, Vazquez, J and **Amstrong, E.** 2013. A multi-scale, high-resolution analysis of global sea surface temperature. *Algorithm Theor Basis Doc version 13*.

Choi, J-K, Park, YJ, Ahn, JH, Lim, H-S, Eom, J and **Ryu, J-H.** 2012. GOCI, the world's first geostationary ocean color observation satellite, for the monitoring of temporal variability in coastal water turbidity. *J Geophys Res Ocean* **117**(C09): 004. DOI: https://doi.org/10.1029/2012JC008046

Chowdhary, J, Cairns, B, Mishchenko, M and **Travis, L.** 2001. Retrieval of aerosol properties over the ocean using multispectral and multiangle photopolarimetric measurements from the Research Scanning Polarimeter. *Geophys Res Lett* **28**(2): 243–246. DOI: https://doi.org/10.1029/2000GL011783

Chowdhary, J, Cairns, B and **Travis, LD.** 2006. Contribution of water-leaving radiances to multiangle, multispectral polarimetric observations over the open ocean: bio-optical model results for case 1 waters. *Appl Opt* **45**(22): 5542–5567. DOI: https://doi.org/10.1364/AO.45.005542

Churnside, JH, McCarty, BJ and **Lu, X.** 2013. Subsurface ocean signals from an orbiting polarization lidar. *Remote Sens* **5**(7): 3457–3475. DOI: https://doi.org/10.3390/rs5073457

Chust, G and **Sagarminaga, Y.** 2007. The multi-angle view of MISR detects oil slicks under sun glitter conditions. *Remote Sens Environ* **107**(1–2): 232–239. DOI: https://doi.org/10.1016/j.rse.2006.09.024

Ciotti, AM and **Bricaud, A.** 2006. Retrievals of a size parameter for phytoplankton and spectral light absorption by colored detrital matter from water-leaving radiances at SeaWiFS channels in a continental shelf region off Brazil. *Limnol Oceanogr Methods* **4**(7): 237–253. DOI: https://doi.org/10.4319/lom.2006.4.237

Claustre, H, Bishop, J, Boss, E, Bernard, S, Berthon, J-F, Coatanoan, C, Johnson, KS, Lotiker, A, Ulloa, O, Perry, MJ, D'Ortenzio, F, Fanton d'Andon, OH and **Uitz, J.** 2010. Bio-Optical Profiling Floats as New Observational Tools for Biogeochemical and Ecosystem Studies: Potential Synergies with Ocean Color Remote Sensing. *Proc Ocean Sustain Ocean Obs Inf Soc* **1**: 177–183. DOI: https://doi.org/10.5270/OceanObs09.cwp.17

Collins, DB, Bertram, TH, Sultana, CM, Lee, C, Axson, JL and **Prather, KA.** 2016. Phytoplankton blooms weakly influence the cloud forming ability of sea spray aerosol. *Geophys Res Lett* **43**(18): 9975–9983. DOI: https://doi.org/10.1002/2016GL069922

Collins, DB, Burkart, J, Chang, RY-W, Lizotte, M, Boivin-Rioux, A, Blais, M, Mungall, EL, Boyer, M, Irish, VE, Massé, G, Kunkel, D, Tremblay, J-É, Papakyriakou, T, Bertram, AK, Bozem, H, Gosselin, M, Levasseur, M and **Abbatt, JPD.** 2017. Frequent Ultrafine Particle Formation and Growth in the Canadian Arctic Marine Environment. *Atmos Chem Phys* **17**: 13119–13138. DOI: https://doi.org/10.5194/acp-2017-411

Costantino, L and **Bréon, F-M.** 2013. Aerosol indirect effect on warm clouds over South-East Atlantic, from co-located MODIS and CALIPSO observations. *Atmos Chem Phys* **13**(1): 69–88. DOI: https://doi.org/10.5194/acp-13-69-2013

Cox, C and **Munk, W.** 1954. Measurement of the roughness of the sea surface from photographs of the Sun's glitter. *J Opt Soc Am* **44**(11): 838–850. DOI: https://doi.org/10.1364/JOSA.44.000838

Cross, JN, Mordy, CW, Tabisola, HM, Meinig, C, Cokelet, ED and **Stabeno, PJ.** 2015. Innovative technology development for Arctic Exploration. *OCEANS 2015 – MTS/IEEE Washington*, 1–8. DOI: https://doi.org/10.23919/OCEANS.2015.7404632

Dall'Osto, M, Beddows, DCS, Tunved, P, Krejci, R, Ström, J, Hansson, H-C, Yoon, YJ, Park, K-T, Becagli, S, Udisti, R, Onasch, T, O'Dowd, CD, Simó, R and **Harrison, RM.** 2017. Arctic sea ice melt leads to atmospheric new particle formation. *Sci Rep* **7**(1): 3318. DOI: https://doi.org/10.1038/s41598-017-03328-1

Danckwerts, PV. 1951. Significance of Liquid-Film Coefficients in Gas Absorption. *Ind Eng Chem* **43**(6): 1460–1467. DOI: https://doi.org/10.1021/ie50498a055

de Paepe, B, Ignatov, A, Dewitte, S and **Ipe, A.** 2008. Aerosol retrieval over ocean from SEVIRI for the use in GERB Earth's radiation budget analyses. *Remote Sens Environ* **112**(5): 2455–2468. DOI: https://doi.org/10.1016/j.rse.2007.11.005

Decho, AW, Kawaguchi, T, Allison, MA, Louchard, EM, Reid, RP, Stephens, FC, Voss, KJ, Wheatcroft, RA and **Taylor, BB.** 2003. Sediment properties influencing upwelling spectral reflectance signatures: The "biofilm gel effect." *Limnol Oceanogr* **48**(1part2): 431–443. DOI: https://doi.org/10.4319/lo.2003.48.1_part_2.0431

Deschamps, P-Y, Breon, F-M, Leroy, M, Podaire, A, Bricaud, A, Buriez, J-C and **Seze, G.** 1994. The POLDER mission: instrument characteristics and scientific objectives. *IEEE Trans Geosci Remote Sens* **32**(3): 598–615. DOI: https://doi.org/10.1109/36.297978

Deuzé, JL, Bréon, FM, Devaux, C, Goloub, P, Herman, M, Lafrance, B, Maignan, F, Marchand, A, Nadal, F, Perry, G and **Tanré, D.** 2001. Remote sensing of aerosols over land surfaces from POLDER-ADEOS-1 polarized measurements. *J Geophys Res Atmos* **106**(D5): 4913–4926. DOI: https://doi.org/10.1029/2000JD900364

Dierking, W. 2013. Sea Ice Monitoring by Synthetic Aperture Radar. *Oceanography* **26**(2): 100–111. DOI: https://doi.org/10.5670/oceanog.2013.33

Dierssen, HM, Chlus, A and **Russell, B.** 2015. Hyperspectral discrimination of floating mats of seagrass wrack and the macroalgae Sargassum in coastal waters of Greater Florida Bay using airborne remote sensing. *Remote Sens Environ* **167**: 247–258. DOI: https://doi.org/10.1016/j.rse.2015.01.027

Dubovik, O, Herman, M, Holdak, A, Lapyonok, T, Tanré, D, Deuzé, JL, Ducos, F, Sinyuk, A and **Lopatin, A.** 2011. Statistically optimized inversion algorithm for enhanced retrieval of aerosol properties from spectral multi-angle polarimetric satellite observations. *Atmos Meas Tech* **4**: 975–1018. DOI: https://doi.org/10.5194/amt-4-975-2011

Dubovik, O and **King, MD.** 2000. A flexible inversion algorithm for retrieval of aerosol optical properties from Sun and sky radiance measurements. *J Geophys Res Atmos* **105**(D16): 20673–20696. DOI: https://doi.org/10.1029/2000JD900282

Dubovik, O, Lapyonok, T, Litvinov, P, Herman, M, Fuertes, D, Ducos, F, Torres, B, Derimian, Y, Huang, X, Lopatin, A, Chaikovsky, A, Aspetsberger, M and **Federspiel, C.** 2014. GRASP: a versatile algorithm for characterizing the atmosphere. *SPIE Newsroom*: 2–5. DOI: https://doi.org/10.1117/2.1201408.005558

Dunne, JP, Armstrong, RA, Gnanadesikan, A and **Sarmiento, JL.** 2005. Empirical and mechanistic models for the particle export ratio. *Global Biogeochem Cycles* **19**: GB4026. DOI: https://doi.org/10.1029/2004GB002390

Durand, M, Fu, L-L, Lettenmaier, DP, Alsdorf, DE, Rodriguez, E and **Esteban-Fernandez, D.** 2010. The Surface Water and Ocean Topography Mission: Observing Terrestrial Surface Water and Oceanic Submesoscale Eddies. *Proc IEEE* **98**(5): 766–779. DOI: https://doi.org/10.1109/JPROC.2010.2043031

Engel, A, Bange, HW, Cunliffe, M, Burrows, SM, Friedrichs, G, Galgani, L, Herrmann, H, Hertkorn,

N, Johnson, M, Liss, PS, Quinn, PK, Schartau, M, Soloviev, A, Stolle, C, Upstill-Goddard, RC, van Pinxteren, M and **Zäncker, B.** 2017. The Ocean's Vital Skin: Toward an Integrated Understanding of the Sea Surface Microlayer. *Front Mar Sci* **4**(165): 165. DOI: https://doi.org/10.3389/fmars.2017.00165

Esselborn, M, Wirth, M, Fix, A, Tesche, M and **Ehret, G.** 2008. Airborne high spectral resolution lidar for measuring aerosol extinction and backscatter coefficients. *Appl Opt* **47**(3): 346–58. DOI: https://doi.org/10.1364/AO.47.000346

Estapa, ML, Boss, E, Mayer, LM and **Roesler, CS.** 2012. Role of iron and organic carbon in mass-specific light absorption by particulate matter from Louisiana coastal waters. *Limnol Oceanogr* **57**(1): 97–112. DOI: https://doi.org/10.4319/lo.2012.57.1.0097

Esters, L, Landwehr, S, Sutherland, G, Bell, TG, Christensen, KH, Saltzman, ES, Miller, SD and **Ward, B.** 2017. Parameterizing air-sea gas transfer velocity with dissipation. *J Geophys Res Ocean* **122**. DOI: https://doi.org/10.1002/2016JC012088

Fasham, MJR, Ducklow, HW and **McKelvie, SM.** 1990. A nitrogen-based model of plankton dynamics in the oceanic mixed layer. *J Mar Res* **48**(3): 591–639. DOI: https://doi.org/10.1357/002224090784984678

Forbes, RM, Geer, AJ, Lonitz, K and **Ahlgrimm, M.** 2016. Reducing systematic errors in cold-air outbreaks. *ECMWF Newsletter No. 146* **14616**(146): 17–22. DOI: https://doi.org/10.21957/s41h7q7l

Fournier, G and **Neukermans, G.** 2017. An analytical model for light backscattering by coccoliths and coccospheres of Emiliania huxleyi. *Opt Express* **25**(13): 14996. DOI: https://doi.org/10.1364/OE.25.014996

Fu, L-L, Alsdorf, D, Rodriguez, E, Morrow, R, Mognard, N, Lambin, J, Vaze, P and **Lafon, T.** 2009. The SWOT (Surface Water and Ocean Topography) Mission: Spaceborne Radar Interferometry for Oceanographic and Hydrological Applications. *Proc Ocean 2009 Sustain Ocean Obs Inf Soc*.

Gade, M, Alpers, W, Hühnerfuss, H, Masuko, H and **Kobayashi, T.** 1998. Imaging of biogenic and anthropogenic ocean surface films by the multifrequency/multipolarization SIR-C/X-SAR. *J Geophys Res Ocean* **103**(C9): 18851–18866. DOI: https://doi.org/10.1029/97JC01915

Galí, M, Devred, E, Levasseur, M, Royer, SJ and **Babin, M.** 2015. A remote sensing algorithm for planktonic dimethylsulfoniopropionate (DMSP) and an analysis of global patterns. *Remote Sens Environ* **171**: 171–184. DOI: https://doi.org/10.1016/j.rse.2015.10.012

Galí, M, Levasseur, M, Devred, E, Simó, R and **Babin, M.** 2018. Sea-surface dimethylsulfide (DMS) concentration from satellite data at global and regional scales. *Biogeosciences* **15**: 3497–3519. DOI: https://doi.org/10.5194/bg-15-3497-2018

Garaba, SP and **Dierssen, HM.** 2018. An airborne remote sensing case study of synthetic hydrocarbon detection using short wave infrared absorption features identified from marine-harvested macro- and microplastics. *Remote Sens Environ* **205**: 224–235. DOI: https://doi.org/10.1016/j.rse.2017.11.023

Garver, SA and **Siegel, DA.** 1997. Inherent optical property inversion of ocean color spectra and its biogeochemical interpretation: 1. Time series from the Sargasso Sea. *J Geophys Res* **102**(C8): 18607–18625. DOI: https://doi.org/10.1029/96JC03243

Glover, DM, Frew, NM and **McCue, SJ.** 2007. Air-sea gas transfer velocity estimates from the Jason-1 and TOPEX altimeters: Prospects for a long-term global time series. *J Mar Syst* **66**(1–4): 173–181. DOI: https://doi.org/10.1016/j.jmarsys.2006.03.020

Glover, DM, Frew, NM, McCue, SJ and **Bock, EJ.** 2002. A multi-year time series of global gas transfer velocity from the TOPEX dual frequency, normalized radar backscatter algorithm. In: *Gas Transfer at Water Surfaces. Geophysical Monograph* **127**: 325–331. DOI: https://doi.org/10.1029/GM127p0325

Goddijn-Murphy, L, Woolf, DK, Callaghan, AH, Nightingale, PD and **Shutler, JD.** 2016. A reconciliation of empirical and mechanistic models of the air-sea gas transfer velocity. *J Geophys Res Ocean* **121**(1): 818–835. DOI: https://doi.org/10.1002/2015JC011096

Goddijn-Murphy, L, Woolf, DK, Chapron, B and **Queffeulou, P.** 2013. Improvements to estimating the air-sea gas transfer velocity by using dual-frequency, altimeter backscatter. *Remote Sens Environ* **139**: 1–5. DOI: https://doi.org/10.1016/j.rse.2013.07.026

Goddijn-Murphy, L, Woolf, DK and **Marandino, C.** 2012. Space-based retrievals of air-sea gas transfer velocities using altimeters: Calibration for dimethyl sulfide. *J Geophys Res* **117**(C8): 028. DOI: https://doi.org/10.1029/2011JC007535

González-Gaya, B, Fernández-Pinos, M-C, Morales, L, Méjanelle, L, Abad, E, Piña, B, Duarte, CM, Jiménez, B and **Dachs, J.** 2016. High atmosphere–ocean exchange of semivolatile aromatic hydrocarbons. *Nat Geosci* (May). DOI: https://doi.org/10.1038/ngeo2714

Gordon, HR. 1997. Atmospheric correction of ocean color imagery in the Earth Observing System era. *J Geophys Res Atmos* **102**(D14): 17081–17106. DOI: https://doi.org/10.1029/96JD02443

Gordon, HR and **Morel, AY.** 1983. *Remote Assessment of Ocean Color for Interpretation of Satellite Visible Imagery: A Review*. (Lecture Notes on Coastal and Estuarine Studies; Vol. 4). DOI: https://doi.org/10.1029/LN004

Gordon, HR and **Wang, M.** 1994. Retrieval of water-leaving radiance and aerosol optical thickness over the oceans with SeaWiFS: a preliminary algorithm. *Appl Opt* **33**(3): 443. DOI: https://doi.org/10.1364/AO.33.000443

Graff, JR, Westberry, TK, Milligan, AJ, Brown, MB, Dall'Olmo, G, van Dongen-Vogels, V, Reifel, KM and **Behrenfeld, MJ.** 2015. Analytical phytoplankton carbon measurements spanning diverse ecosystems.

Deep Res Part I Oceanogr Res Pap **102**: 16–25. DOI: https://doi.org/10.1016/j.dsr.2015.04.006

Grimes, DJ, Ford, TE, Colwell, RR, Baker-Austin, C, Martinez-Urtaza, J, Subramaniam, A and **Capone, DG.** 2014. Viewing Marine Bacteria, Their Activity and Response to Environmental Drivers from Orbit. *Microb Ecol* **67**(3): 489–500. DOI: https://doi.org/10.1007/s00248-013-0363-4

Groß, S, Esselborn, M, Weinzierl, B, Wirth, M, Fix, A and **Petzold, A.** 2013. Aerosol classification by airborne high spectral resolution lidar observations. *Atmos Chem Phys* **13**(5): 2487–2505. DOI: https://doi.org/10.5194/acp-13-2487-2013

Groß, S, Freudenthaler, V, Wirth, M and **Weinzierl, B.** 2015. Towards an aerosol classification scheme for future EarthCARE lidar observations and implications for research needs. *Atmos Sci Lett* **16**(1): 77–82. DOI: https://doi.org/10.1002/asl2.524

Hair, J, Hostetler, C, Hu, Y, Behrenfeld, M, Butler, C, Harper, D, Hare, R, Berkoff, T, Cook, A, Collins, J, Stockley, N, Twardowski, M, Cetinić, I, Ferrare, R and **Mack, T.** 2016. Combined Atmospheric and Ocean Profiling from an Airborne High Spectral Resolution Lidar. Gross, B, Moshary, F and Arend, M (eds.), *EPJ Web Conf* **119**: 22001. DOI: https://doi.org/10.1051/epjconf/201611922001

Hair, JW, Hostetler, CA, Cook, AL, Harper, DB, Ferrare, RA, Mack, TL, Welch, W, Izquierdo, LR and **Hovis, FE.** 2008. Airborne High Spectral Resolution Lidar for profiling aerosol optical properties. *Appl Opt* **47**(36): 6734. DOI: https://doi.org/10.1364/AO.47.006734

Harmel, T. 2016. Recent developments in the use of polarization for marine environment monitoring from space. In: Kokhanovsky, AA (ed.), *Light Scattering Reviews*, 41–84. DOI: https://doi.org/10.1007/978-3-662-46762-6_2

Harmel, T and **Chami, M.** 2008. Invariance of polarized reflectance measured at the top of atmosphere by PARASOL satellite instrument in the visible range with marine constituents in open ocean waters. *Opt Express* **16**(9). DOI: https://doi.org/10.1364/OE.16.006064

Harmel, T and **Chami, M.** 2011. Influence of polarimetric satellite data measured in the visible region on aerosol detection and on the performance of atmospheric correction procedure over open ocean waters. *Opt Express* **19**(21). DOI: https://doi.org/10.1364/OE.19.020960

Harmel, T and **Chami, M.** 2012. Determination of sea surface wind speed using the polarimetric and multidirectional properties of satellite measurements in visible bands. *Geophys Res Lett* **39**(19). DOI: https://doi.org/10.1029/2012GL053508

Harmel, T and **Chami, M.** 2013. Estimation of the sunglint radiance field from optical satellite imagery over open ocean: Multidirectional approach and polarization aspects. *J Geophys Res Ocean* **118**(1): 76–90. DOI: https://doi.org/10.1029/2012JC008221

Harmel, T, Chami, M, Tormos, T, Reynaud, N and **Danis, PA.** 2018. Sunglint correction of the Multi-Spectral Instrument (MSI)-SENTINEL-2 imagery over inland and sea waters from SWIR bands. *Remote Sensing of Environment* **204**: 308–321. DOI: https://doi.org/10.1016/j.rse.2017.10.022

Harmel, T, Hieronymi, M, Slade, W, Röttgers, R, Roullier, F and **Chami, M.** 2016. Laboratory experiments for inter-comparison of three volume scattering meters to measure angular scattering properties of hydrosols. *Opt Express* **24**(2): A234. DOI: https://doi.org/10.1364/OE.24.00A234

Hasekamp, OP and **Landgraf, J.** 2007. Retrieval of aerosol properties over land surfaces: capabilities of multiple-viewing-angle intensity and polarization measurements. *Appl Opt* **46**(16): 3332. DOI: https://doi.org/10.1364/AO.46.003332

Hasekamp, OP, Litvinov, P and **Butz, A.** 2011. Aerosol properties over the ocean from PARASOL multiangle photopolarimetric measurements. *J Geophys Res* **116**(D14): D14204. DOI: https://doi.org/10.1029/2010JD015469

Hashiguchi, T, Okamura, Y, Tanaka, K, Nakajima, Y, Suzuki, K, Sakashita, T and **Amano, T.** 2016. Radiometric performance of Second-generation Global Imager (SGLI) using integrating spheres. Meynart, R, Neeck, SP, Kimura, T and Shimoda, H (eds.), DOI: https://doi.org/10.1117/12.2241955

Haynes, JM, Vonder Haar, TH, L'Ecuyer, T and **Henderson, D.** 2013. Radiative heating characteristics of Earth's cloudy atmosphere from vertically resolved active sensors. *Geophys Res Lett* **40**(3): 624–630. DOI: https://doi.org/10.1002/grl.50145

He, X, Pan, D, Bai, Y, Wang, D and **Hao, Z.** 2015. A new simple concept for ocean colour remote sensing using parallel polarisation radiance. *Sci Rep* **4**(1): 3748. DOI: https://doi.org/10.1038/srep03748

Heintzenberg, J, Tunved, P, Galí, M and **Leck, C.** 2017. New particle formation in the Svalbard region 2006–2015. *Atmos Chem Phys* **17**(10): 6153–6175. DOI: https://doi.org/10.5194/acp-17-6153-2017

Herman, M, Deuzé, J-L, Marchand, A, Roger, B and **Lallart, P.** 2005. Aerosol remote sensing from POLDER/ADEOS over the ocean: Improved retrieval using a nonspherical particle model. *J Geophys Res* **110**(D10): D10S02. DOI: https://doi.org/10.1029/2004JD004798

Hess, M, Koepke, P, Schult, I, Hess, M, Koepke, P and **Schult, I.** 1998. Optical Properties of Aerosols and Clouds: The Software Package OPAC. *Bull Am Meteorol Soc* **79**(5): 831–844. DOI: https://doi.org/10.1175/1520-0477(1998)079<0831:OPOAAC>2.0.CO;2

Higbie, R. 1935. The rate of absorption of a pure gas into still liquid during short periods of exposure. *Trans AIChE* **31**: 365–389. Available at: http://ci.nii.ac.jp/naid/10003391803/.

Hill, VJ, Matrai, PA, Olson, E, Suttles, S, Steele, M, Codispoti, LA and **Zimmerman, RC.** 2013. Synthesis of integrated primary production in the Arctic

Ocean: II. In situ and remotely sensed estimates. *Prog Oceanogr* **110**: 107–125. DOI: https://doi.org/10.1016/j.pocean.2012.11.005

Hoge, FE, Swift, RN, Yungel, JK and **Vodacek, A.** 1993. Fluorescence of dissolved organic matter: A comparison of north Pacific and north Atlantic oceans during April 1991. *J Geophys Res* **98**(C12): 22779. DOI: https://doi.org/10.1029/93JC01772

Hostetler, CA, Behrenfeld, MJ, Hu, Y, Hair, JW and **Schulien, JA.** 2018. Spaceborne Lidar in the Study of Marine Systems. *Ann Rev Mar Sci* **10**(1): 121–147. DOI: https://doi.org/10.1146/annurev-marine-121916-063335

Hu, C. 2011. An empirical approach to derive MODIS ocean color patterns under severe sun glint. *Geophys Res Lett* **38**(1): L01603. DOI: https://doi.org/10.1029/2010GL045422

Hu, Y, Rodier, S, Xu, K, Sun, W, Huang, J, Lin, B, Zhai, P and **Josset, D.** 2010. Occurrence, liquid water content, and fraction of supercooled water clouds from combined CALIOP/IIR/MODIS measurements. *J Geophys Res* **115**(D4): D00H34. DOI: https://doi.org/10.1029/2009JD012384

Hu, Y, Stamnes, K, Vaughan, M, Pelon, J, Weimer, C, Wu, D, Cisewski, M, Sun, W, Yang, P, Lin, B, Omar, A, Flittner, D, Hostetler, C, Trepte, C, Winker, D, Gibson, G and **Santa-Maria, M.** 2008. Sea surface wind speed estimation from space-based lidar measurements. *Atmos Chem Phys* **8**: 3593–3601. DOI: https://doi.org/10.5194/acp-8-3593-2008

Ibrahim, A, Gilerson, A, Chowdhary, J and **Ahmed, S.** 2016. Retrieval of macro- and micro-physical properties of oceanic hydrosols from polarimetric observations. *Remote Sens Environ* **186**: 548–566. DOI: https://doi.org/10.1016/j.rse.2016.09.004

Ignatov, A, Sapper, J, Cox, S, Laszlo, I, Nalli, NR and **Kidwell, KB.** 2004. Operational Aerosol Observations (AEROBS) from AVHRR/3 On Board NOAA-KLM Satellites. *J Atmos Ocean Technol* **21**(1): 3–26. DOI: https://doi.org/10.1175/1520-0426(2004)021<0003:OAOAFO>2.0.CO;2

Illingworth, AJ, Barker, HW, Beljaars, A, Ceccaldi, M, Chepfer, H, Clerbaux, N, Cole, J, Delanoë, J, Domenech, C, Donovan, DP, Fukuda, S, Hirakata, M, Hogan, RJ, Huenerbein, A, Kollias, P, Kubota, T, Nakajima, T, Nakajima, TY, Nishizawa, T, Ohno, Y, Okamoto, H, Oki, R, Sato, K, Satoh, M, Shephard, MW, Velázquez-Blázquez, A, Wandinger, U, Wehr, T, van Zadelhoff, G-J, Illingworth, AJ, Barker, HW, Beljaars, A, Ceccaldi, M, Chepfer, H, Clerbaux, N, Cole, J, Delanoë, J, Domenech, C, Donovan, DP, Fukuda, S, Hirakata, M, Hogan, RJ, Huenerbein, A, Kollias, P, Kubota, T, Nakajima, T, Nakajima, TY, Nishizawa, T, Ohno, Y, Okamoto, H, Oki, R, Sato, K, Satoh, M, Shephard, MW, Velázquez-Blázquez, A, Wandinger, U, Wehr, T and **van Zadelhoff, G-J.** 2015. The EarthCARE Satellite: The Next Step Forward in Global Measurements of Clouds, Aerosols, Precipitation, and Radiation. *Bull Am Meteorol Soc* **96**(8): 1311–1332. DOI: https://doi.org/10.1175/BAMS-D-12-00227.1

IOCCG. 2006. Remote sensing of inherent optical properties: fundamentals, tests of algorithms, and applications. Lee, ZP (ed.), Reports and Monographs of the International Ocean Colour Coordinating Group. Dartmouth, Canada.

IOCCG. 2010. *Atmospheric Correction for Remotely-Sensed Ocean-Colour Products*. Wang, M (ed.), Reports and Monographs of the International Ocean Colour Coordinating Group. Dartmouth, Canada.

IOCCG. 2014. *Phytoplankton Functional Types from Space*. Sathyendranath, S (ed.), Reports and Monographs of the International Ocean Colour Coordinating Group. Dartmouth, Canada.

Isern-Fontanet, J, Ballabrera-Poy, J, Turiel, A and **García-Ladona, E.** 2017. Remote sensing of ocean surface currents: A review of what is being observed and what is being assimilated. *Nonlinear Process Geophys* **24**(4): 613–643. DOI: https://doi.org/10.5194/npg-24-613-2017

Jackson, C. 2007. Internal wave detection using the moderate resolution imaging spectroradiometer (MODIS). *J Geophys Res* **112**: C11012. DOI: https://doi.org/10.1029/2007JC004220

Johnson, MS, Meskhidze, N, Kiliyanpilakkil, VP and **Gassó, S.** 2011. Understanding the transport of Patagonian dust and its influence on marine biological activity in the South Atlantic Ocean. *Atmos Chem Phys* **11**(6): 2487–2502. DOI: https://doi.org/10.5194/acp-11-2487-2011

Johnson, MT. 2010. A numerical scheme to calculate temperature and salinity dependent air-water transfer velocities for any gas. *Ocean Sci* **6**(4): 913–932. DOI: https://doi.org/10.5194/os-6-913-2010

Kahn, RA, Sayer, AM, Ahmad, Z, Franz, BA, Kahn, RA, Sayer, AM, Ahmad, Z and **Franz, BA.** 2016. The Sensitivity of SeaWiFS Ocean Color Retrievals to Aerosol Amount and Type. *J Atmos Ocean Technol* **33**(6): 1185–1209. DOI: https://doi.org/10.1175/JTECH-D-15-0121.1

Kato, S, Rose, FG, Sun-Mack, S, Miller, WF, Chen, Y, Rutan, DA, Stephens, GL, Loeb, NG, Minnis, P, Wielicki, BA, Winker, DM, Charlock, TP, Stackhouse, PW, Xu, K-M and **Collins, WD.** 2011. Improvements of top-of-atmosphere and surface irradiance computations with CALIPSO-, CloudSat-, and MODIS-derived cloud and aerosol properties. *J Geophys Res* **116**(D19): D19209. DOI: https://doi.org/10.1029/2011JD016050

Kattawar, GW. 2013. Genesis and evolution of polarization of light in the ocean. *Appl Opt* **52**(5): 940–948. DOI: https://doi.org/10.1364/AO.52.000940

Kaufman, YJ, Martins, JV, Remer, L, Schoeberl, MR and **Yamasoe, MA.** 2002. Satellite retrieval of aerosol absorption over the oceans using sunglint. *Geophys Res Lett* **29**(19): 31–34. DOI: https://doi.org/10.1029/2002GL015403

Keene, WC, Maring, H, Maben, JR, Kieber, DJ, Pszenny, AAP, Dahl, EE, Izaguirre, MA, Davis, AJ, Long,

MS, Zhou, X, Smoydzin, L and **Sander, R.** 2007. Chemical and physical characteristics of nascent aerosols produced by bursting bubbles at a model air-sea interface. *J Geophys Res* **112**(D21): D21202. DOI: https://doi.org/10.1029/2007JD008464

Kieber, DJ, Keene, WC, Frossard, AA, Long, MS, Maben, JR, Russell, LM, Kinsey, JD, Tyssebotn, IMB, Quinn, PK and **Bates, TS.** 2016. Coupled ocean-atmosphere loss of marine refractory dissolved organic carbon. *Geophys Res Lett* **43**(6): 2765–2772. DOI: https://doi.org/10.1002/2016GL068273

Kim, H-D, Kang, G-S, Lee, D-K, Jin, K-W, Seo, S-B, Oh, H-J, Ryu, J-H, Lambert, H, Laine, I, Meyer, P, Coste, P and **Duquesne, J-L.** 2012. COMS, the New Eyes in the Sky for Geostationary Remote Sensing. In: Escalante, B (ed.), *Remote Sensing–Advanced Techniques*, 235–268. DOI: https://doi.org/10.5772/37926

Kitaigorodskii, SA and **Donelan, MA.** 1984. Wind-Wave Effects on Gas Transfer. In: Brutsaert, W and Jirka, GH (eds.), *Gas Transfer at Water Surfaces. Water Science and Technology Library* **2**: 147–170. DOI: https://doi.org/10.1007/978-94-017-1660-4_14

Klüser, L, Martynenko, D and **Holzer-Popp, T.** 2011. Thermal infrared remote sensing of mineral dust over land and ocean: a spectral SVD based retrieval approach for IASI. *Atmos Meas Tech* **4**: 757–773. DOI: https://doi.org/10.5194/amt-4-757-2011

Knobelspiesse, K, Cairns, B, Mishchenko, M, Chowdhary, J, Tsigaridis, K, van Diedenhoven, B, Martin, W, Ottaviani, M and **Alexandrov, M.** 2012. Analysis of fine-mode aerosol retrieval capabilities by different passive remote sensing instrument designs. *Opt Express* **20**(19): 21457. DOI: https://doi.org/10.1364/OE.20.021457

Koffi, B, Schulz, M, Bréon, F-M, Dentener, F, Steensen, BM, Griesfeller, J, Winker, D, Balkanski, Y, Bauer, SE, Bellouin, N, Berntsen, T, Bian, H, Chin, M, Diehl, T, Easter, R, Ghan, S, Hauglustaine, DA, Iversen, T, Kirkevåg, A, Liu, X, Lohmann, U, Myhre, G, Rasch, P, Seland, Ø, Skeie, RB, Steenrod, SD, Stier, P, Tackett, J, Takemura, T, Tsigaridis, K, Vuolo, MR, Yoon, J and **Zhang, K.** 2016. Evaluation of the aerosol vertical distribution in global aerosol models through comparison against CALIOP measurements: AeroCom phase II results. *J Geophys Res Atmos* **121**(12): 7254–7283. DOI: https://doi.org/10.1002/2015JD024639

Kokhanovsky, AA, Deuzé, JL, Diner, DJ, Dubovik, O, Ducos, F, Emde, C, Garay, MJ, Grainger, RG, Heckel, A, Herman, M, Katsev, IL, Keller, J, Levy, R, North, PRJ, Prikhach, AS, Rozanov, VV, Sayer, AM, Ota, Y, Tanré, D, Thomas, GE and **Zege, EP.** 2010. The inter-comparison of major satellite aerosol retrieval algorithms using simulated intensity and polarization characteristics of reflected light. *Atmos Meas Tech* **3**: 909–932. DOI: https://doi.org/10.5194/amt-3-909-2010

Koren, I and **Feingold, G.** 2013. Adaptive behavior of marine cellular clouds. *Sci Rep* **3**(1): 2507. DOI: https://doi.org/10.1038/srep02507

Kostadinov, TS, Milutinović, S, Marinov, I and **Cabré, A.** 2016. Carbon-based phytoplankton size classes retrieved via ocean color estimates of the particle size distribution. *Ocean Sci* **12**(2): 561–575. DOI: https://doi.org/10.5194/os-12-561-2016

Kostadinov, TS, Siegel, DA and **Maritorena, S.** 2009. Retrieval of the particle size distribution from satellite ocean color observations. *J Geophys Res* **114**(C9): C09015. DOI: https://doi.org/10.1029/2009JC005303

Krug, M, Swart, S and **Hermes, J.** 2018. Ocean Gliders Ride the Research Wave in the Agulhas Current. *Eos (Washington DC)* **99**. DOI: https://doi.org/10.1029/2018EO100105

Kudryavtsev, V, Yurovskaya, M, Chapron, B, Collard, F and **Donlon, C.** 2017a. Sun glitter imagery of ocean surface waves. Part 1: Directional spectrum retrieval and validation. *J Geophys Res Ocean* **122**(2): 1369–1383. DOI: https://doi.org/10.1002/2016JC012425

Kudryavtsev, V, Yurovskaya, M, Chapron, B, Collard, F and **Donlon, C.** 2017b. Sun glitter imagery of surface waves. Part 2: Waves transformation on ocean currents. *J Geophys Res Ocean* **122**(2): 1384–1399. DOI: https://doi.org/10.1002/2016JC012426

Kulmala, M, Kontkanen, J, Junninen, H, Lehtipalo, K, Manninen, HE, Nieminen, T, Petäjä, T, Sipilä, M, Schobesberger, S, Rantala, P, Franchin, A, Jokinen, T, Järvinen, E, Äijälä, M, Kangasluoma, J, Hakala, J, Aalto, PP, Paasonen, P, Mikkilä, J, Vanhanen, J, Aalto, J, Hakola, H, Makkonen, U, Ruuskanen, T, Mauldin, RL, Duplissy, J, Vehkamäki, H, Bäck, J, Kortelainen, A, Riipinen, I, Kurtén, T, Johnston, MV, Smith, JN, Ehn, M, Mentel, TF, Lehtinen, KEJ, Laaksonen, A, Kerminen, V-M and **Worsnop, DR.** 2013. Direct Observations of Atmospheric Aerosol Nucleation. *Science* **339**(6122). DOI: https://doi.org/10.1126/science.1227385

Kurata, N, Vella, K, Hamilton, B, Shivji, M, Soloviev, A, Matt, S, Tartar, A and **Perrie, W.** 2016. Surfactant-associated bacteria in the near-surface layer of the ocean. *Sci Rep* **6**(1): 19123. DOI: https://doi.org/10.1038/srep19123

Lagerloef, G, Colomb, FR, Le Vine, D, Wentz, F, Yueh, S, Ruf, C, Lilly, J, Gunn, J, Chao, YI, Decharon, A, Feldman, G and **Swift, C.** 2008. The Aquarius/SAC-D mission. *Oceanography* **21**(1): 68–81. DOI: https://doi.org/10.5670/oceanog.2008.68

Lamont, JC and **Scott, DS.** 1970. An eddy cell model of mass transfer into the surface of a turbulent liquid. *AIChE J* **16**(4): 513–519. DOI: https://doi.org/10.1002/aic.690160403

Lana, A, Simó, R, Vallina, SM and **Dachs, J.** 2012. Potential for a biogenic influence on cloud microphysics over the ocean: a correlation study with satellite-derived data. *Atmos Chem Phys* **12**(17): 7977–7993. DOI: https://doi.org/10.5194/acp-12-7977-2012

Lary, DJ, Alavi, AH, Gandomi, AH and **Walker, AL.** 2016. Machine learning in geosciences and remote

sensing. *Geosci Front* **7**(1): 3–10. DOI: https://doi.org/10.1016/j.gsf.2015.07.003

Law, CS, Brévière, E, de Leeuw, G, Garçon, V, Guieu, C, Kieber, DJ, Kontradowitz, S, Paulmier, A, Quinn, PK, Saltzman, ES, Stefels, J and **von Glasow, R.** 2013. Evolving research directions in Surface Ocean – Lower Atmosphere (SOLAS) science. *Environ Chem* **10**(1): 1. DOI: https://doi.org/10.1071/EN12159

Leaitch, WR, Sharma, S, Huang, L, Toom-Sauntry, D, Chivulescu, A, Macdonald, AM, von Salzen, K, Pierce, JR, Bertram, AK, Schroder, JC, Shantz, NC, Chang, RYW and **Norman, A-L.** 2013. Dimethyl sulfide control of the clean summertime Arctic aerosol and cloud. *Elem Sci Anth* **1**(1): 17. DOI: https://doi.org/10.12952/journal.elementa.000017

Lee, Z, Carder, KL and **Arnone, RA.** 2002. Deriving inherent optical properties from water color: a multiband quasi-analytical algorithm for optically deep waters. *Appl Opt* **41**(27): 5755–5772. DOI: https://doi.org/10.1364/AO.41.005755

Lehahn, Y, D'Ovidio, F and **Koren, I.** 2018. A Satellite-Based Lagrangian View on Phytoplankton Dynamics. *Ann Rev Mar Sci* **10**: 99–119. DOI: https://doi.org/10.1146/annurev-marine-121916-063204

Lehahn, Y, Koren, I, Rudich, Y, Bidle, KD, Trainic, M, Flores, JM, Sharoni, S and **Vardi, A.** 2014. Decoupling atmospheric and oceanic factors affecting aerosol loading over a cluster of mesoscale North Atlantic eddies. *Geophys Res Lett* **41**(11): 4075–4081. DOI: https://doi.org/10.1002/2014GL059738

Lehahn, Y, Koren, I, Sharoni, S, d'Ovidio, F, Vardi, A and **Boss, E.** 2017. Dispersion/dilution enhances phytoplankton blooms in low-nutrient waters. *Nat Commun* **8**: 14868. DOI: https://doi.org/10.1038/ncomms14868

Lehtipalo, K, Rondo, L, Kontkanen, J, Schobesberger, S, Jokinen, T, Sarnela, N, Kürten, A, Ehrhart, S, Franchin, A, Nieminen, T, Riccobono, F, Sipilä, M, Yli-Juuti, T, Duplissy, J, Adamov, A, Ahlm, L, Almeida, J, Amorim, A, Bianchi, F, Breitenlechner, M, Dommen, J, Downard, AJ, Dunne, EM, Flagan, RC, Guida, R, Hakala, J, Hansel, A, Jud, W, Kangasluoma, J, Kerminen, VM, Keskinen, H, Kim, J, Kirkby, J, Kupc, A, Kupiainen-Määttä, O, Laaksonen, A, Lawler, MJ, Leiminger, M, Mathot, S, Olenius, T, Ortega, IK, Onnela, A, Petäjä, T, Praplan, A, Rissanen, MP, Ruuskanen, T, Santos, FD, Schallhart, S, Schnitzhofer, R, Simon, M, Smith, JN, Tröstl, J, Tsagkogeorgas, G, Tomé, A, Vaattovaara, P, Vehkamäki, H, Vrtala, AE, Wagner, PE, Williamson, C, Wimmer, D, Winkler, PM, Virtanen, A, Donahue, NM, Carslaw, KS, Baltensperger, U, Riipinen, I, Curtius, J, Worsnop, DR and **Kulmala, M.** 2016. The effect of acid-base clustering and ions on the growth of atmospheric nano-particles. *Nat Commun* **7**: 11594. DOI: https://doi.org/10.1038/ncomms11594

Le Quéré, C, Harrison, SP, Prentice, IC, Buitenhuis, ET, Aumont, O, Bopp, L, Claustre, H, Da Cunha, LC, Geider, R, Giraud, X, Klaas, C, Kohfeld, KE, Legendre, L, Manizza, M, Platt, T, Rivkin, RB, Sathyendranath, S, Uitz, J, Watson, AJ and **Wolf-Gladrow, D.** 2005. Ecosystem dynamics based on plankton functional types for global ocean biogeochemistry models. *Glob Chang Biol* **11**(11): 2016–2040. DOI: https://doi.org/10.1111/j.1365-2486.2005.01004.x

Le Quéré, C and **Saltzman, ES.** 2013. Surface Ocean-Lower Atmosphere Processes. Le Quéré, C and Saltzman, ES (eds.). DOI: https://doi.org/10.1029/GM187

Li, X. 2015. The first Sentinel-1 SAR image of a typhoon. *Acta Oceanol Sin* **34**(1): 1–2. DOI: https://doi.org/10.1007/s13131-015-0589-8

Li, X, Zheng, W, Yang, X, Zhang, JA, Pichel, WG and **Li, Z.** 2013. Coexistence of Atmospheric Gravity Waves and Boundary Layer Rolls Observed by SAR. *J Atmos Sci* **70**(11): 3448–3459. DOI: https://doi.org/10.1175/JAS-D-12-0347.1

Limbacher, JA and **Kahn, RA.** 2017. Updated MISR dark water research aerosol retrieval algorithm-Part 1: Coupled 1.1 km ocean surface chlorophyll a retrievals with empirical calibration corrections. *Atmos Meas Tech* **10**(4): 1539–1555. DOI: https://doi.org/10.5194/amt-10-1539-2017

Lin, I-I, Wen, L-S, Liu, K-K, Tsai, W-T and **Liu, AK.** 2002. Evidence and quantification of the correlation between radar backscatter and ocean colour supported by simultaneously acquired in situ sea truth. *Geophys Res Lett* **29**(10): 102-1–102-4. DOI: https://doi.org/10.1029/2001GL014039

Lin, Z, Li, W, Gatebe, C, Poudyal, R and **Stamnes, K.** 2016. Radiative transfer simulations of the two-dimensional ocean glint reflectance and determination of the sea surface roughness. *Appl Opt* **55**(6): 1206. DOI: https://doi.org/10.1364/AO.55.001206

Liss, PS and **Johnson, MT.** 2014. Ocean-Atmosphere Interactions of Gases and Particles. Liss, PS and Johnson, MT (eds.). DOI: https://doi.org/10.1007/978-3-642-25643-1

Liu, J, He, X, Liu, J, Bai, Y, Wang, D, Chen, T, Wang, Y and **Zhu, F.** 2017. Polarization-based enhancement of ocean color signal for estimating suspended particulate matter: radiative transfer simulations and laboratory measurements. *Opt Express* **25**(8): A323. DOI: https://doi.org/10.1364/OE.25.00A323

Liu, Y and **Diner, DJ.** 2017. Multi-Angle Imager for Aerosols. *Public Health Rep* **132**(1): 14–17. DOI: https://doi.org/10.1177/0033354916679983

Liu, Z, Vaughan, M, Winker, D, Kittaka, C, Getzewich, B, Kuehn, R, Omar, A, Powell, K, Trepte, C and **Hostetler, C.** 2009. The CALIPSO lidar cloud and aerosol discrimination: Version 2 algorithm and initial assessment of performance. *J Atmos Ocean Technol* **26**(7): 1198–1213. DOI: https://doi.org/10.1175/2009JTECHA1229.1

Loisel, H, Duforet, L, Dessailly, D, Chami, M and **Dubuisson, P.** 2008. Investigation of the variations

in the water leaving polarized reflectance from the POLDER satellite data over two biogeochemical contrasted oceanic areas. *Opt Express* **16**(17): 12905. DOI: https://doi.org/10.1364/OE.16.012905

Loisel, H, Nicolas, J-M, Sciandra, A, Stramski, D and **Poteau, A.** 2006. Spectral dependency of optical backscattering by marine particles from satellite remote sensing of the global ocean. *J Geophys Res* **111**(C9): C09024. DOI: https://doi.org/10.1029/2005JC003367

Loisel, H, Vantrepotte, V, Dessailly, D and **Mériaux, X.** 2014. Assessment of the colored dissolved organic matter in coastal waters from ocean color remote sensing. *Opt Express* **22**(11): 13109. DOI: https://doi.org/10.1364/OE.22.013109

Loose, B, Kelly, RP, Bigdeli, A, Williams, W, Krishfield, R, Rutgers van der Loeff, M and **Moran, SB.** 2017. How well does wind speed predict air-sea gas transfer in the sea ice zone? A synthesis of radon deficit profiles in the upper water column of the Arctic Ocean. *J Geophys Res Ocean* **122**(5): 3696–3714. DOI: https://doi.org/10.1002/2016JC012460

Loose, B, Miller, L, Elliot, S and **Papakyriakou, T.** 2011. Sea Ice Biogeochemistry and Material Transport Across the Frozen Interface. *Oceanography* **24**(3): 202–218. DOI: https://doi.org/10.5670/oceanog.2011.72

Lu, X, Hu, Y, Trepte, C, Zeng, S and **Churnside, JH.** 2014. Ocean subsurface studies with the CALIPSO spaceborne lidar. *J Geophys Res Ocean* **119**(7): 4305–4317. DOI: https://doi.org/10.1002/2014JC009970

Lu, Y, Sun, S, Zhang, M, Murch, B and **Hu, C.** 2016. Refinement of the critical angle calculation for the contrast reversal of oil slicks under sunglint. *J Geophys Res Ocean* **121**(1): 148–161. DOI: https://doi.org/10.1002/2015JC011001

Lu, Y, Zhou, Y, Liu, Y, Mao, Z, Qian, W, Wang, M, Zhang, M, Xu, J, Sun, S and **Du, P.** 2017. Using remote sensing to detect the polarized sunglint reflected from oil slicks beyond the critical angle. *J Geophys Res Ocean* **122**(8): 6342–6354. DOI: https://doi.org/10.1002/2017JC012793

Lubac, B, Loisel, H, Guiselin, N, Astoreca, R, Felipe Artigas, L and **Mériaux, X.** 2008. Hyperspectral and multispectral ocean color inversions to detect *Phaeocystis globosa* blooms in coastal waters. *J Geophys Res* **113**(C6): C06026. DOI: https://doi.org/10.1029/2007JC004451

Lyden, JD, Hammond, RR, Lyzenga, DR and **Shuchman, RA.** 1988. Synthetic aperture radar imaging of surface ship wakes. *J Geophys Res* **93**(C10): 12293. DOI: https://doi.org/10.1029/JC093iC10p12293

Mace, GG and **Zhang, Q.** 2014. The CloudSat radar-lidar geometrical profile product (RL-GeoProf): Updates, improvements, and selected results. *J Geophys Res Atmos* **119**(15): 9441–9462. DOI: https://doi.org/10.1002/2013JD021374

Mace, GG, Zhang, Q, Vaughan, M, Marchand, R, Stephens, G, Trepte, C and **Winker, D.** 2009. A description of hydrometeor layer occurrence statistics derived from the first year of merged Cloudsat and CALIPSO data. *J Geophys Res* **114**(D8): D00A26. DOI: https://doi.org/10.1029/2007JD009755

MacIntyre, S, Jonsson, A, Jansson, M, Aberg, J, Turney, DE and **Miller, SD.** 2010. Buoyancy flux, turbulence, and the gas transfer coefficient in a stratified lake. *Geophys Res Lett* **37**: L24604. DOI: https://doi.org/10.1029/2010GL044164

Marbach, T, Phillips, P, Lacan, A and **Schlüssel, P.** 2013. The Multi-Viewing, -Channel, -Polarisation Imager (3MI) of the EUMETSAT Polar System – Second Generation (EPS-SG) dedicated to aerosol characterisation. Meynart, R, Neeck, SP and Shimoda, H (eds.). 2013 Oct 16. DOI: https://doi.org/10.1117/12.2028221

Maritorena, S, Siegel, DA and **Peterson, AR.** 2002. Optimization of a semianalytical ocean color model for global-scale applications. *Appl Opt* **41**(15): 2705–2714. DOI: https://doi.org/10.1364/AO.41.002705

Martinez-Vicente, V, Dall'Olmo, G, Tarran, G, Boss, E and **Sathyendranath, S.** 2013. Optical backscattering is correlated with phytoplankton carbon across the Atlantic Ocean. *Geophys Res Lett* **40**(6): 1154–1158. DOI: https://doi.org/10.1002/grl.50252

Martins, JV, Marshak, A, Remer, LA, Rosenfeld, D, Kaufman, YJ, Fernandez-Borda, R, Koren, I, Correia, AL, Zubko, V and **Artaxo, P.** 2011. Remote sensing the vertical profile of cloud droplet effective radius, thermodynamic phase, and temperature. *Atmos Chem Phys* **11**: 9485–9501. DOI: https://doi.org/10.5194/acp-11-9485-2011

Martins, JV, Nielsen, T, Fish, C, Sparr, L, Fernandez-Borda, R, Schoeberl, M and **Remer, L.** 2014. HARP CubeSat – An innovative Hyperangular Imaging Polarimeter for Earth Science Applications. *AIAA/USU Conf Small Satell*, in press. Available at: https://digitalcommons.usu.edu/smallsat/2014/Workshop/13. Accessed 2018 Feb 28.

Martonchik, JV, Diner, DJ, Kahn, RA, Ackerman, TP, Verstraete, MM, Pinty, B and **Gordon, HR.** 1998. Techniques for the retrieval of aerosol properties over land and ocean using multiangle imaging. *IEEE Trans Geosci Remote Sens* **36**(4): 1212–1227. DOI: https://doi.org/10.1109/36.701027

Matsuoka, A, Babin, M and **Devred, EC.** 2016. A new algorithm for discriminating water sources from space: A case study for the southern Beaufort Sea using MODIS ocean color and SMOS salinity data. *Remote Sens Environ* **184**(June): 124–138. DOI: https://doi.org/10.1016/j.rse.2016.05.006

Matsuoka, A, Boss, E, Babin, M, Karp-boss, L, Hafez, M, Chekalyuk, A, Proctor, CW, Werdell, PJ and **Bricaud, A.** 2017. Pan-Arctic optical characteristics of colored dissolved organic matter : Tracing dissolved organic carbon in changing Arctic waters using satellite ocean color data. *Remote Sens Environ* **200**: 89–101. DOI: https://doi.org/10.1016/j.rse.2017.08.009

Matsuoka, A, Hooker, SB, Bricaud, A, Gentili, B and **Babin, M.** 2013. Estimating absorption coefficients of colored dissolved organic matter (CDOM) using a

semi-analytical algorithm for southern Beaufort Sea waters: application to deriving concentrations of dissolved organic carbon from space. *Biogeosciences* **10**(2): 917–927. DOI: https://doi.org/10.5194/bg-10-917-2013

Matus, AV, L'Ecuyer, TS, Kay, JE, Hannay, C, Lamarque, J-F, Matus, AV, L'Ecuyer, TS, Kay, JE, Hannay, C and **Lamarque, J-F.** 2015. The Role of Clouds in Modulating Global Aerosol Direct Radiative Effects in Spaceborne Active Observations and the Community Earth System Model. *J Clim* **28**(8): 2986–3003. DOI: https://doi.org/10.1175/JCLI-D-14-00426.1

McCoy, DT, Burrows, SM, Wood, R, Grosvenor, DP, Elliott, SM, Ma, P-L, Rasch, PJ and **Hartmann, DL.** 2015. Natural aerosols explain seasonal and spatial patterns of Southern Ocean cloud albedo. *Sci Adv* **1**: e1500157. DOI: https://doi.org/10.1126/sciadv.1500157

McGillis, WR, Edson, JB, Zappa, CJ, Ware, JD, McKenna, SP, Terray, EA, Hare, JE, Fairall, CW, Drennan, W, Donelan, M, DeGrandpre, MD, Wanninkhof, R and **Feely, RA.** 2004. Air-sea CO_2 exchange in the equatorial Pacific. *J Geophys Res C Ocean* **109**: C08S02. DOI: https://doi.org/10.1029/2003JC002256

McKinna, LIW. 2015. Three decades of ocean-color remote-sensing Trichodesmium spp. in the World's oceans: A review. *Progress in Oceanography*. DOI: https://doi.org/10.1016/j.pocean.2014.12.013

Meissner, T, Ricciadulli, L and **Wentz, FJ.** 2017. Capability of the SMAP mission to measure ocean surface winds in storms. *Bull Am Meteorol Soc*, in press. DOI: https://doi.org/10.1175/BAMS-D-16-0052.1

Mélin, F, Clerici, M, Zibordi, G, Holben, BN and Smirnov, A. 2010. Validation of SeaWiFS and MODIS aerosol products with globally distributed AERONET data. *Remote Sens Environ* **114**(2): 230–250. DOI: https://doi.org/10.1016/J.RSE.2009.09.003

Merchant, CJ, Embury, O, Rayner, NA, Berry, DI, Corlett, GK, Lean, K, Veal, KL, Kent, EC, Llewellyn-Jones, DT, Remedios, JJ and **Saunders, R.** 2012. A 20 year independent record of sea surface temperature for climate from Along-Track Scanning Radiometers. *J Geophys Res Ocean* **117**: C12013. DOI: https://doi.org/10.1029/2012JC008400

Meskhidze, N and **Nenes, A.** 2006. Phytoplankton and Cloudiness in the Southern Ocean. *Science* **314**(5804): 1419–1423. DOI: https://doi.org/10.1126/science.1131779

Miller, SD, Haddock, SHD, Elvidge, CD and **Lee, TF.** 2005. Detection of a bioluminescent milky sea from space. *Proc Natl Acad Sci USA* **102**(40): 14181–14184. DOI: https://doi.org/10.1073/pnas.0507253102

Mishchenko, MI, Geogdzhayev, IV, Cairns, B, Carlson, BE, Chowdhary, J, Lacis, AA, Liu, L, Rossow, WB and **Travis, LD.** 2007. Past, present, and future of global aerosol climatologies derived from satellite observations: A perspective. **106**(1–3): 325–347. DOI: https://doi.org/10.1016/j.jqsrt.2007.01.007

Mishchenko, MI and **Travis, LD.** 1997. Satellite retrieval of aerosol properties over the ocean using polarization as well as intensity of reflected sunlight. *J Geophys Res Atmos* **102**(D14): 16989–17013. DOI: https://doi.org/10.1029/96JD02425

Morel, A and **Bricaud, A.** 1981. Theoretical results concerning light absorption in a discrete medium, and application to specific absorption of phytoplankton. *Deep Sea Res Part A, Oceanogr Res Pap* **28**(11): 1375–1393. DOI: https://doi.org/10.1016/0198-0149(81)90039-X

Müller, D, Hostetler, CA, Ferrare, RA, Burton, SP, Chemyakin, E, Kolgotin, A, Hair, JW, Cook, AL, Harper, DB, Rogers, RR, Hare, RW, Cleckner, CS, Obland, MD, Tomlinson, J, Berg, LK and **Schmid, B.** 2014. Airborne Multiwavelength High Spectral Resolution Lidar (HSRL-2) observations during TCAP 2012: vertical profiles of optical and microphysical properties of a smoke/urban haze plume over the northeastern coast of the US. *Atmos Meas Tech* **7**(10): 3487–3496. DOI: https://doi.org/10.5194/amt-7-3487-2014

Müller, D, Krasemann, H, Brewin, RJW, Brockmann, C, Deschamps, PY, Doerffer, R, Fomferra, N, Franz, BA, Grant, MG, Groom, SB, Mélin, F, Platt, T, Regner, P, Sathyendranath, S, Steinmetz, F and **Swinton, J.** 2015. The Ocean Colour Climate Change Initiative: I. A methodology for assessing atmospheric correction processors based on in-situ measurements. *Remote Sens Environ* **162**: 242–256. DOI: https://doi.org/10.1016/j.rse.2013.11.026

Mungall, EL, Abbatt, JPD, Wentzell, JJB, Lee, AKY, Thomas, JL, Blais, M, Gosselin, M, Miller, LA, Papakyriakou, T, Willis, MD and **Liggio, J.** 2017. Microlayer source of oxygenated volatile organic compounds in the summertime marine Arctic boundary layer. *Proc Natl Acad Sci* **114**(24): 6203–6208. DOI: https://doi.org/10.1073/pnas.1620571114

Munk, W. 2009. An Inconvenient Sea Truth: Spread, Steepness, and Skewness of Surface Slopes. *Ann Rev Mar Sci* **1**(1): 377–415. DOI: https://doi.org/10.1146/annurev.marine.010908.163940

Nelson, NB and **Siegel, DA.** 2013. The Global Distribution and Dynamics of Chromophoric Dissolved Organic Matter. *Ann Rev Mar Sci* **5**(1): 447–476. DOI: https://doi.org/10.1146/annurev-marine-120710-100751

Neukermans, G and **Fournier, G.** 2018. Optical Modeling of Spectral Backscattering and Remote Sensing Reflectance From Emiliania huxleyi Blooms. *Front Mar Sci* **5**: 146. DOI: https://doi.org/10.3389/fmars.2018.00146

Neukermans, G, Loisel, H, Mériaux, X, Astoreca, R and **McKee, D.** 2012b. In situ variability of mass-specific beam attenuation and backscattering of marine particles with respect to particle size, density, and composition. *Limnol Oceanogr* **57**(1): 124–144. DOI: https://doi.org/10.4319/lo.2012.57.1.0124

Neukermans, G, Reynolds, RA and **Stramski, D.** 2014. Contrasting inherent optical properties and particle

characteristics between an under-ice phytoplankton bloom and open water in the Chukchi Sea. *Deep Res Part II Top Stud Oceanogr* **105**: 59–73. DOI: https://doi.org/10.1016/j.dsr2.2014.03.014

Neukermans, G, Reynolds, RA and **Stramski, D.** 2016. Optical classification and characterization of marine particle assemblages within the western Arctic Ocean. *Limnol Oceanogr* **61**(4): 1472–1494. DOI: https://doi.org/10.1002/lno.10316

Neukermans, G, Ruddick, KG and **Greenwood, N.** 2012a. Diurnal variability of turbidity and light attenuation in the southern North Sea from the SEVIRI geostationary sensor. *Remote Sens Environ* **124**: 564–580. DOI: https://doi.org/10.1016/j.rse.2012.06.003

O'Brien, DM and **Mitchell, RM.** 1988. Retrieval of Surface Wind Speed and Aerosol Optical Depth over the Oceans from AVHRR Images of Sun Glint. *J Appl Meteorol* **27**(12): 1395–1403. DOI: https://doi.org/10.1175/1520-0450(1988)027<1395:ROSWSA>2.0.CO;2

O'Dowd, C, Ceburnis, D, Ovadnevaite, J, Bialek, J, Stengel, DB, Zacharias, M, Nitschke, U, Connan, S, Rinaldi, M, Fuzzi, S, Decesari, S, Cristina Facchini, M, Marullo, S, Santoleri, R, Dell'Anno, A, Corinaldesi, C, Tangherlini, M and **Danovaro, R.** 2015. Connecting marine productivity to sea-spray via nanoscale biological processes: Phytoplankton Dance or Death Disco? *Sci Rep* **5**: 14883. DOI: https://doi.org/10.1038/srep14883

O'Dowd, CD, Facchini, MC, Cavalli, F, Ceburnis, D, Mircea, M, Decesari, S, Fuzzi, S, Yoon, YJ and **Putaud, J-P.** 2004. Biogenically driven organic contribution to marine aerosol. *Nature* **431**(7009): 676–680. DOI: https://doi.org/10.1038/nature02959

O'Malley, RT, Behrenfeld, MJ, Westberry, TK, Milligan, AJ, Shang, S and **Yan, J.** 2014. Geostationary satellite observations of dynamic phytoplankton photophysiology. *Geophys Res Lett* **41**(14): 5052–5059. DOI: https://doi.org/10.1002/2014GL060246

Oikawa, E, Nakajima, T, Inoue, T and **Winker, D.** 2013. A study of the shortwave direct aerosol forcing using ESSP/CALIPSO observation and GCM simulation. *J Geophys Res Atmos* **118**(9): 3687–3708. DOI: https://doi.org/10.1002/jgrd.50227

Olmedo, E, Martínez, J, Umbert, M, Hoareau, N, Portabella, M, Ballabrera-Poy, J and **Turiel, A.** 2016. Improving time and space resolution of SMOS salinity maps using multifractal fusion. *Remote Sens Environ* **180**: 246–263. DOI: https://doi.org/10.1016/j.rse.2016.02.038

Omar, AH, Winker, DM, Vaughan, MA, Hu, Y, Trepte, CR, Ferrare, RA, Lee, K-P, Hostetler, CA, Kittaka, C, Rogers, RR, Kuehn, RE, Liu, Z, Omar, AH, Winker, DM, Vaughan, MA, Hu, Y, Trepte, CR, Ferrare, RA, Lee, K-P, Hostetler, CA, Kittaka, C, Rogers, RR, Kuehn, RE and **Liu, Z.** 2009. The CALIPSO Automated Aerosol Classification and Lidar Ratio Selection Algorithm. *J Atmos Ocean Technol* **26**(10): 1994–2014. DOI: https://doi.org/10.1175/2009JTECHA1231.1

Ooki, A, Nomura, D, Nishino, S, Kikuchi, T and **Yokouchi, Y.** 2015. A global-scale map of isoprene and volatile organic iodine in surface seawater of the Arctic, Northwest Pacific, Indian, and Southern Oceans. *J Geophys Res Ocean* **120**(6): 4108–4128. DOI: https://doi.org/10.1002/2014JC010519

Ottaviani, M, Cairns, B, Chowdhary, J, Van Diedenhoven, B, Knobelspiesse, K, Hostetler, C, Ferrare, R, Burton, S, Hair, J, Obland, MD and **Rogers, R.** 2012. Polarimetric retrievals of surface and cirrus clouds properties in the region affected by the Deepwater Horizon oil spill. *Remote Sens Environ* **121**(0): 389–403. DOI: https://doi.org/10.1016/j.rse.2012.02.016

Ottaviani, M, Knobelspiesse, K, Cairns, B and **Mishchenko, M.** 2013. Information content of aerosol retrievals in the sunglint region. *Geophys Res Lett* **40**(3): 631–634. DOI: https://doi.org/10.1002/grl.50148

Park, K-T, Lee, K, Yoon, Y-J, Lee, H-W, Kim, H-C, Lee, B-Y, Hermansen, O, Kim, T-W and **Holmén, K.** 2013. Linking atmospheric dimethyl sulfide and the Arctic Ocean spring bloom. *Geophys Res Lett* **40**(1): 155–160. DOI: https://doi.org/10.1029/2012GL054560

Petrenko, M and **Ichoku, C.** 2013. Coherent uncertainty analysis of aerosol measurements from multiple satellite sensors. *Atmos Chem Phys* **13**: 6777–6805. DOI: https://doi.org/10.5194/acp-13-6777-2013

Piironen, P and **Eloranta, EW.** 1994. Demonstration of a high-spectral-resolution lidar based on an iodine absorption filter. *Opt Lett* **19**(3): 234. DOI: https://doi.org/10.1364/OL.19.000234

Platt, T and **Sathyendranath, S.** 1988. Oceanic Primary Production: Estimation by Remote Sensing at Local and Regional Scales. *Science* **241**(4873): 1613–1620. DOI: https://doi.org/10.1126/science.241.4873.1613

Pleskachevsky, AL, Rosenthal, W and **Lehner, S.** 2016. Meteo-marine parameters for highly variable environment in coastal regions from satellite radar images. *ISPRS J Photogramm Remote Sens* **119**: 464–484. DOI: https://doi.org/10.1016/j.isprsjprs.2016.02.001

Popp, T, de Leeuw, G, Bingen, C, Brühl, C, Capelle, V, Chedin, A, Clarisse, L, Dubovik, O, Grainger, R, Griesfeller, J, Heckel, A, Kinne, S, Klüser, L, Kosmale, M, Kolmonen, P, Lelli, L, Litvinov, P, Mei, L, North, P, Pinnock, S, Povey, A, Robert, C, Schulz, M, Sogacheva, L, Stebel, K, Stein Zweers, D, Thomas, G, Tilstra, L, Vandenbussche, S, Veefkind, P, Vountas, M and **Xue, Y.** 2016. Development, Production and Evaluation of Aerosol Climate Data Records from European Satellite Observations (Aerosol_cci). *Remote Sens* **8**(5): 421. DOI: https://doi.org/10.3390/rs8050421

Powell, KA, Hostetler, CA, Liu, Z, Vaughan, MA, Kuehn, RE, Hunt, WH, Lee, KP, Trepte, CR, Rogers, RR, Young, SA and **Winker, DM.** 2009. Calipso lidar calibration algorithms. Part I: Nighttime 532-nm parallel channel and 532-nm perpendicular

channel. *J Atmos Ocean Technol* **26**(10): 2015–2033. DOI: https://doi.org/10.1175/2009JTECHA1242.1

Prytherch, J, Brooks, IM, Crill, PM, Thornton, BF, Salisbury, DJ, Tjernström, M, Anderson, LG, Geibel, MC and **Humborg, C.** 2017. Direct determination of the air-sea CO_2 gas transfer velocity in Arctic sea ice regions. *Geophys Res Lett* **44**(8): 3770–3778. DOI: https://doi.org/10.1002/2017GL073593

Quinby-Hunt, MS, Hunt, AJ, Lofftus, K and **Shapiro, D.** 1989. Polarized-light scattering studies of marine Chlorella. *Limnol Oceanogr* **34**(8): 1587–1600. DOI: https://doi.org/10.4319/lo.1989.34.8.1587

Quinn, PK and **Bates, TS.** 2011. The case against climate regulation via oceanic phytoplankton sulphur emissions. *Nature* **480**(7375): 51–56. DOI: https://doi.org/10.1038/nature10580

Quinn, PK, Bates, TS, Schulz, KS, Coffman, DJ, Frossard, AA, Russell, LM, Keene, WC and **Kieber, DJ.** 2014. Contribution of sea surface carbon pool to organic matter enrichment in sea spray aerosol. *Nat Geosci* **7**(3): 228–232. DOI: https://doi.org/10.1038/ngeo2092.

Quinn, PK, Coffman, DJ, Johnson, JE, Upchurch, LM and **Bates, TS.** 2017. Small fraction of marine cloud condensation nuclei made up of sea spray aerosol. *Nat Geosci* **10**: 674–679. DOI: https://doi.org/10.1038/ngeo3003

Remer, LA, Kaufman, YJ, Tanré, D, Mattoo, S, Chu, DA, Martins, JV, Li, RR, Ichoku, C, Levy, RC, Kleidman, RG, Eck, TF, Vermote, E and **Holben, BN.** 2005. The MODIS Aerosol Algorithm, Products, and Validation. *J Atmos Sci* **62**(4): 947–973. DOI: https://doi.org/10.1175/JAS3385.1

Reul, N, Fournier, S, Boutin, J, Hernandez, O, Maes, C, Chapron, B, Alory, G, Quilfen, Y, Tenerelli, J, Morisset, S, Kerr, Y, Mecklenburg, S and **Delwart, S.** 2014. Sea Surface Salinity Observations from Space with the SMOS Satellite: A New Means to Monitor the Marine Branch of the Water Cycle. *Surv Geophys* **35**(3): 681–722. DOI: https://doi.org/10.1007/s10712-013-9244-0

Reynolds, RA, Stramski, D and **Neukermans, G.** 2016. Optical backscattering by particles in Arctic seawater and relationships to particle mass concentration, size distribution, and bulk composition. *Limnol Oceanogr* **61**(5): 1869–1890. DOI: https://doi.org/10.1002/lno.10341

Riser, SC, Freeland, HJ, Roemmich, D, Wijffels, S, Troisi, A, Belbéoch, M, Gilbert, D, Xu, J, Pouliquen, S, Thresher, A and **Le Traon, P.** 2016. Fifteen years of ocean observations with the global Argo array. *Nat Clim Chang* **6**: 145–153. DOI: https://doi.org/10.1038/nclimate2872

Roesler, CS and **Perry, MJ.** 1995. In situ phytoplankton absorption, fluorescence emission, and particulate backscattering spectra determined from reflectance. *J Geophys Res* **100**(C7): 13279–13294. DOI: https://doi.org/10.1029/95JC00455

Rosenfeld, D, Williams, E, Andreae, MO, Freud, E, Pöschl, U and **Rennó, NO.** 2012. The scientific basis for a satellite mission to retrieve CCN concentrations and their impacts on convective clouds. *Atmos Meas Tech* **5**(8): 2039–2055. DOI: https://doi.org/10.5194/amt-5-2039-2012

Rosenfeld, D, Zheng, Y, Hashimshoni, E, Pöhlker, ML, Jefferson, A, Pöhlker, C, Yu, X, Zhu, Y, Liu, G, Yue, Z, Fischman, B, Li, Z, Giguzin, D, Goren, T, Artaxo, P, Barbosa, HMJ, Pöschl, U and **Andreae, MO.** 2016. Satellite retrieval of cloud condensation nuclei concentrations by using clouds as CCN chambers. *Proc Natl Acad Sci U S A* **113**(21): 5828–34. DOI: https://doi.org/10.1073/pnas.1514044113

Ruddick, K, Vanhellemont, Q, Yan, J, Neukermans, G, Wei, G and **Shang, S.** 2012. Variability of suspended particulate matter in the Bohai Sea from the geostationary Ocean Color Imager (GOCI). *Ocean Sci J* **47**(3): 331–345. DOI: https://doi.org/10.1007/s12601-012-0032-4

Ruddick, KG, Ovidio, F and **Rijkeboer, M.** 2000. Atmospheric correction of SeaWiFS imagery for turbid coastal and inland waters. *Appl Opt* **39**(6): 897. DOI: https://doi.org/10.1364/AO.39.000897

Rutgersson, A, Smedman, A and **Sahle, E.** 2011. Oceanic convective mixing and the impact on air-sea gas transfer velocity. *Geophys Res Lett*, L02602. DOI: https://doi.org/10.1029/2010GL045581

Sabbaghzadeh, B, Upstill-Goddard, RC, Beale, R, Pereira, R and **Nightingale, PD.** 2017. The Atlantic Ocean surface microlayer from 50°N to 50°S is ubiquitously enriched in surfactants at wind speeds up to 13 ms^{-1}. *Geophys Res Lett* **44**(6): 2852–2858. DOI: https://doi.org/10.1002/2017GL072988

Saiz-Lopez, A, Mahajan, AS, Salmon, RA, Bauguitte, SJ-B, Jones, AE, Roscoe, HK, Plane, JMC. 2007. Boundary layer halogens in coastal Antarctica. *Science* **317**(5836): 348–351. DOI: https://doi.org/10.1126/science.1141408

Salter, ME, Upstill-Goddard, RC, Nightingale, PD, Archer, SD, Blomquist, B, Ho, DT, Huebert, B, Schlosser, P and **Yang, M.** 2011. Impact of an artificial surfactant release on air-sea gas fluxes during Deep Ocean Gas Exchange Experiment II. *J Geophys Res* **116**(C11): C11016. DOI: https://doi.org/10.1029/2011JC007023

Sauzède, R, Bittig, HC and **Claustre, H, Pasqueron de Fommervault, O, Gattuso, J-P, Legendre, L, Johnson, KS.** 2017. Estimates of Water-Column Nutrient Concentrations and Carbonate System Parameters in the Global Ocean: A Novel Approach Based on Neural Networks. *Front Mar Sci* **4**: 128. DOI: https://doi.org/10.3389/fmars.2017.00128

Sawamura, P, Moore, RH, Burton, SP, Chemyakin, E, Müller, D, Kolgotin, A, Ferrare, RA, Hostetler, CA, Ziemba, LD, Beyersdorf, AJ and **Anderson, BE.** 2017. HSRL-2 aerosol optical measurements and microphysical retrievals vs. airborne in situ measurements during DISCOVER-AQ 2013: an intercomparison study. *Atmos Chem Phys* **17**(11): 7229–7243. DOI: https://doi.org/10.5194/acp-17-7229-2017

Sayer, AM, Hsu, NC, Bettenhausen, C, Ahmad, Z, Holben, BN, Smirnov, A, Thomas, GE and **Zhang, J.** 2012. SeaWiFS Ocean Aerosol Retrieval (SOAR): Algorithm, validation, and comparison with other data sets. *J Geophys Res Atmos* **117**: D03206. DOI: https://doi.org/10.1029/2011JD016599

Sayer, AM, Thomas, GE and **Grainger, RG.** 2010. A sea surface reflectance model for (A)ATSR, and application to aerosol retrievals. *Atmos Meas Tech* **3**: 813–838. DOI: https://doi.org/10.5194/amt-3-813-2010

Schmidtko, S, Stramma, L and **Visbeck, M.** 2017. Decline in global oceanic oxygen content during the past five decades. *Nature* **542**(7641): 335–339. DOI: https://doi.org/10.1038/nature21399

Schulien, JA, Behrenfeld, MJ, Hair, JW, Hostetler, CA and **Twardowski, MS.** 2017. Vertically- resolved phytoplankton carbon and net primary production from a high spectral resolution lidar. *Opt Express* **25**(12): 13577. DOI: https://doi.org/10.1364/OE.25.013577

Sellegri, K, O'Dowd, CD, Yoon, YJ, Jennings, SG and **de Leeuw, G.** 2006. Surfactants and submicron sea spray generation. *J Geophys Res* **111**(D22): D22215. DOI: https://doi.org/10.1029/2005JD006658

Shao, H, Li, Y and **Li, L.** 2011. Sun glitter imaging of submarine sand waves on the Taiwan Banks: Determination of the relaxation rate of short waves. *J Geophys Res* **116**(C6): C06024. DOI: https://doi.org/10.1029/2010JC006798

Shipley, ST, Tracy, DH, Eloranta, EW, Trauger, JT, Sroga, JT, Roesler, FL and **Weinman, JA.** 1983. High spectral resolution lidar to measure optical scattering properties of atmospheric aerosols. 1: theory and instrumentation. *Appl Opt* **22**(23): 3716–24. DOI: https://doi.org/10.1364/AO.22.003716

Shutler, JD, Quartly, GD, Donlon, CJ, Sathyendranath, S, Platt, T, Chapron, B, Johannessen, JA, Girard-Ardhuin, F, Nightingale, PD, Woolf, DK and **Høyer, JL.** 2016. Progress in satellite remote sensing for studying physical processes at the ocean surface and its borders with the atmosphere and sea-ice. *Prog Phys Geogr* **40**(2): 215–246. DOI: https://doi.org/10.1177/0309133316638957

Siegel, DA, Maritorena, S, Nelson, NB and **Behrenfeld, MJ.** 2005. Independence and interdependencies among global ocean color properties: Reassessing the bio-optical assumption. *J Geophys Res* **110**(C7): C07011. DOI: https://doi.org/10.1029/2004JC002527

Simó, R. 2011. The role of marine microbiota in short-term climate regulation. In: Duarte, CM and Agustí, S (eds.), *The Role of Marine Biota in the Functioning of the Biosphere*, 107–130. Available at: http://digital.csic.es/handle/10261/73663.

Slade, WH and **Boss, E.** 2015. Spectral attenuation and backscattering as indicators of average particle size. *Appl Opt* **54**(24): 7264. DOI: https://doi.org/10.1364/AO.54.007264

Smirnov, A, Holben, BN, Giles, DM, Slutsker, I, O'Neill, NT, Eck, TF, Macke, A, Croot, P, Courcoux, Y, Sakerin, SM, Smyth, TJ, Zielinski, T, Zibordi, G, Goes, JI, Harvey, MJ, Quinn, PK, Nelson, NB, Radionov, VF, Duarte, CM, Losno, R, Sciare, J, Voss, KJ, Kinne, S, Nalli, NR, Joseph, E, Krishna Moorthy, K, Covert, DS, Gulev, SK, Milinevsky, G, Larouche, P, Belanger, S, Horne, E, Chin, M, Remer, LA, Kahn, RA, Reid, JS, Schulz, M, Heald, CL, Zhang, J, Lapina, K, Kleidman, RG, Griesfeller, J, Gaitley, BJ, Tan, Q and **Diehl, TL.** 2011. Maritime aerosol network as a component of AERONET – first results and comparison with global aerosol models and satellite retrievals. *Atmos Meas Tech* **4**(3): 583–597. DOI: https://doi.org/10.5194/amt-4-583-2011

Spooner, N, Keely, BJ and **Maxwell, JR.** 1994. Biologically mediated defunctionalization of chlorophyll in the aquatic environment-I. Senescence/decay of the diatom Phaeodactylum tricornutum. *Org Geochem* **21**(5): 509–516. DOI: https://doi.org/10.1016/0146-6380(94)90101-5

Stamnes, S, Hostetler, C, Ferrare, R, Burton, S, Liu, X, Hair, J, Hu, Y, Wasilewski, A, Martin, W, van Diedenhoven, B, Chowdhary, J, Stamnes, K and **Cairns, B.** 2018. Simultaneous polarimeter retrievals of microphysical aerosol and ocean color parameters from the "MAPP" algorithm with comparison to high spectral resolution lidar aerosol and ocean products. *Appl Opt*, in press. DOI: https://doi.org/10.1364/AO.57.002394

Stein, AF, Draxler, RR, Rolph, GD, Stunder, BJB, Cohen, MD, Ngan, F, Stein, AF, Draxler, RR, Rolph, GD, Stunder, BJB, Cohen, MD and **Ngan, F.** 2015. NOAA's HYSPLIT Atmospheric Transport and Dispersion Modeling System. *Bull Am Meteorol Soc* **96**(12): 2059–2077. DOI: https://doi.org/10.1175/BAMS-D-14-00110.1

Stephens, G, Winker, D, Pelon, J, Trepte, C, Vane, D, Yuhas, C, L'Ecuyer, T and **Lebsock, M.** 2017. CloudSat and CALIPSO within the A-Train: Ten years of actively observing the Earth system. *Bull Am Meteorol Soc.* DOI: https://doi.org/10.1175/BAMS-D-16-0324.1

Stephens, GL, Vane, DG, Tanelli, S, Im, E, Durden, S, Rokey, M, Reinke, D, Partain, P, Mace, GG, Austin, R, L'Ecuyer, T, Haynes, J, Lebsock, M, Suzuki, K, Waliser, D, Wu, D, Kay, J, Gettelman, A, Wang, Z and **Marchand, R.** 2008. CloudSat mission: Performance and early science after the first year of operation. *J Geophys Res* **113**(D8): D00A18. DOI: https://doi.org/10.1029/2008JD009982

Stocker, TF, Qin, D, Plattner, G-K, Alexander, LV, Allen, SK, Bindoff, NL, Bréon, F-M, Church, JA, Cubasch, U, Emori, S, Forster, P, Friedlingstein, P, Gillett, N, Gregory, JM, Hartmann, DL, Jansen, E, Kirtman, B, Knutti, R, Krishna Kumar, K, Lemke, P, Marotzke, J, Masson-Delmotte, V, Meehl, GA, Mokhov, II, Piao, S, Ramaswamy, V, Randall, D, Rhein, M, Rojas, M, Sabine, C, Shindell, D, Talley, LD, Vaughan, DG and **Xie, S-P.** 2013. Technical Summary. In: Stocker, TF, Qin, D, Plattner, G-K, Tignor, M, Allen, SK, Boschung, J, Nauels, A, Xia, Y,

Bex, V and Midgley, PM (eds.), *Climate Change 2013: The Physical Science Basis. Contribution of Working Group I to the Fifth Assessment Report of the Intergovernmental Panel on Climate Change*, 33–115.

Stramski, D, Reynolds, RA, Babin, M, Kaczmarek, S, Lewis, MR, Röttgers, R, Sciandra, A, Stramska, M, Twardowski, MS and **Claustre, H.** 2008. Relationships between the surface concentration of particulate organic carbon and optical properties in the eastern South Pacific and eastern Atlantic Oceans. *Biogeosciences* **5**: 171–201. DOI: https://doi.org/10.5194/bg-5-171-2008

Tan, S-C and **Shi, G-Y.** 2012. Transport of a Severe Dust Storm in March 2007 and Impacts on Chlorophyll a Concentration in the Yellow Sea. **8**: 2012–22. DOI: https://doi.org/10.2151/sola.2012-022

Tanré, D, Bréon, FM, Deuzé, JL, Dubovik, O, Ducos, F, François, P, Goloub, P, Herman, M, Lifermann, A and **Waquet, F.** 2011. Remote sensing of aerosols by using polarized, directional and spectral measurements within the A-Train: the PARASOL mission. *Atmos Meas Tech* **4**: 1383–1395. DOI: https://doi.org/10.5194/amt-4-1383-2011

Tanré, D, Kaufman, YJ, Herman, M and **Mattoo, S.** 1997. Remote sensing of aerosol properties over oceans using the MODIS/EOS spectral radiances. *J Geophys Res Atmos* **102**(D14): 16971–16988. DOI: https://doi.org/10.1029/96JD03437

Tedford, EW, MacIntyre, S, Miller, SD and **Czikowsky, MJ.** 2014. Similarity scaling of turbulence in a temperate lake during fall cooling. *J Geophys Res Ocean* **119**(8): 4689–4713. DOI: https://doi.org/10.1002/2014JC010135

Tesdal, J-E, Christian, JR, Monahan, AH and **von Salzen, K.** 2016. Evaluation of diverse approaches for estimating sea-surface DMS concentration and air–sea exchange at global scale. *Environ Chem* **13**(2): 390. DOI: https://doi.org/10.1071/EN14255

Tonizzo, A, Gilerson, A, Harmel, T, Ibrahim, A, Chowdhary, J, Gross, B, Moshary, F and **Ahmed, S.** 2011. Estimating particle composition and size distribution from polarized water-leaving radiance. *Appl Opt* **50**(25): 5047. DOI: https://doi.org/10.1364/AO.50.005047

Torrance, KE, Sparrow, EM and **Birkebak, RC.** 1966. Polarization, directional distribution, and off-specular peak phenomena in light reflected from roughened surfaces. *JOSA* **56**(7): 916–924. DOI: https://doi.org/10.1364/JOSA.56.000916

Twomey, S. 1974. Pollution and the Planetary Albedo. *Atmos Environ* **8**: 1251–1256. DOI: https://doi.org/10.1016/j.atmosenv.2007.10.062

Vallina, SM, Simó, R and **Gassó, S.** 2006. What controls CCN seasonality in the Southern Ocean? A statistical analysis based on satellite-derived chlorophyll and CCN and model-estimated OH radical and rainfall. *Global Biogeochem Cycles* **20**: GB1014. DOI: https://doi.org/10.1029/2005GB002597

van Diedenhoven, B, Cairns, B, Fridlind, AM, Ackerman, AS and **Garrett, TJ.** 2013. Remote sensing of ice crystal asymmetry parameter using multi-directional polarization measurements–Part 2: Application to the Research Scanning Polarimeter. *Atmos Chem Phys* **13**(6): 3185–3203. DOI: https://doi.org/10.5194/acp-13-3185-2013

Vandenbussche, S, Kochenova, S, Vandaele, AC, Kumps, N and **De Mazière, M.** 2013. Retrieval of desert dust aerosol vertical profiles from IASI measurements in the TIR atmospheric window. *Atmos Meas Tech* **6**: 2577–2591. DOI: https://doi.org/10.5194/amt-6-2577-2013

Vantrepotte, V, Danhiez, F-P, Loisel, H, Ouillon, S, Mériaux, X, Cauvin, A and **Dessailly, D.** 2015. CDOM-DOC relationship in contrasted coastal waters: implication for DOC retrieval from ocean color remote sensing observation. *Opt Express* **23**(1): 33. DOI: https://doi.org/10.1364/OE.23.000033

Vila, DA, Scofield, RA and **Davenport, J.** 2001. Satellite rainfall estimation over South America: Evaluation of two major events. *AMS 16th Conference on Hydrology*.

Vodacek, A, Blough, NV, DeGrandpre, MD and **Nelson, RK.** 1997. Seasonal variation of CDOM and DOC in the Middle Atlantic Bight: Terrestrial inputs and photooxidation. *Limnol Oceanogr* **42**(4): 674–686. DOI: https://doi.org/10.4319/lo.1997.42.4.0674

Vogelzang, J, Stoffelen, A, Verhoef, A and **Figa-Saldaña, J.** 2011. On the quality of high-resolution scatterometer winds. *J Geophys Res Ocean* **116**(10). DOI: https://doi.org/10.1029/2010JC006640

von Glasow, R and **Crutzen, PJ.** 2004. Model study of multiphase DMS oxidation with a focus on halogens. *Atmos Chem Phys* **4**: 589–608. DOI: https://doi.org/10.5194/acp-4-589-2004

Voss, KJ and **Fry, ES.** 1984. Measurement of the Mueller matrix for ocean water. *Appl Opt* **23**(23): 4427. DOI: https://doi.org/10.1364/AO.23.004427

Wald, L and **Monget, J-M.** 1983. Sea surface winds from sun glitter observations. *J Geophys Res Ocean* **88**(C4): 2547–2555. DOI: https://doi.org/10.1029/JC088iC04p02547

Wang, M and **Shi, W.** 2007. The NIR-SWIR combined atmospheric correction approach for MODIS ocean color data processing. *Opt Express* **15**(24): 15722–33. DOI: https://doi.org/10.1364/OE.15.015722

Wanninkhof, R. 2014. Relationship between wind speed and gas exchange over the ocean revisited. *Limnol Oceanogr Methods* **12**(6): 351–362. DOI: https://doi.org/10.4319/lom.2014.12.351

Wanninkhof, R, Asher, WE, Ho, DT, Sweeney, C and **McGillis, WR.** 2009. Advances in Quantifying Air-Sea Gas Exchange and Environmental Forcing. *Ann Rev Mar Sci* **1**(1): 213–244. DOI: https://doi.org/10.1146/annurev.marine.010908.163742

Wentz, FJ. 2015. A 17-Yr Climate Record of Environmental Parameters Derived from the Tropical Rainfall Measuring Mission (TRMM) Microwave Imager. *J Clim* **28**(17): 6882–6902. DOI: https://doi.org/10.1175/JCLI-D-15-0155.1

Werdell, PJ, Franz, BA, Bailey, SW, Feldman, GC, Boss, E, Brando, VE, Dowell, M, Hirata, T, Lavender, SJ, Lee, Z, Loisel, H, Maritorena, S, Mélin, F, Moore, TS, Smyth, TJ and **Antoine, D.** 2013. Generalized ocean color inversion model for retrieving marine inherent optical properties. *Appl Opt* **52**(10).

Willis, MD, Burkart, J, Thomas, JL, Köllner, F, Schneider, J, Bozem, H, Hoor, PM, Aliabadi, AA, Schulz, H, Herber, AB, Leaitch, WR and **Abbatt, JPD.** 2016. Growth of nucleation mode particles in the summertime Arctic: a case study. *Atmos Chem Phys* **16**: 7663–7679. DOI: https://doi.org/10.5194/acp-2016-256

Wilson, TW, Ladino, LA, Alpert, PA, Breckels, MN, Brooks, IM, Browse, J, Burrows, SM, Carslaw, KS, Huffman, JA, Judd, C, Kilthau, WP, Mason, RH, McFiggans, G, Miller, LA, Nájera, JJ, Polishchuk, E, Rae, S, Schiller, CL, Si, M, Temprado, JV, Whale, TF, Wong, JPS, Wurl, O, Yakobi-Hancock, JD, Abbatt, JPD, Aller, JY, Bertram, AK, Knopf, DA and **Murray, BJ.** 2015. A marine biogenic source of atmospheric ice-nucleating particles. *Nature* **525**(7568): 234–238. DOI: https://doi.org/10.1038/nature14986

Winker, DM, Couch, RH and **McCormick, MP.** 1996. An overview of LITE: NASA's Lidar In-space Technology Experiment. *Proc IEEE* **84**(2): 164–180. DOI: https://doi.org/10.1109/5.482227

Winker, DM, Tackett, JL, Getzewich, BJ, Liu, Z, Vaughan, MA and **Rogers, RR.** 2013. The global 3-D distribution of tropospheric aerosols as characterized by CALIOP. *Atmos Chem Phys* **13**(6): 3345–3361. DOI: https://doi.org/10.5194/acp-13-3345-2013

Winker, DM, Vaughan, MA, Omar, A, Hu, Y, Powell, KA, Liu, Z, Hunt, WH and **Young, SA.** 2009. Overview of the CALIPSO Mission and CALIOP Data Processing Algorithms. *J Atmos Ocean Technol* **26**(11): 2310–2323. DOI: https://doi.org/10.1175/2009JTECHA1281.1

Woolf, DK. 2005. Parametrization of gas transfer velocities and sea-state-dependent wave breaking. *Tellus, Ser B Chem Phys Meteorol* **57**(2): 87–94. DOI: https://doi.org/10.1111/j.1600-0889.2005.00139.x

Xu, F, Dubovik, O, Zhai, P-W, Diner, DJ, Kalashnikova, OV, Seidel, FC, Litvinov, P, Bovchaliuk, A, Garay, MJ, van Harten, G and **Davis, AB.** 2016. Joint retrieval of aerosol and water-leaving radiance from multispectral, multiangular and polarimetric measurements over ocean. *Atmos Meas Tech* **9**(7): 2877–2907. DOI: https://doi.org/10.5194/amt-9-2877-2016

Xu, F, van Harten, G, Diner, DJ, Davis, AB, Seidel, FC, Rheingans, B, Tosca, M, Alexandrov, MD, Cairns, B, Ferrare, RA, Burton, SP, Fenn, MA, Hostetler, CA, Wood, R and **Redemann, J.** 2018. Coupled Retrieval of Liquid Water Cloud and Aerosol Above Cloud Properties using the Airborne Multiangle SpectroPolarimetric Imager (AirMSPI). *J Geophys Res Atmos* **123**: 3175–3204. DOI: https://doi.org/10.1002/2017JD027926

Yin, X, Boutin, J, Dinnat, E, Song, Q and **Martin, A.** 2016. Roughness and foam signature on SMOS-MIRAS brightness temperatures: A semi-theoretical approach. *Remote Sens Environ* **180**: 221–233. DOI: https://doi.org/10.1016/j.rse.2016.02.005

Yorks, JE, McGill, MJ, Palm, SP, Hlavka, DL, Selmer, PA, Nowottnick, EP, Vaughan, MA, Rodier, SD and **Hart, WD.** 2016. An overview of the CATS level 1 processing algorithms and data products. *Geophys Res Lett* **43**(9): 4632–4639. DOI: https://doi.org/10.1002/2016GL068006

Young, SA, Vaughan, MA, Kuehn, RE and **Winker, DM.** 2013. The Retrieval of Profiles of Particulate Extinction from *Cloud–Aerosol Lidar and Infrared Pathfinder Satellite Observations* (*CALIPSO*) Data: Uncertainty and Error Sensitivity Analyses. *J Atmos Ocean Technol* **30**(3): 395–428. DOI: https://doi.org/10.1175/JTECH-D-12-00046.1

Young, SA and **Vaughan, MA.** 2009. The Retrieval of Profiles of Particulate Extinction from Cloud-Aerosol Lidar Infrared Pathfinder Satellite Observations (CALIPSO) Data: Algorithm Description. *J Atmos Ocean Technol* **26**(6): 1105–1119. DOI: https://doi.org/10.1175/2008JTECHA1221.1

Yu, H, Chin, M, Winker, DM, Omar, AH, Liu, Z, Kittaka, C and **Diehl, T.** 2010. Global view of aerosol vertical distributions from CALIPSO lidar measurements and GOCART simulations: Regional and seasonal variations. *J Geophys Res* **115**(D4): D00H30. DOI: https://doi.org/10.1029/2009JD013364

Yu, H, Chin, M, Yuan, T, Bian, H, Remer, LA, Prospero, JM, Omar, A, Winker, D, Yang, Y, Zhang, Y, Zhang, Z and **Zhao, C.** 2015. The fertilizing role of African dust in the Amazon rainforest: A first multiyear assessment based on data from Cloud-Aerosol Lidar and Infrared Pathfinder Satellite Observations. *Geophys Res Lett* **42**(6): 1984–1991. DOI: https://doi.org/10.1002/2015GL063040

Zeng, S, Riedi, J, Trepte, CR, Winker, DM and **Hu, Y-X.** 2014. Study of global cloud droplet number concentration with A-Train satellites. *Atmos Chem Phys* **14**(14): 7125–7134. DOI: https://doi.org/10.5194/acp-14-7125-2014

Zhai, L, Gudmundsson, K, Miller, P, Peng, W, Guðfinnsson, H, Debes, H, Hátún, H, White, GN, Hernández Walls, R, Sathyendranath, S and **Platt, T.** 2012. Phytoplankton phenology and production around Iceland and Faroes. *Cont Shelf Res* **37**: 15–25. DOI: https://doi.org/10.1016/j.csr.2012.01.013

Zhai, P-W, Hu, Y, Trepte, CR, Winker, DM, Josset, DB, Lucker, PL and **Kattawar, GW.** 2013. Inherent optical properties of the coccolithophore: Emiliania huxleyi. *Opt Express* **21**(15): 17625–17638. DOI: https://doi.org/10.1364/OE.21.017625

Zhang, JA, Katsaros, KB, Black, PG, Lehner, S, French, JR and **Drennan, WM.** 2008. Effects of roll vortices on turbulent fluxes in the hurricane boundary layer. *Boundary-Layer Meteorol* **128**(2): 173–189. DOI: https://doi.org/10.1007/s10546-008-9281-2

Zhang, Z, Cai, W, Liu, L, Liu, C and **Chen, F.** 2003. Direct determination of thickness of sea surface microlayer using a pH microelectrode at original location. *Sci China Ser B* **46**(4): 339. DOI: https://doi.org/10.1360/02yb0192

Zhang, Z, Meyer, K, Yu, H, Platnick, S, Colarco, P, Liu, Z and **Oreopoulos, L.** 2016. Shortwave direct radiative effects of above-cloud aerosols over global oceans derived from 8 years of CALIOP and MODIS observations. *Atmos Chem Phys* **16**(5): 2877–2900. DOI: https://doi.org/10.5194/acp-16-2877-2016

Zheng, G and **Stramski, D.** 2013. A model for partitioning the light absorption coefficient of suspended marine particles into phytoplankton and nonalgal components. *J Geophys Res Ocean* **118**(6): 2977–2991. DOI: https://doi.org/10.1002/jgrc.20206

How to cite this article: Neukermans, G, Harmel, T, Galí, M, Rudorff, N, Chowdhary, J, Dubovik, O, Hostetler, C, Hu, Y, Jamet, C, Knobelspiesse, K, Lehahn, Y, Litvinov, P, Sayer, AM, Ward, B, Boss, E, Koren, I and Miller, LA. 2018. Harnessing remote sensing to address critical science questions on ocean-atmosphere interactions. *Elem Sci Anth*, 6: 71. DOI: https://doi.org/10.1525/elementa.331

Domain Editor-in-Chief: Jody W. Deming, Department of Biological Oceanography, University of Washington, US

Associate Editor: Kevin Arrigo, Environmental Earth System Science, Stanford University, US

Knowledge Domain: Ocean Science

Submitted: 05 March 2018 **Accepted:** 16 October 2018 **Published:** 28 November 2018

ELEMENTA Science of the Anthropocene

Elem Sci Anth is a peer-reviewed open access journal published by University of California Press.

OPEN ACCESS